THE UNIVERSITY OF MANITOBA

"THE THERMAL WAKE BEHIND A CYLINDER IN FULLY-DEVELOPED TURBULENT PIPE FLOW"

BY

YOU QIN WANG

A THESIS

SUBMITTED TO THE FACULTY OF

GRADUATE STUDIES IN PARTIAL FULFILLMENT

OF THE REQUIREMENTS FOR THE DEGREE OF

MASTER OF SCIENCE IN DEPARTMENT OF

MECHANICAL AND INDUSTRIAL ENGINEERING

WINNIPEG, MANITOBA

AUGUST, 1994

ISBN 0-612-13551-9

Canada

Name YOU QIN WANG

Dissertation Abstracts International is arranged by broad, general subject categories. Please select the one subject which most nearly describes the content of your dissertation. Enter the corresponding four-digit code in the spaces provided.

Engineering Heat and Thermodynamics Applied Sciences
SUBJECT TERM

0348
SUBJECT CODE

U·M·I

Subject Categories

THE HUMANITIES AND SOCIAL SCIENCES

COMMUNICATIONS AND THE ARTS
Architecture 0729
Art History 0377
Cinema 0900
Dance 0378
Fine Arts 0357
Information Science 0723
Journalism 0391
Library Science 0399
Mass Communications 0708
Music 0413
Speech Communication 0459
Theater 0465

EDUCATION
General 0515
Administration 0514
Adult and Continuing 0516
Agricultural 0517
Art 0273
Bilingual and Multicultural 0282
Business 0688
Community College 0275
Curriculum and Instruction 0727
Early Childhood 0518
Elementary 0524
Finance 0277
Guidance and Counseling 0519
Health 0680
Higher 0745
History of 0520
Home Economics 0278
Industrial 0521
Language and Literature 0279
Mathematics 0280
Music 0522
Philosophy of 0998
Physical 0523
Psychology 0525
Reading 0535
Religious 0527
Sciences 0714
Secondary 0533
Social Sciences 0534
Sociology of 0340
Special 0529
Teacher Training 0530
Technology 0710
Tests and Measurements 0288
Vocational 0747

LANGUAGE, LITERATURE AND LINGUISTICS
Language
- General 0679
- Ancient 0289
- Linguistics 0290
- Modern 0291

Literature
- General 0401
- Classical 0294
- Comparative 0295
- Medieval 0297
- Modern 0298
- African 0316
- American 0591
- Asian 0305
- Canadian (English) 0352
- Canadian (French) 0355
- English 0593
- Germanic 0311
- Latin American 0312
- Middle Eastern 0315
- Romance 0313
- Slavic and East European 0314

PHILOSOPHY, RELIGION AND THEOLOGY
Philosophy 0422
Religion
- General 0318
- Biblical Studies 0321
- Clergy 0319
- History of 0320
- Philosophy of 0322

Theology 0469

SOCIAL SCIENCES
American Studies 0323
Anthropology
- Archaeology 0324
- Cultural 0326
- Physical 0327

Business Administration
- General 0310
- Accounting 0272
- Banking 0770
- Management 0454
- Marketing 0338

Canadian Studies 0385
Economics
- General 0501
- Agricultural 0503
- Commerce-Business 0505
- Finance 0508
- History 0509
- Labor 0510
- Theory 0511

Folklore 0358
Geography 0366
Gerontology 0351
History
- General 0578
- Ancient 0579
- Medieval 0581
- Modern 0582
- Black 0328
- African 0331
- Asia, Australia and Oceania 0332
- Canadian 0334
- European 0335
- Latin American 0336
- Middle Eastern 0333
- United States 0337

History of Science 0585
Law 0398
Political Science
- General 0615
- International Law and Relations 0616
- Public Administration 0617

Recreation 0814
Social Work 0452
Sociology
- General 0626
- Criminology and Penology 0627
- Demography 0938
- Ethnic and Racial Studies 0631
- Individual and Family Studies 0628
- Industrial and Labor Relations 0629
- Public and Social Welfare 0630
- Social Structure and Development 0700
- Theory and Methods 0344

Transportation 0709
Urban and Regional Planning 0999
Women's Studies 0453

THE SCIENCES AND ENGINEERING

BIOLOGICAL SCIENCES
Agriculture
- General 0473
- Agronomy 0285
- Animal Culture and Nutrition 0475
- Animal Pathology 0476
- Food Science and Technology 0359
- Forestry and Wildlife 0478
- Plant Culture 0479
- Plant Pathology 0480
- Plant Physiology 0817
- Range Management 0777
- Wood Technology 0746

Biology
- General 0306
- Anatomy 0287
- Biostatistics 0308
- Botany 0309
- Cell 0379
- Ecology 0329
- Entomology 0353
- Genetics 0369
- Limnology 0793
- Microbiology 0410
- Molecular 0307
- Neuroscience 0317
- Oceanography 0416
- Physiology 0433
- Radiation 0821
- Veterinary Science 0778
- Zoology 0472

Biophysics
- General 0786
- Medical 0760

EARTH SCIENCES
Biogeochemistry 0425
Geochemistry 0996
Geodesy 0370
Geology 0372
Geophysics 0373
Hydrology 0388
Mineralogy 0411
Paleobotany 0345
Paleoecology 0426
Paleontology 0418
Paleozoology 0985
Palynology 0427
Physical Geography 0368
Physical Oceanography 0415

HEALTH AND ENVIRONMENTAL SCIENCES
Environmental Sciences 0768
Health Sciences
- General 0566
- Audiology 0300
- Chemotherapy 0992
- Dentistry 0567
- Education 0350
- Hospital Management 0769
- Human Development 0758
- Immunology 0982
- Medicine and Surgery 0564
- Mental Health 0347
- Nursing 0569
- Nutrition 0570
- Obstetrics and Gynecology 0380
- Occupational Health and Therapy 0354
- Ophthalmology 0381
- Pathology 0571
- Pharmacology 0419
- Pharmacy 0572
- Physical Therapy 0382
- Public Health 0573
- Radiology 0574
- Recreation 0575
- Speech Pathology 0460
- Toxicology 0383

Home Economics 0386

PHYSICAL SCIENCES
Pure Sciences
Chemistry
- General 0485
- Agricultural 0749
- Analytical 0486
- Biochemistry 0487
- Inorganic 0488
- Nuclear 0738
- Organic 0490
- Pharmaceutical 0491
- Physical 0494
- Polymer 0495
- Radiation 0754

Mathematics 0405
Physics
- General 0605
- Acoustics 0986
- Astronomy and Astrophysics 0606
- Atmospheric Science 0608
- Atomic 0748
- Electronics and Electricity 0607
- Elementary Particles and High Energy 0798
- Fluid and Plasma 0759
- Molecular 0609
- Nuclear 0610
- Optics 0752
- Radiation 0756
- Solid State 0611

Statistics 0463

Applied Sciences
Applied Mechanics 0346
Computer Science 0984
Engineering
- General 0537
- Aerospace 0538
- Agricultural 0539
- Automotive 0540
- Biomedical 0541
- Chemical 0542
- Civil 0543
- Electronics and Electrical 0544
- Heat and Thermodynamics 0348
- Hydraulic 0545
- Industrial 0546
- Marine 0547
- Materials Science 0794
- Mechanical 0548
- Metallurgy 0743
- Mining 0551
- Nuclear 0552
- Packaging 0549
- Petroleum 0765
- Sanitary and Municipal 0554
- System Science 0790

Geotechnology 0428
Operations Research 0796
Plastics Technology 0795
Textile Technology 0994

PSYCHOLOGY
General 0621
Behavioral 0384
Clinical 0622
Developmental 0620
Experimental 0623
Industrial 0624
Personality 0625
Physiological 0989
Psychobiology 0349
Psychometrics 0632
Social 0451

THE THERMAL WAKE BEHIND A CYLINDER

IN FULLY-DEVELOPED TURBULENT PIPE FLOW

BY

YOU QIN WANG

A thesis submitted to the Faculty of Graduate Studies of the University of Manitoba in partial fulfillment of the requirements of the degree of

MASTER OF SCIENCE

ABSTRACT

In this report, the characteristics of the thermal wake created by a heated cylinder in pipe flow are studied. The measurements were made in a fully-developed turbulent pipe flow, at 13 stations from 16.7 to 166.7 filament diameters downstream of the heat source at a Reynolds number of 180,000 based on the centerline mean velocity and the pipe diameter (or 11,000 based on the cylinder diameter). The results include the transverse distributions of the mean and r.m.s. velocity and the first four moments of the temperatures as well as the probability density functions of temperature fluctuation. The data have validated Derksen and Sullivan's maximum entropy formulation. It has been shown that the maximum entropy method is a very effective method to approximate the pdf of a turbulent contaminate fluctuation when only the moments up to fourth order are known. The data also indicate that the characteristics of the thermal wake are symmetric.

ACKNOWLEDGMENTS

I would like to thank all of the people who have assisted me throughout this project.

Thanks to Dr. R. W. Derksen for his invaluable guidance and enthusiastic assistance. It was an honor to have him as my advisor; Thanks to Dr. R. S. Azad for his helpful suggestion which he has provided during the experiment; Thanks to Dr. D. Burn for the thesis reviewing and Mr. K. Tart for assisting with the experimental set-up; Thanks to my parents for their encouragement and my husband, Mingchuan Lu, for his support.

Thanks to the University of Manitoba which provided a Graduate Fellowship for my second year of study.

TABLE OF CONTENTS

ABSTRACT i

ACKNOWLEDGMENTS ii

TABLE OF CONTENTS iii

LIST OF FIGURES v

LIST OF TABLES ix

NOMENCLATURE x

Chapter Page

I. INTRODUCTION 1

II. EQUIPMENT AND PROCEDURE 10

2.1 The Wind Tunnel and its Calibration 10
2.2 The Velocity Measurement Instruments 12
2.3 The Temperature Measurement Instruments 15
2.4 Data Acquisition 17

III. RESULTS AND DISCUSSION 18

3.1 The Velocity Field 18
3.2 The Temperature Field 19
3.3 Statistical Characteristics of the Flow 23

IV. CONCLUSIONS 26

REFERENCES 27

FIGURES 30

APPENDIX (TABLES OF EXPERIMENTAL DATA) 83

LIST OF FIGURES

Figure		page
1.	The general layout of the wind tunnel	30
2.	Sketch of the wind-tunnel test section	31
3.	Tunnel calibration curve (centerline dynamic pressure)	32
4.	Tunnel calibration curve (centerline mean velocity)	33
5.	Transverse distributions of the mean velocity	34
6.	Transverse distributions of the r.m.s. velocity	35
7.	Downstream development of centerline maen velocity	36
8.	Downstream development of centerline r.m.s. velocity	37
9.	Transverse distributions of the mean velocity measured by both hot-wire and pitot tube at x/d = 16.7	38
10.	Transverse distributions of the mean velocity measured by both hot-wire and pitot tube at x/d = 25.0	39
11.	Transverse distributions of the mean velocity measured by both hot-wire and pitot tube at x/d = 33.3	40
12.	Transverse distributions of the mean velocity measured by both hot-wire and pitot tube at x/d = 41.7	41
13.	Transverse distributions of the mean velocity measured by both hot-wire and pitot tube at x/d = 50.0	42

Figure page

14. Transverse distributions of the mean velocity measured by both hot-wire and pitot tube at x/d = 58.3 43

15. Transverse distributions of the mean velocity measured by both hot-wire and pitot tube at x/d = 66.7 44

16. Transverse profiles of the mean temperature rise..... 45

17. Transverse distribution of the mean temperature rise at x/d = 16.7 (solid smooth line represents the Gaussian distribution and the symbols of the open circle represent measured data)..... 46

18. Transverse distribution of the mean temperature rise at x/d = 25.0 (symbols as in Figure 17.)..... 47

19. Transverse distribution of the mean temperature rise at x/d = 33.3 (symbols as in Figure 17.)..... 48

20. Transverse distribution of the mean temperature rise at x/d = 41.7 (symbols as in Figure 17.)..... 49

21. Transverse distribution of the mean temperature rise at x/d = 50.0 (symbols as in Figure 17.)..... 50

22. Transverse distribution of the mean temperature rise at x/d = 58.3 (symbols as in Figure 17.)..... 51

23. Downstream development of the centerline mean temperature..... 52

24. Locus of positions with $k = \Delta\overline{T} / \Delta\overline{T}_c$ = 0.9,0.5,0.3, respectively..... 53

25. Transverse distributions of the r.m.s. temperature fluctuation..... 54

26. Downstream development of the centerline r.m.s. temperature fluctuation..... 55

27. Downstream development of half-width of the wake..... 56

28. Transverse distributions of temperature skewness..... 57

29. Transverse distributions of temperature flatness..... 58

Figure page

30. Distributions of probability density function of temperature fluctuation at r/d =0.0 and x/d = 16.7 59

31. Distributions of probability density function of temperature fluctuation at r/d =0.0 and x/d = 25.0 60

32. Distributions of probability density function of temperature fluctuation at r/d =0.0 and x/d = 33.3 61

33. Distributions of probability density function of temperature fluctuation at r/d =0.0 and x/d = 41.7 62

34. Distributions of probability density function of temperature fluctuation at r/d =0.0 and x/d = 50.0 63

35. Distributions of probability density function of temperature fluctuation at r/d =0.0 and x/d = 58.3 64

36. Distributions of probability density function of temperature fluctuation at r/d =1.3 and x/d = 16.7 65

37. Distributions of probability density function of temperature fluctuation at r/d =1.3 and x/d = 25.0 66

38. Distributions of probability density function of temperature fluctuation at r/d =1.3 and x/d = 33.3 67

39. Distributions of probability density function of temperature fluctuation at r/d =1.3 and x/d = 41.7 68

40. Distributions of probability density function of temperature fluctuation at r/d =1.3 and x/d = 50.0 69

41. Distributions of probability density function of temperature fluctuation at r/d =1.3 and x/d = 58.3 70

42. Distributions of probability density function of temperature fluctuation at r/d =2.7 and x/d = 16.7 71

43. Distributions of probability density function of temperature fluctuation at r/d =2.7 and x/d = 25.0 72

Figure page

44. Distributions of probability density function of temperature fluctuation at r/d =2.7 and x/d = 33.3 73

45. Distributions of probability density function of temperature fluctuation at r/d =2.7 and x/d = 41.7 74

46. Distributions of probability density function of temperature fluctuation at r/d =2.7 and x/d = 50.0 75

47. Distributions of probability density function of temperature fluctuation at r/d =2.7 and x/d = 58.3 76

48. Distributions of probability density function of temperature fluctuation at r/d =5.0 and x/d = 16.7 77

49. Distributions of probability density function of temperature fluctuation at r/d =5.0 and x/d = 25.0 78

50. Distributions of probability density function of temperature fluctuation at r/d =5.0 and x/d = 33.3 79

51. Distributions of probability density function of temperature fluctuation at r/d =5.0 and x/d = 41.7 80

52. Distributions of probability density function of temperature fluctuation at r/d =5.0 and x/d = 50.0 81

53. Distributions of probability density function of temperature fluctuation at r/d =5.0 and x/d = 58.3 82

LIST OF TABLES

Table		Page
1.	Pitot-tube measurements	83
2.	Hot-wire measurements (radial distributions)	85
3.	Hot-wire measurements (axial distributions)	89
4.	Cold-wire measurements (radial distributions)	90
5.	Cold-wire measurements (axial distributions)	91
6.	The skewness and flatness distributions	92
7.	The parameters of the curve fitting and the development of the wake width	94

NOMENCLATURE

a	a constant or overheating ratio
b	a constant
A	a constant
B	a constant
c_n	the height order moments of contaminant concentration
$\overline{c^n}$	The height order central moments of contaminant concentration
C	the local mean contaminant concentration
C_d	drag coefficient
C_0	the maximum mean contaminant concentration
d	diameter of the cylinder
D	diameter of the pipe
F( )	flatness factor of ( )
$\vec{g}$	gravity vector
h	the momentum thickness of the wake
H	the entropy of a pdf
k	a constant
K	a constant

l local length scale

p( ) probability density function of ( )

P_{dyn} dynamic pressure

ΔP_{cone} contraction cone pressure drop

r distance in cross-stream direction

R probe hot resistance

R_0 probe cold resistance at ambient temperature

R_T bridge resistance

ΔR_C comparison resistance

S( ) skewness factor of ( )

t time

$\overline{T}$ mean temperature

$\overline{T}_c$ centerline mean temperature

T_a ambient temperature

$\overline{T}_{min}$ the lowest value of the mean temperature at that transverse location

$\overline{T}_{max}$ the maximum value of the mean temperature in present experiment

$\Delta\overline{T}$ mean temperature rise with respect to the lowest value at that transverse location

$\Delta\overline{T}^*$ mean temperature rise with respect to the ambient temperature

$\Delta\overline{T}_c$ centerline mean temperature rise with respect to the lowest value at that transverse location

$\Delta\overline{T}_c^*$ centerline mean temperature rise with respect to the ambient temperature

$\Delta\overline{T}^{*}_{max}$ the maximum value of the mean temperature rise with respect to the ambient temperature

$\Delta\overline{T}_{p}$ peak value of mean temperature rise

u fluctuating velocity in the direction of increasing x

u' r.m.s. fluctuating velocity in the direction of increasing x

u'_{c} centerline r.m.s. fluctuating velocity in the direction of increasing x

U the velocity component in the direction of increasing x

$\overline{U}$ mean velocity in the direction of increasing x

$\overline{U}_{c}$ centerline mean velocity

U_{ref} mean axial centerline velocity

U_{s} the cross-stream variation of the mean velocity component in the x direction

U_{0} the velocity of the mean flow in the x direction

v fluctuating velocity in the direction of increasing y

V the velocity component in the direction of increasing y

$\overline{V}$ mean velocity in the direction of increasing y

V_{CTA} anemometer output voltage

V_{LIN} linearizer output voltage

w half-width of the wake or the fluctuating velocity in the direction of increasing z

W the velocity component in the direction of increasing z

$\overline{W}$ mean velocity in the direction of increasing z

x distance in streamwise direction or component of Cartesian coordinate

x_0 the location of virtual origin of the self-similar wake

y distance in cross-stream direction or component of Cartesian coordinate

z distance parallel to the cylinder or component of Cartesian coordinate

Z ratio of local mean concentration to the maximum mean concentration

Greek Symbols

α function of downstream or time for unsteady flow

α_0 temperature coefficient

β function of downstream or time for unsteady flow

ε dissipation rate of turbulent kinetic energy

γ fluctuating instantaneous contaminant concentration

Γ instantaneous contaminant concentration at position x and time t

$\overline{\Gamma}$ mean instantaneous contaminant concentration

θ instantaneous contaminant concentration or temperature fluctuation or the random variable

θ' r.m.s. temperature fluctuation

θ'_c centerline r.m.s. temperature fluctuation

κ diffusion coefficient

λ cut-off length

λ_i constants

ν kinematic viscosity

ρ air density

ζ non-dimensional fluctuating temperature

CHAPTER I

INTRODUCTION

The objective of this work was to provide experimental data on turbulent diffusion. The specific measurements were the distribution of moments, up to fourth order, and probability density functions in the wake of a heated cylinder in fully-developed pipe flow. This will provide valuable data in assessing the α - β model of Chatwin and Sullivan (1990) and the maximum entropy method of Derksen and Sullivan (1990).

Turbulence is the most common state of fluid motion in nature, and it is also the most complex physical problem for engineers to solve. Wall-jet, thermal wake, and shear layer, etc. are different turbulent flows but they have many characteristics in common. Turbulence is not a fluid property, but of the flows. Besides the irregularity and dissipation, the diffusivity, which causes rapid mixing and increased rates of contaminant transfer, is an important feature of all turbulent flows. Thus turbulence is the predominant mechanism for mixing and transporting contaminants in fluids. Here the fluctuations in the fluid velocities result in large mean fluxes which transport the contaminant. These motions also serve to stretch and fold contaminated regions which results in increased local, instantaneous concentration gradients and hence speed up dilution. Turbulent flow has eluded first principle analytical solution to date. Current solutions to turbulent flow problems rely very heavily on empirical data and simplified models, which cannot be readily extended to other situations. The solution of turbulent mixing problems

has become more urgent with our current concern about environmental issues. Additionally, many industrial processes depend on efficient turbulent mixing and transport of heat, moisture, and chemical reactants. Thus a strong interest in the physics of turbulent mixing has motivated a great deal of research since the pioneering work of Taylor (1921).

Before we discuss some related recent research results on turbulent diffusion, let us first provide the derivation of the turbulent contaminant transport equation. Instantaneous transport of a contaminant in a fluid is governed by

$$\frac{\partial \Gamma}{\partial t} + U\frac{\partial \Gamma}{\partial x} + V\frac{\partial \Gamma}{\partial y} + W\frac{\partial \Gamma}{\partial z} = \kappa\left(\frac{\partial^2 \Gamma}{\partial x^2} + \frac{\partial^2 \Gamma}{\partial y^2} + \frac{\partial^2 \Gamma}{\partial z^2}\right), \qquad 1$$

where Γ is the instantaneous contaminant concentration, t is time, x, y, z are three components with respect to the Cartesian coordinate and U, V, W denote respectively the velocity components in the directions of increasing x, y, and z, and κ is the diffusion coefficient. We can show that

$$U\frac{\partial \Gamma}{\partial x} + V\frac{\partial \Gamma}{\partial y} + W\frac{\partial \Gamma}{\partial z} = \frac{\partial U\Gamma}{\partial x} + \frac{\partial V\Gamma}{\partial y} + \frac{\partial W\Gamma}{\partial z} - \Gamma\left(\frac{\partial U}{\partial x} + \frac{\partial V}{\partial y} + \frac{\partial W}{\partial z}\right). \qquad 2$$

As $\nabla \cdot \mathbf{V}$ is zero for an incompressible flow, we have

$$U\frac{\partial \Gamma}{\partial x} + V\frac{\partial \Gamma}{\partial y} + W\frac{\partial \Gamma}{\partial z} = \frac{\partial U\Gamma}{\partial x} + \frac{\partial V\Gamma}{\partial y} + \frac{\partial W\Gamma}{\partial z}. \qquad 3$$

Thus we have

$$\frac{\partial \Gamma}{\partial t} + \frac{\partial U\Gamma}{\partial x} + \frac{\partial V\Gamma}{\partial y} + \frac{\partial W\Gamma}{\partial z} = \kappa\left(\frac{\partial^2 \Gamma}{\partial x^2} + \frac{\partial^2 \Gamma}{\partial y^2} + \frac{\partial^2 \Gamma}{\partial z^2}\right). \qquad 4$$

The Reynolds decomposition allows us to write

$$\begin{aligned}\Gamma &= \overline{\Gamma} + \gamma, \\ U &= \overline{U} + u, \\ V &= \overline{V} + v, \\ W &= \overline{W} + w,\end{aligned} \qquad 5$$

where the overbar indicates the mean value and lower case indicates fluctuation from the mean. Hence

$$\begin{aligned}&\frac{\partial(\overline{\Gamma}+\gamma)}{\partial t} + \frac{\partial}{\partial x}(\overline{U\Gamma} + u\overline{\Gamma} + \overline{U}\gamma + u\gamma) + \frac{\partial}{\partial y}(\overline{V\Gamma} + v\overline{\Gamma} + \overline{V}\gamma + v\gamma) \\ &+ \frac{\partial}{\partial z}(\overline{W\Gamma} + w\overline{\Gamma} + \overline{W}\gamma + w\gamma) = \kappa\left[\frac{\partial^2(\overline{\Gamma}+\gamma)}{\partial x^2} + \frac{\partial^2(\overline{\Gamma}+\gamma)}{\partial y^2} + \frac{\partial^2(\overline{\Gamma}+\gamma)}{\partial z^2}\right].\end{aligned} \qquad 6$$

The mean value of this equation is

$$\frac{\partial\overline{\Gamma}}{\partial t} + \frac{\partial(\overline{U\Gamma} + \overline{u\gamma})}{\partial x} + \frac{\partial(\overline{V\Gamma} + \overline{v\gamma})}{\partial y} + \frac{\partial(\overline{W\Gamma} + \overline{w\gamma})}{\partial z} = \kappa\left(\frac{\partial^2\overline{\Gamma}}{\partial x^2} + \frac{\partial^2\overline{\Gamma}}{\partial y^2} + \frac{\partial^2\overline{\Gamma}}{\partial z^2}\right). \qquad 7$$

For a stationary flow ($\partial\overline{\Gamma}/\partial t = 0$) we can write

$$\frac{\partial\overline{U\Gamma}}{\partial x} + \frac{\partial\overline{V\Gamma}}{\partial y} + \frac{\partial\overline{W\Gamma}}{\partial z} = \kappa\left(\frac{\partial^2\overline{\Gamma}}{\partial x^2} + \frac{\partial^2\overline{\Gamma}}{\partial y^2} + \frac{\partial^2\overline{\Gamma}}{\partial z^2}\right) - \left(\frac{\partial\overline{u\gamma}}{\partial x} + \frac{\partial\overline{v\gamma}}{\partial y} + \frac{\partial\overline{w\gamma}}{\partial z}\right). \qquad 8$$

The LHS is the mean convection and the RHS consists of two terms: molecular diffusion due to mean concentration gradients and turbulent transport.

Recently, Chatwin and Sullivan (1990) obtained a universal expression for the moments of the probability density function (pdf) of the concentration in self-similar turbulent flows such as jets, wakes, boundary layers and plumes. This work was later extended to non-self-similar flows, see Chatwin, Sullivan and Yip (1990). These moments could then be used to find the shape of the pdf using the maximum entropy as shown by Derksen and Sullivan (1990).

The expression for all of the asymptotic moments of the pdf for self-similar turbulent flows as given by Chatwin and Sullivan (1990) is

$$\overline{c^n} = \beta^n \frac{C_0^n}{\alpha}[Z(\alpha - Z)^n + (-1)^n(\alpha - Z)Z^n], \qquad 9$$

where $Z = C / C_0$, is the ratio of local mean concentration (C) to the maximum mean concentration (C_0). The mean and higher central moments are defined as,

$$C = \overline{\Gamma} = \int_0^\infty \theta \; p(\theta) \, d\theta , \qquad 10$$

and

$$\overline{c^n} = \overline{(\Gamma - C)^n} = \int_0^\infty (\theta - C)^n \; p(\theta) \, d\theta . \qquad 11$$

where $p(\theta)$ is the probability density function (pdf) of the instantaneous contaminant concentration, Γ (i.e., $p(\theta) = \text{prob}\{ \theta < \Gamma < \theta + d\theta \}$). The ranges of the two parameters α and β that appear in Eq. 9 are relatively narrow (i.e., $1 \leq \alpha \leq 1.5$ and $0.1 \leq \beta \leq 0.75$).

For non-self-similar flows, Eq. 9 is still valid if we allow the α and β to be slowly varying functions of downstream distance (or time for unsteady flow),

as shown by Sullivan and Yip (1988) and Chatwin, Sullivan and Yip (1990). A further study by Moseley (1991) has shown that the α value determines the modality of the mean-square fluctuation. A value between 1 and 2 implies a bimodal distribution, while $\alpha > 2$ denotes a unimodal distribution. The β value determines the magnitude of the mean-square fluctuation.

In turbulence, it is very common that more unknowns exit than equations. This lack of equations creates the need to impose conditions, often empirically, to effect closure. However, a further consequence of the above is that it leads to a very simple closure hypothesis (i.e., in a scheme the number of unknowns is equal to the number of equations).

Because complete mixing between two fluids can only take place through molecular diffusivity κ, let us begin with the convective-diffusion equation (Eq.4) to discuss closure hypothesis. Equation 4 can be used to derive an equation for the higher moments, which is

$$\frac{\partial}{\partial t} c_{n+1} + \nabla \cdot \overline{(U\Gamma^{n+1})} = \kappa \nabla^2 c_{n+1} - n(n+1)\,\kappa\, \overline{\Gamma^{n-1}(\nabla\Gamma)\cdot(\nabla\Gamma)}. \qquad 12$$

where the overbar denotes an ensemble average and the higher moments are defined as

$$c_n = \overline{\Gamma^n} = \int_0^\infty \theta^n\, p(\theta)\, d\theta\,. \qquad 13$$

Integration over all space (a.s.) of Eq. 12 results in

$$\frac{\partial}{\partial t} \int_{a.s.} \overline{\Gamma^{n+1}} dV = -n(n+1)\,\kappa \int_{a.s.} \overline{\Gamma^{n-1}(\nabla\Gamma)^2} dV\,, \qquad n \geq 1\,. \qquad 14$$

A simple, physically based closure approximation given by Moseley (1991) is

$$(\nabla\Gamma)^2 = A\frac{(\Gamma - C)^2}{\lambda^2(t)}. \qquad 15$$

Where A is a closure constant which can be estimated using experimental data, and the conduction cut-off length λ is given by

$$\lambda = (\frac{\nu\kappa^2}{\varepsilon})^{\frac{1}{4}}, \qquad 16$$

where ν is the kinematic viscosity and ε is the dissipation rate of turbulent kinetic energy. It is believed that λ (10^{-3} to 10^{-4} m in most flows) is the smallest length-scale associated with the diffusion of a contaminant within a turbulent fluid.

Let $(\nabla\Gamma)^2$ in Eq. 14 be replace with Eq. 15, we then have

$$\frac{\partial}{\partial t}\int_{a.s.}\overline{\Gamma^{n+1}}dV = -n(n+1)\,\kappa\, A\int_{a.s.}\frac{\overline{\Gamma^{n-1}(\Gamma - C)^2}}{\lambda^2}dV\,, \qquad n \geq 1\,. \qquad 17$$

Thus a closure scheme for a non-self-similar flow is complete.

Besides the successful approach described above, there is another remarkable approach obtained by Derksen and Sullivan (1990) - the maximum entropy formulation for approximating a pdf. This method is based upon the maximization of an integral of the pdf. Briefly, the entropy of a pdf is defined as

$$H = -\int_a^b p(\theta)\,\ln(p(\theta))\,d\theta\,, \qquad 18$$

where H is the entropy of the pdf $p(\theta)$, a and b are the two limits that bound the random variable, θ. The constraints are the first few moments which are given by

$$c_i = \int_a^b \theta^i \, p(\theta) \, d\theta . \qquad 19$$

The order of the moments would be between 0 and some finite value n. The solution of the Euler-Lagrange equation for the variational problem posed by Eq. 18 is

$$p(\theta) = \exp\left(\sum_{i=0}^{n} \lambda_i \theta^i \right), \qquad 20$$

where the n constants λ_i appearing in Eq. 20 satisfy the constraints given by Eq.19. The Gaussian solution is obtained analytically when n = 2. When n > 2, a numerical solution for the constants is required. In practice a Newton-Raphson method was used to evaluate the λ_i in Eq.20 using Eq.19 with starting values of $\lambda_i = 0$ and integrals computed using Simpson's rule.

In conclusion, the above theoretical research results are important, either in a self-similar or non-self-similar turbulent flow. Once the α and β values are obtained through a complete closure scheme, we can get the lower order central moments of the concentration from Eq.9. Then, using the maximum entropy method to approximate the pdf of the turbulent contaminate fluctuation, we can estimate the range of concentration values. However, these hypotheses require further extensive and accurate experimental data for verification.

The fluctuations in the concentration of a passive scalar (e.g., a neutral density contaminant, such as temperature, dye, foreign gas) have been investigated

in many experimental programs. But basically only four different types of flow / source scenario can be identified:

(i) Laboratory (wind tunnel) tests with continuous release (e.g., experiments in grid turbulence with a line source by Stapountzis et al. [1986] and with two line sources by Warhaft [1984]; experiments with a line source in a uniformly sheared turbulent flow by Karnik and Tavoularis [1989] and in a plane turbulent wake by LaRue and Libby [1974]).

(ii) Laboratory (wind tunnel) tests with instantaneous release (e.g., research on dispersion by injecting "marked fluid" into an open channel flow, see Sullivan [1971a]).

(iii) Large-scale trials with continuous release (e.g., experiments with dye plumes in Lake Huron, see Sullivan [1971b] and Chatwin and Sullivan [1979]).

(iv) Large-scale trials with instantaneous release (e.g., research on dense-gas dispersion in the atmospheric boundary layer, see Picknett [1981]).

A laboratory test usually focuses on a specific mixing process in an idealized flow with a smaller test range while a large-scale trial focuses on a whole mixing process in nature (e.g., lake, river, sea and ocean etc.) with a larger test range. The present work belongs to a laboratory test with a continuous release source. Measurements were made of the thermal wake created by a heated circular cylinder mounted along a diameter of a pipe, in a fully-developed turbulent pipe flow. A pipe flow is fully-developed when the profile of mean velocity is independent of the downstream distance. However, it should be noted that in our case the profile of the mean velocity varied with the downstream distance because

of the mounted cylinder. Heat was chosen instead of a contaminant concentration as both quantities are analogs of each other, and as temperature is more easily measured than contaminate concentration. The statistics of interest are the pdf and its moments.

CHAPTER II

EQUIPMENT AND PROCEDURE

During the course of this research, all experiments were carried out in the Turbulence Laboratory of the Department of Mechanical and Industrial Engineering, at the University of Manitoba. Measurements included: mean velocity and r.m.s. velocity; mean temperature and r.m.s. temperature; higher moments of temperature and the pdf of the temperature. The experimental equipment and the measurement procedures are briefly described in this chapter.

2.1 The Wind Tunnel and its Calibration

All the experiments were performed in a straight, open return tunnel. The general layout of the wind tunnel is shown in Figure 1. The wind tunnel is described briefly in what follows (see Derksen [1986] for more detail).

Air was drawn into the tunnel through a large radial flow fan driven by a 25 hp DC electric motor with a continuously variable speed control. Its inlet was a 1.0 m circular opening, coaxial with the fan axis with adjustable guide vanes, and its outlet was a 33.0 cm by 70.0 cm rectangular discharge.

Flow conditioning was obtained by use of the rectangular to circular diffuser, settling chamber and contraction cone. A rectangular to circular diffuser of overall length 2.1 m followed the fan. There were guide vanes installed inside this section to straighten and condition the flow from the fan. The settling chamber (2.2 m long) was a heavy sheet metal circular tube, which contains 3 sets of copper

screens used to breakup any residual flow structures from the fan. The contraction cone (area ratio, 89:1, length 1.45 m) was made of a stack of plywood rings, constructed to form a smooth curved surface. The flow rate was measured and monitored using the static pressure drop across the contraction cone. This pressure drop was measured using a Trimount inclined manometer, calibrated in inches of water. The manometer range was from 0.00 in.H_2O to 8.00 in.H_2O in divisions of 0.02 in.H_2O.

A vibration isolator was used to reduce fan and motor vibration that could be transmitted along the tunnel. The flow was tripped using a sandpaper trip which was used to force transition to turbulent flow immediately.

The pipe section was composed of two straight steel pipes with a smooth inside surface. They were supported by wheeled jack posts and connected butt to butt. The first one was 2.05 m long and the second one was 4.05 m long. Their internal diameter was 10.16 cm.

The test section is shown in Figure 2. It was composed of a 1.83 m long plastic pipe with 10.16 cm internal diameter. There were three sets of holes in the surface of the pipe which were used for holding the heated filament. The holes were located 40, 70 and 100 cm from the outlet, so it was possible to move the filament between these three positions in order to get the measurement distance from 0 cm to 100 cm (from the probe to the filament). A power supply was used to heat the cylindrical filament which was 6 mm diameter and 10 cm long. The power supply could supply up to 75 w. The traversing mechanism at the outlet of the test section consisted of a two-axis rotatable milling table.

Before the experiments were performed, the wind tunnel had been calibrated. First the dynamic pressure, on the pipe centerline, was measured using a pitot tube and a Betz manometer. The data is plotted in Figure 3, where it can be seen that from 0.2 in.H_2O to 4 in.H_2O of contraction cone pressure drop, the dynamic pressure was linear on cone pressure. The linear approximation to this line is given by

$$P_{dyn} = 22.547 \Delta P_{cone} + 0.012 \qquad 21$$

where P_{dyn} is dynamic pressure and ΔP_{cone} is contraction cone pressure drop. A velocity calibration curve plotted in Figure 4 was obtained on the basis of Bernoulli's equation for ideal incompressible flow ($U_{ref} \propto \sqrt{\Delta P_{cone} / \rho}$, where U_{ref} is the mean axial centerline velocity [reference velocity], and ρ is air density). From the calibration curve, we can see that ΔP_{cone} =2.0 in.H_2O yields a U_{ref} =27.5 m/s. The Reynolds number based on this reference velocity and the pipe diameter is 180,000 (or 11,000 based on the filament diameter). It should be noted that all the measurements discussed later were carried out at this Reynolds number.

2.2 The Velocity Measurement Instruments

The measurements of $\overline{U}$ (mean velocity) were made using both pitot tube and hot-wire. The reasoning for repeating these measurements is to have some means to check on the quality of the measurements. If the mean velocity distribution for the hot-wire matches the pitot tube results, then the u' (r.m.s. of the fluctuating velocity) should match too.

First the distributions of $\overline{U}$ were obtained through measuring the static pressure and total pressure. The instruments used for pressure measurements were:

a static pressure tube of 1.2 mm outer diameter (United Sensor, U.S.A., USC-E-120-04); a pitot tube of 1.2 mm outer diameter (United Sensor, U.S.A., USC-E-120-03). The pressure was measured using a Betz manometer with a range of -17 to 400 mm H_2O with an accuracy of $\pm$0.05 mm H_2O, and a MKS BARATRON type 223B pressure transducer (0 to 10 mm Hg range, 0.01% F.S. accuracy). The measurements were made at 13 locations (from 16.7 to 166.7 filament diameters downstream of the unheated cylinder). In the cross-stream direction, the measurements were made from 6 mm to 82 mm in 4 mm increments. The pitot tube and Betz manometer were used in all 13 locations while the BARATRON was used at only 2 of 13 locations. The BARATRON was also used for checking on the quality of the measurements. The difference between these two sets is negligible (within 0.5%). The velocity measurement error is estimated at $\pm$0.1% due to the pressure fluctuation .

Then the measurements of $\overline{U}$ and u' were made with an Auspect probe type ASPS-100 (approx. 1 mm long, 5 μm diameter). The electronic equipment included a constant temperature anemometer, DISA 55M10 standard bridge and a 55M01 main unit ; a linearizer, DISA 55M25; an r.m.s. meter, DISA 55D35; a digital voltmeter, DISA 55D31; and a Telequipment oscilloscope type D1011. The DISA 55D90 calibration stand used for the calibration of the anemometer system included a pressure control unit, DISA 55D44; a nozzle unit, DISA 55D45; and a pressure converter, DISA 55D46. A x-y recorder was also used for the calibration of the anemometer system. The measurements were made at the same positions as those of the pressure measurements.

The main steps of hot-wire calibration procedure included:

(1) **selecting and installing cables**: checking the cable length and selecting several cables of the proper length for connecting the instruments;

(2) **initial settings of controls**: plugging 55M10 standard bridge into 55M01 main unit, checking the initial settings as described in menu;

(3) **applying power**: allowed sufficient warm-up time before beginning any measurement;

(4) **measurement of probe resistance**: measuring the probe cold resistance at room temperature;

(5) **calculation and adjustment of overheating ratio**: calculating the probe hot resistance by

$$R = R_0(1 + a) \qquad 22$$

where R is probe hot resistance, R_0 is probe cold resistance at ambient temperature, and a is overheating ratio selected as 0.5;

(6) **setting up type 55D90 calibration equipment**: calculating the primary pressure and nozzle pressure, using them to adjust the flow speed;

(7) **electronic linearization**: adjusting the 55M25 linearizer to obtain an output voltage proportional to the flow velocity;

The basic principle of a electronic linearization is given below:

The relation between flow velocity U and anemometer output voltage V_{CTA} can be expressed by King's Law

$$V_{CTA}^2 = A + BU^n = A + BU^{\frac{1}{m}}. \qquad 23$$

A and B are constants whose value depend on the probe used. The 55M25 linearizer is , basically, an electronic analog computer which linearizes the anemometer output voltage with the aid of the function

$$V_{LIN} = K(V_{CTA}^2 - A)^m . \qquad 24$$

K is a constant depending on the conditions of measurements. Let V_{CTA}^2 in Eq.24 be replace by Eq.23. Thus

$$V_{LIN} = K(BU^{\frac{1}{m}})^m = KB^{\frac{1}{m}}U = kU \qquad 25$$

The linearizer output voltage is therefore proportional to the flow velocity U.

(8) **calibration curve**: plotting a calibration curve using the x-y recorder and the type 55D90 calibration equipment.

The DISA 55M25 linearizer was accuracy to around 1% in our measurement range.

2.3 The Temperature Measurement Instruments

The temperature measurements were made with a DANTEC 55P31 resistance thermometer probe (0.4 mm long, 1 μm - dia., platinum wire). Besides the instruments which are already mentioned above, others included are: a DANTEC temperature bridge type 55M20; a DISA signal conditioner type 55D26. The probe was calibrated using a hot-air blow dryer and a mercury thermometer.

Some steps of the cold wire calibration were similar to those of the hot-wire calibration. The five main steps were:

(1) **compensating of lead resistance**

(2) **selection of probe current**

(3) **determining temperature coefficient**: measuring probe resistance at ambient temperature; heating probe by known temperature difference (e.g., 50°C); measuring probe resistance at that temperature; calculating temperature coefficient from the following formula

$$\alpha_0 = \frac{\Delta R \times 100}{\Delta T \times R_0} \quad (\% \text{ per } ^\circ\text{C}). \tag{26}$$

(4) **determining decade resistance change for given temperature change**: calculating decade resistance change (comparison resistance) for temperature range under consideration, using the formula

$$\Delta R_C = -\Delta R \frac{R + R_T}{R + R_T + \Delta R} \tag{27}$$

where R_T is a bridge resistance (i.e., 50Ω), and ΔR_C is the comparison resistance.

(5) **adjustment of gain and output voltage**

Before beginning the temperature measurements, the cylinder was electrically heated using heater wire. A DC power supply was adjusted so that a fixed amount of power was dissipated for each experiment.

The measurements of $\overline{T}$ (mean temperature) and θ' (r.m.s. of the fluctuating temperature) were made at the same 13 locations as those of velocity measurements. But in the cross-stream direction, the measurement locations were from 5 mm to 95 mm in 3 (or 4) mm increments.

2.4 Data Acquisition

For data acquisition, an IBM XT computer with a DAS-1602 12 bit data acquisition board was used. The board was supported by the software package STREAMER. It allows data to be collected at up to 99 kHz. All data was collected at 50 kHz, collecting 350,000 samples per record (7 seconds). Measurements were made at the same 13 locations as those mentioned above, in the cross-stream direction, the range was from 20 mm to 50 mm in 5 mm increments. Finally, the pdf and higher moments were calculated from the digital data.

CHAPTER III

RESULTS AND DISCUSSION

3.1 The Velocity Field

All velocity measurements were performed in the unheated flow since the heating effect on the velocity field was negligible. The transverse distributions of the mean and r.m.s. fluctuating velocity profiles at six downstream stations are shown in Figure 5 and Figure 6, respectively. It can be seen that both the distributions of mean velocity and r.m.s. fluctuating velocity are, as to be expected, nearly symmetric. For the mean velocity profiles, distinct double peaks can be found. The peak value decreases with downstream distance. For the r.m.s. fluctuating velocity profiles, near the source, the distributions have one peak on the symmetry axis. In the cross-stream direction, the values decrease with the distance away from the centerline until reaching 26 mm (i.e. r/d = $\pm$ 4.33) after that the values increase again in the near wall region of the pipe. For the positions farther downstream than 50 diameters of the cylinder the peaks are no longer distinct. All these profiles are non-dimensional profiles, the mean and r.m.s fluctuating velocity have been normalized by the reference velocity U_{ref} and the distance has been normalized by the diameter of the cylinder d.

The downstream development of the mean and r.m.s. fluctuating velocity along the pipe centerline are presented in Figure 7 and Figure 8 , respectively. The centerline mean velocity $\overline{U}_c$ increases with the downstream distance whereas

the centerline r.m.s. fluctuating velocity u_c' decreases with the downstream distance.

The transverse distributions of mean velocity obtained by using both hot-wire and pitot tube are presented from Figure 9 to Figure 15. It can be seen that they nearly match each other. The maximum absolute error is 11.5%. At most measured points the absolute errors are less than 4%. In Figure 7 to Figure 15, the data have been normalized by the same parameters as in Figure 5 and Figure 6.

3.2 The Temperature Field

The characteristics of the thermal wake are presented here. First the mean temperature distributions and r.m.s. temperature fluctuation distributions are presented. Then the development of the wake width is discussed. Finally, the location of the virtual origin of the self-preserving wake is indicated and the characteristics of self-preservation are discussed.

Figure 16 shows the transverse distributions of the mean temperature rise $\Delta\overline{T}$ ($= \overline{T} - \overline{T}_{min}$; $\overline{T}$ is the mean temperature, $\overline{T}_{min}$ is the lowest value of the mean temperature at that transverse location) which has been normalized by the corresponding centerline mean temperature rise $\Delta\overline{T}_c$ ($= \overline{T}_c - \overline{T}_{min}$; $\overline{T}_c$ is the corresponding centerline mean temperature). The distance has been normalized by the half-width of the wake, w, defined as half the distance between the points having a temperature rise which is 50% of the peak value $\Delta\overline{T}_p$. The same profiles are also presented from Figure 17 to Figure 22 where Gaussian distributions have been used to fit these curves, the regression coefficients

change from 0.94 to 0.97 at six downstream stations and the average is 0.96. The nearly Gaussian distribution of mean temperature, in the downstream stations, is in conformity with the findings of Stapountzis and Britter (1987) and Karnik and Tavoularis (1989). It can be seen that the profiles are nearly symmetric and the peaks are on the axis.

Figure 23 shows the downstream decrease of the centerline mean temperature rise $\Delta\overline{T}_c^*$ ($= \overline{T}_c - T_a$; T_a is the ambient temperature) which is normalized by the maximum mean temperature rise $\Delta\overline{T}_{max}^*$ ($= \overline{T}_{max} - T_a$; $\overline{T}_{max}$ is the maximum value of the mean temperature in the present measurement). The distance has been normalized by the diameter of the cylinder d.

Figure 24 presents the points with mean temperature rise $\Delta\overline{T}$ at a particular fraction of the centerline mean temperature rise $\Delta\overline{T}_c$. From this profile, it can be seen that the virtual origin is at a position upstream of the cylinder (as the curves do not extrapolate to the origin) and the wake width increases with the downstream distance. Further discussion on these two aspects will be provided later.

Figure 25 shows the non-dimensional transverse distributions of the r.m.s. temperature fluctuation θ' at six downstream locations where the transverse positions have been normalized with the half-width of the wake w and the r.m.s. temperature fluctuations have been normalized with the corresponding centerline r.m.s. temperature fluctuation θ_c'. The profiles exhibit distinct double peaks at all six transverse stations and they are nearly symmetric to the centerline. Double peaks have also been observed in the uniformly sheared turbulent flow experiments of Karnik and Tavoularis (1989). In their profiles, the two peaks are

not symmetric. The peak on the high velocity side is greater than that on the low velocity side, hence the reason causing this asymmetric is evident. A possible explanation of the appearance of the double peaks in the temperature fluctuation profiles is given by Karnik and Tavoularis (1989) as: temperature fluctuations are produced "locally" in regions of non-zero mean temperature gradient as well as transported from neighboring regions by turbulent eddies so that at locations of peak mean temperature the local production can not be the source of the temperature fluctuations (if one neglected production by the weak streamwise mean temperature gradient $\partial \overline{T} / \partial x$). In this case the only source of the temperature fluctuations is transport by the turbulent eddies originating in regions with non-zero $\partial \overline{T} / \partial y$ (or $\partial \overline{T} / \partial r$). Therefore at the locations of peak mean temperature the temperature fluctuations are lower than those at neighboring locations.

Figure 26 shows the downstream decrease of the centerline r.m.s. temperature fluctuation θ_c' normalized by the maximum value of mean temperature rise $\Delta\overline{T}^*_{max}$.

Self-preservation (or self-similar) means that there exist appropriate local scaling parameters such that the distribution of velocity and temperature can be made invariant. Let us define l as the local length scale and U_s as the maximum value of $| U_0 - U |$, where U_0 is a scale for the velocity of the mean flow in the x direction (in our case, l = w and $U_0 = U_{ref}$). For a two-dimensional flow, Tennekes and Lumley's (1972) conclusion is that self-preservation is possible only if the velocity and length scales behave as

$$U_s = A(x - x_0)^{-\frac{1}{2}} \quad ; \qquad l = B(x - x_0)^{\frac{1}{2}}, \tag{28}$$

Where x_0 is the virtual origin, A and B are constants which can be determined by

$$A = 1.58U_0 h^{\frac{1}{2}} \quad ; \qquad B = 0.252 h^{\frac{1}{2}}, \tag{29}$$

where h is the momentum thickness of the wake defined by

$$h = \int_{-\infty}^{\infty} \frac{U}{U_0} (1 - \frac{U}{U_0}) dy . \tag{30}$$

The relationship between the momentum thickness and the drag coefficient of the obstacle that produces the wake is

$$C_d = \frac{2h}{d}. \tag{31}$$

If the obstacle is a circular cylinder, for Reynolds numbers between 10^3 and 3×10^5 , $C_d \sim 1$, so that h is about $\frac{1}{2}$d in that range.

Thus we have

$$A = 1.12 U_0 d^{\frac{1}{2}} \quad ; \qquad B = 0.178 d^{\frac{1}{2}} . \tag{32}$$

Finally we obtain

$$U_s = 1.12 U_0 [d / (x - x_0)]^{\frac{1}{2}} \quad ; \qquad l = 0.178 [d (x - x_0)]^{\frac{1}{2}}. \tag{33}$$

Many experiments have been done to determine whether or not Eq. 28 is correct. As early as in 1948, Townsend (1948) conducted detailed measurements of the wake of unheated and heated cylinders. His results indicate that the

development of l and U_s is well described by Eq. 28 for $(x - x_0) / d > 100$ while the more complicated statistical quantities of turbulence such as the intermittence factor, velocity intensity, and the kinetic energy are self-preserving for $(x - x_0) / d > 500$ at Reynolds numbers greater than 860 based on the free stream velocity and cylinder diameter.

The present measurements were performed from x=10 cm to x=100 cm downstream of the cylinder. From Figure 27 it can be seen that the virtual origin is at -5.4 diam, i.e. at 5.4 diam upstream of the cylinder. At x=60 cm we have $(x - x_0) / d \geq 100$ so those previous results imply that part of the present data ($x < 60$ cm) should correspond to the non-self-similar portion of the turbulent wake while the rest ($x \geq 60$ cm) should correspond to the self-similar portion of the turbulent wake. The present data should not be interpreted as self-similar. The data does not fit Eq. 33. However, it can be seen that in Figure 27 from 16.7 to 50 filament diameters downstream of the cylinder the half-width of the wake normalized by the diameter of cylinder is almost linear with the square root of the downstream distance normalized by the same scale. In Figures 5, 16 and 25 (for profiles of $x \geq 25$ cm) these profiles seem to show similar distributions. Hence we can conclude that the temperature distributions are self-similar in the later stages of our flow, although the experimental data does not fit Eq. 33.

3.3 Statistical Characteristics of the Flow

In order to understand the mixing process, we describe the statistical characteristics of turbulent flow using the pdf of the temperature and as well as the third and fourth order moment distributions.

Figure 28 shows the transverse distributions of the skewness at five downstream locations. It is very obvious that the skewness increases with distance from the centerline and near the centerline area, even far downstream, the skewness values are very low. So this implies that the turbulence was very well mixed at that area. At the locations off the centerline , the skewness decreases in magnitude slightly with distance from the heat source. At 100 filament diameters downstream of the cylinder, the transverse distribution of skewness is quite uniform, there is no big difference from centerline to 5 filament diameters from the centerline (see Table 6[b]). The measured maximum value of the skewness appears at the location near the cylinder but off the centerline. It implies that the turbulence was not well mixed at that place. From Table 6(b), both positive and negative values of skewness can be found. A possible explanation is that the negative temperature fluctuation skewness could be attributed to the effect of negative fluctuations in the signal due to "cold" fluid, while the positive temperature fluctuation skewness would be attributed to the effect of positive fluctuation in the signal due to "hot" fluid.

Figure 29 shows the transverse distributions of the flatness at five downstream stations. Close to the centerline, the low value of flatness can be observed in all the locations downstream of the cylinder. Off the centerline, the flatness decreases in magnitude with distance from the source. This is consistent with the conclusion obtained from the skewness that in the region near the source, off the centerline, the turbulence was not mixed as well as in other positions. This is also compatible with the observation in the previously related research by LaRue and Libby (1974).

Figure 30 to Figure 53 show the pdfs of the temperature at seven downstream and four transverse locations, respectively. The solid smooth lines represent the pdf calculated using the maximum entropy formula whereas the symbols of the open circle represent the data obtained from the present experiment. It should be noted that the calculated pdf is in very good agreement with the measured data. Thus it once more proves that the maximum entropy method is a very effective method to approximate the pdf of a turbulent contaminate fluctuation when only the fourth and the lower order moments are known. Comparing the profiles of the pdfs near the centerline with that off the centerline, one can find that different deviation levels from a Gaussian distribution exist. At the locations near the centerline, the profiles are nearly Gaussian whereas at the locations off the centerline, the profiles show that non-Gaussian distributions exist and that is also consistent with their relatively high values of skewness.

CHAPTER IV
CONCLUSIONS

The results of the present work can be summarized as follows:

a) The transverse distributions of mean velocity, r.m.s. fluctuating velocity and mean temperature as well as r.m.s. fluctuating temperature are all nearly symmetric.

b) Although the data do not fit the formulas for self-similar flow, the non-dimensional profiles of the velocity and temperature show that the flow is a self-similar flow in its later stages.

c) The profiles of the pdf of the temperature show that both nearly Gaussian and non-Gaussian distributions exist.

d) Derksen and Sullivan's maximum entropy method is a very effective method to approximate the pdf of a turbulent contaminate fluctuation when only the fourth and lower order moments are known.

REFERENCES

Alexopoulos, C.C., and Keffer, J.F., 1971: "Turbulent Wake in a Passively Field", Phys. Fluids, Vol. 14, No. 2, pp. 216-224.

Chatwin, P.C. and Sullivan, P.J., 1979: "Measurements of Concentration Fluctuations in Relative Turbulent Diffusion", J. Fluid Mech. Vol. 94, Part 1. pp. 83-101.

Chatwin, P.C. and Sullivan, P.J., 1985: "Effects of Instrumentation and Averaging on Turbulent Diffusion Data", 5th Symposium on Turbulent Shear Flows, New York.

Chatwin, P.C., Sullivan, P.J. and Yip, H., 1990: "Dilution and Marked Fluid Particle Analysis", Proc. Int. Conf. on Physical Modeling of Transport and Diffusion.

Chatwin, P.C. and Sullivan, P.J., 1990: "A Simple and Unifying Physical Interpretation of Scalar Fluctuation Measurements from Many Turbulent Shear Flows", J. Fluid Mech. Vol. 212, pp. 533-556.

Csanady, G.T., 1973: "Turbulent Diffusion in the Environment", D. Reidel Publishing Company.

Derksen, R.W., 1981: "The Response of Hot-Wire of Finite Length to Fine-Scale Structure in a Turbulent Flow", M.Sc. Thesis, The University of Manitoba.

Derksen, R.W., 1986: "An Experimental Investigation of the Fluctuating Wall Shear Stresses in an eight Degree Conical Diffuser", Ph.D. Thesis, The University of Manitoba.

Derksen, R.W. and Sullivan, P.J., 1990: "Moment Approximations for Probability Density Functions", Combust. Flame, Vol. 81, pp. 378-391.

Derksen, R.W., Sullivan, P.J. and Yip, H., 1994: "The Asymptotic Probability Density Function of a Scalar", A.I.A.A. Journal, Vol. 31, No. 5, pp. 1083-1084.

Freymuth, P and Uberoi, M.S., 1971, :"Structure of Temperature Fluctuations in the Turbulent Wake behind a Heated Cylinder", Phys. Fluids. Vol. 14. No. 12. pp. 2574-2580.

George, W. K. and Arndt, R., 1989: "Advances in Turbulence", Springer-Verlag.

Hinze, J.O., 1975: "Turbulence", 2nd ed., McGraw Hill.

Karnik, U. and Tavoularis, S. 1989: "Measurements of Heat Diffusion from a Continuous Line Source in a Uniformly Sheared Turbulent Flow", J. Fluid Mech. Vol. 202, pp. 233-261.

LaRue, J.C. and Libby, P.A., 1974: "Temperature Fluctuations in the Plane Turbulent Wake", The Physics of Fluids, Vol. 17, No. 11, pp. 1956-1967.

Monin, A.S., and Yaglom, A.M. 1971: "Statistical Fluid Mechanics: Mechanics of Turbulence", Vol. 1, The MIT Press.

Monin, A.S., and Yaglom, A.M. 1971: "Statistical Fluid Mechanics: Mechanics of Turbulence", Vol. 2, The MIT Press.

Moseley, D.J., 1991: "A Closure Hypothesis for Contaminant Fluctuations in Turbulent Flow", M.Sc. Thesis, University of Western Ontario.

Picknett, R.G., 1981: "Dispersion of Dense Gas Puffs Released in the Atmosphere at Ground level", Atm. Envir. Vol. 15, pp. 509-515

Stapountzis, H., Sawford, L., Hunt, J.C.R. and Britter, R.E., 1986: "Structure of the Temperature Field downwind of Line Source in Grid Turbulence", J. Fluid Mech. Vol. 165, pp. 401-424.

Stapountzis, H. and Britter, R.E., 1987: "Turbulent Diffusion behind a Heated Line Source in a Nearly Homogeneous Turbulent Shear Flow", Proc. Sixth Symp. on Turbulent Shear Flows, Springer-Verlag. pp. 97-108.

Sullivan, P.J., 1971a: "Longitudinal Dispersion within a Two-dimensional Turbulent Shear Flow", J. Fluid Mech. Vol. 49, Part 3, pp. 551-576.

Sullivan, P.J., 1971b: "Some Data on the Distance-neighbor Function for Relative Diffusion", J. Fluid Mech. Vol. 47, Part 3, pp. 601-607.

Sullivan, P.J., 1976: "Dispersion of a Line Source in Grid Turbulence", The Physics of Fluids, Vol. 19, No. 1. pp. 159-162.

Sullivan, P.J. and Yip, H., 1988: "An Approach for Predicting Some Statistics Relevant to Contaminant Spread in the Atmospheric Boundary Layer, Continuum Mechanics on its Applications", Proc. Conf. Simon Fraser University.

Tavoularis, S. and Corrsin, S. 1981a: "Experiment in a Nearly Homogeneous Shear Flow with a Uniform Mean Temperature Gradient. Part 1." J. Fluid Mech. Vol. 104, pp. 311-348.

Tavoularis, S. and Corrsin, S. 1981b: "Experiment in a Nearly Homogeneous Shear Flow with a Uniform Mean Temperature Gradient. Part 2." J. Fluid Mech. Vol. 104, pp. 349-367.

Taylor, G.L., 1921: "Diffusion by Continuous Movements", Proc. Lond. Math. Soc. Vol. A20, pp. 196-212.

Tennekes, H. and Lumley, J.L., 1972: "A First Course in Turbulence", The MIT Press.

Townsend, A.A., 1948, Aust. J. Sci. Res., Vol. A1, pp. 161.

Venkataramani, K.S. and Chevray, R., 1978: "Statistical Features of Heat Transfer in Grid-generated Turbulence: Constant-gradient Case", J. Fluid Mech. Vol. 86, Part 3, pp. 513-543.

Warhaft, Z., 1984: "The Interference of Thermal Fields from Line Sources in Grid Turbulence", J. Fluid. Mech. Vol. 144, pp. 363-387.

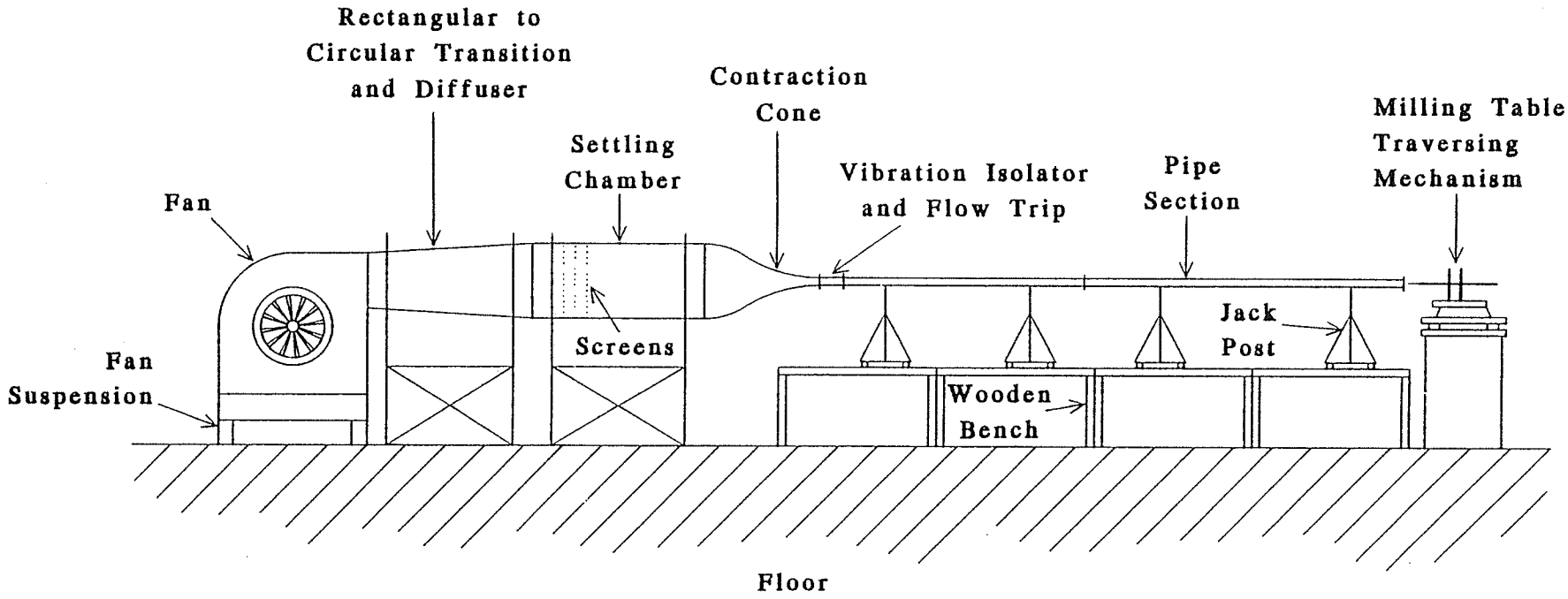

Figure 1. The general layout of the wind tunnel.

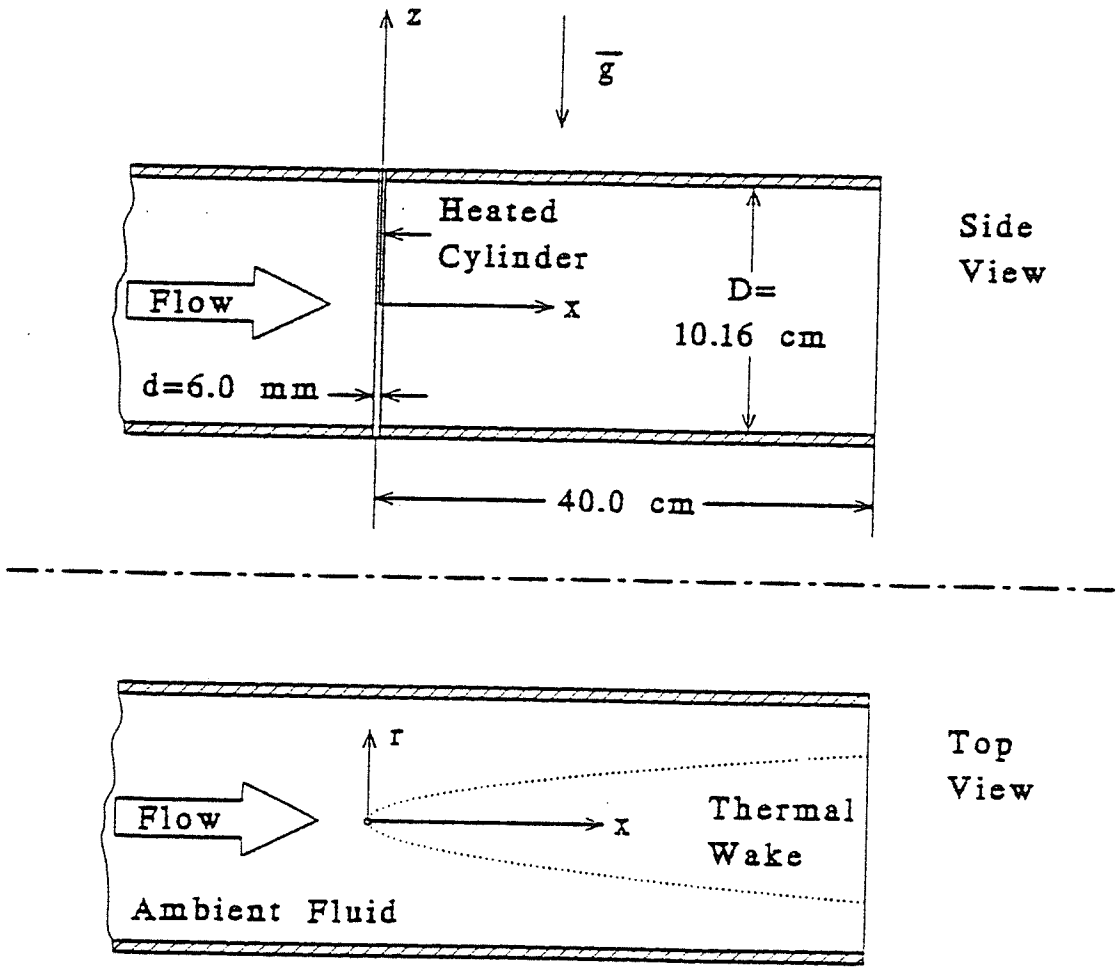

Figure 2. Sketch of the wind-tunnel test section.

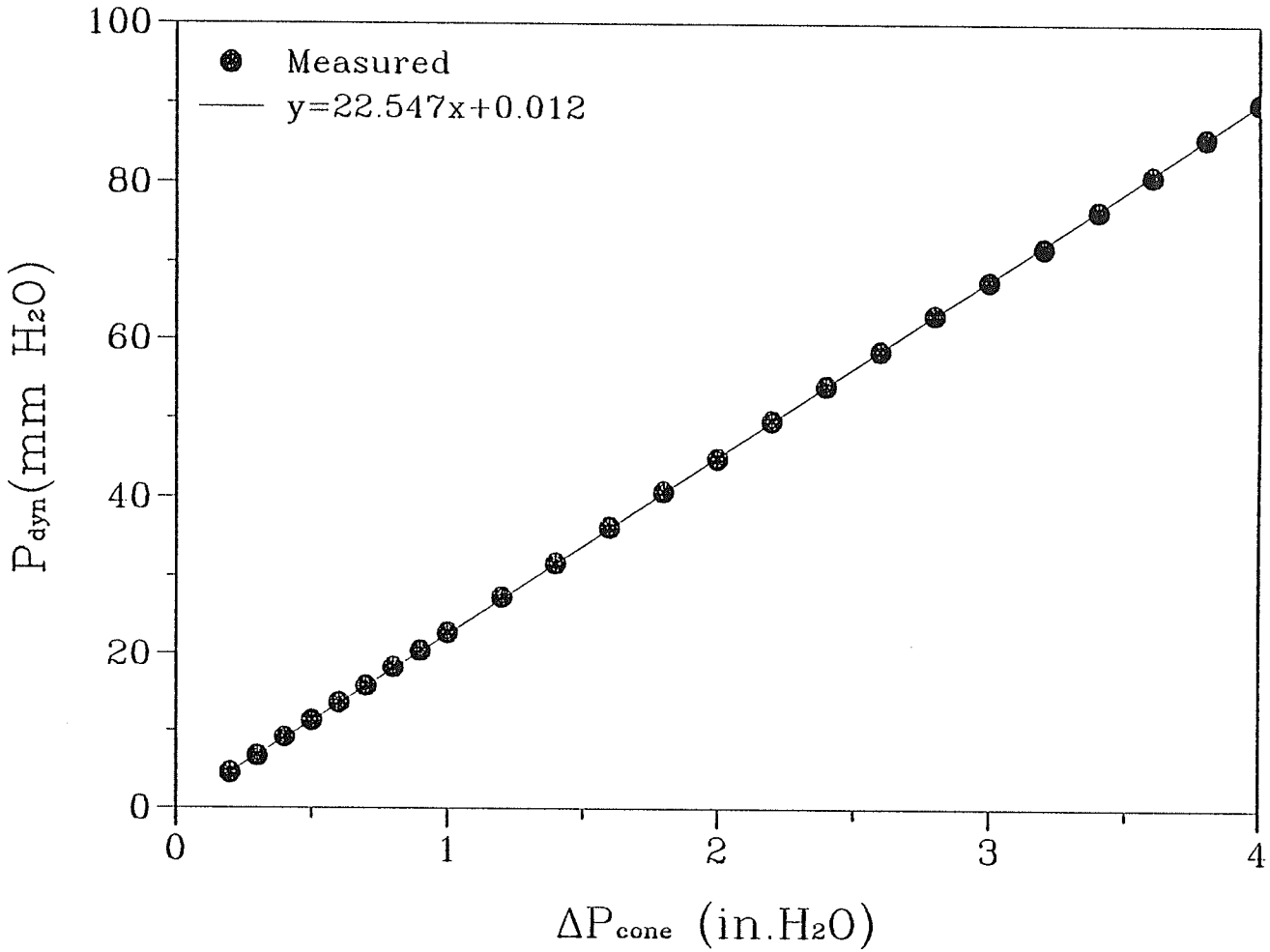

Figure 3. Tunnel calibration curve (centerline dynamic pressure).

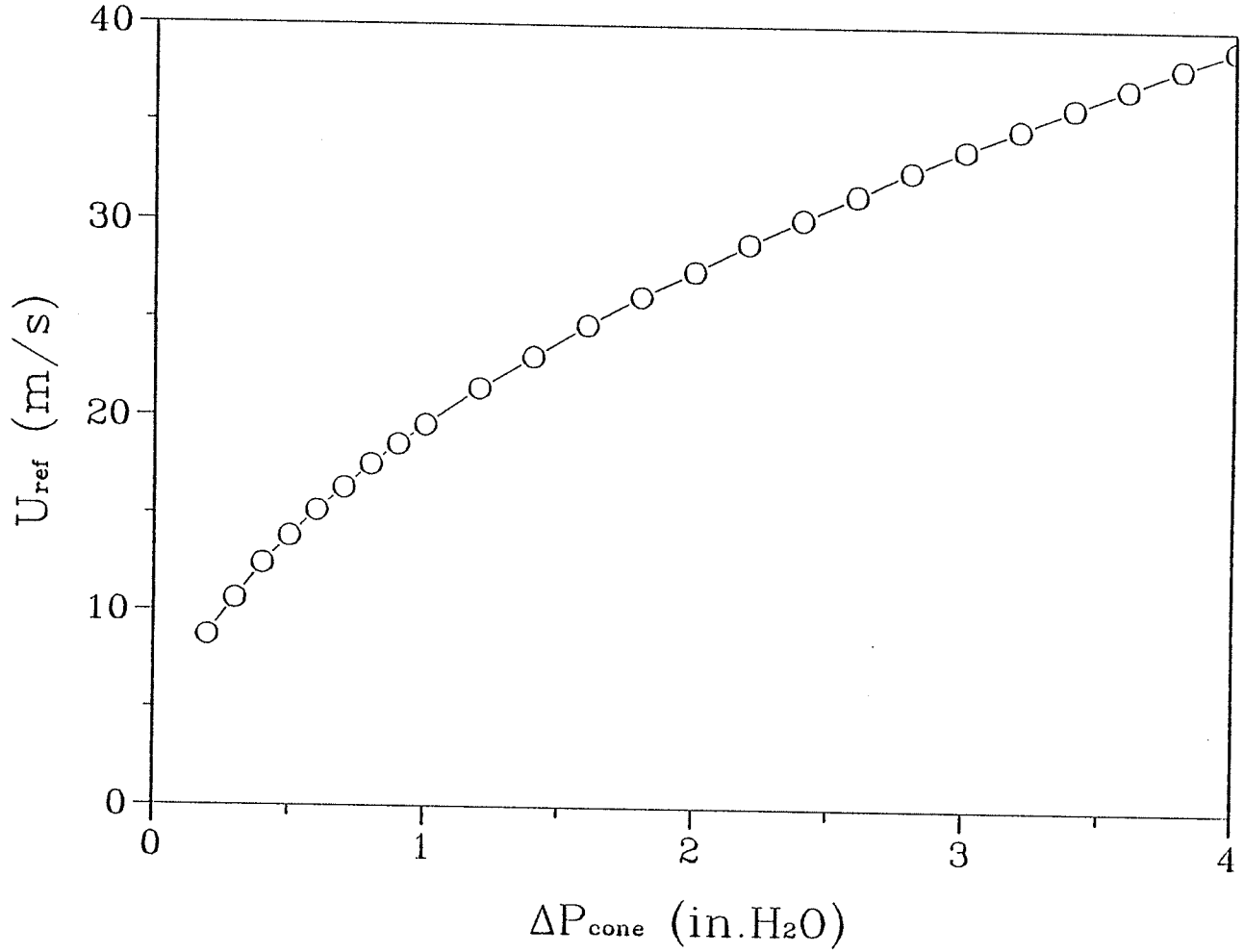

Figure 4. Tunnel calibration curve (centerline mean velocity).

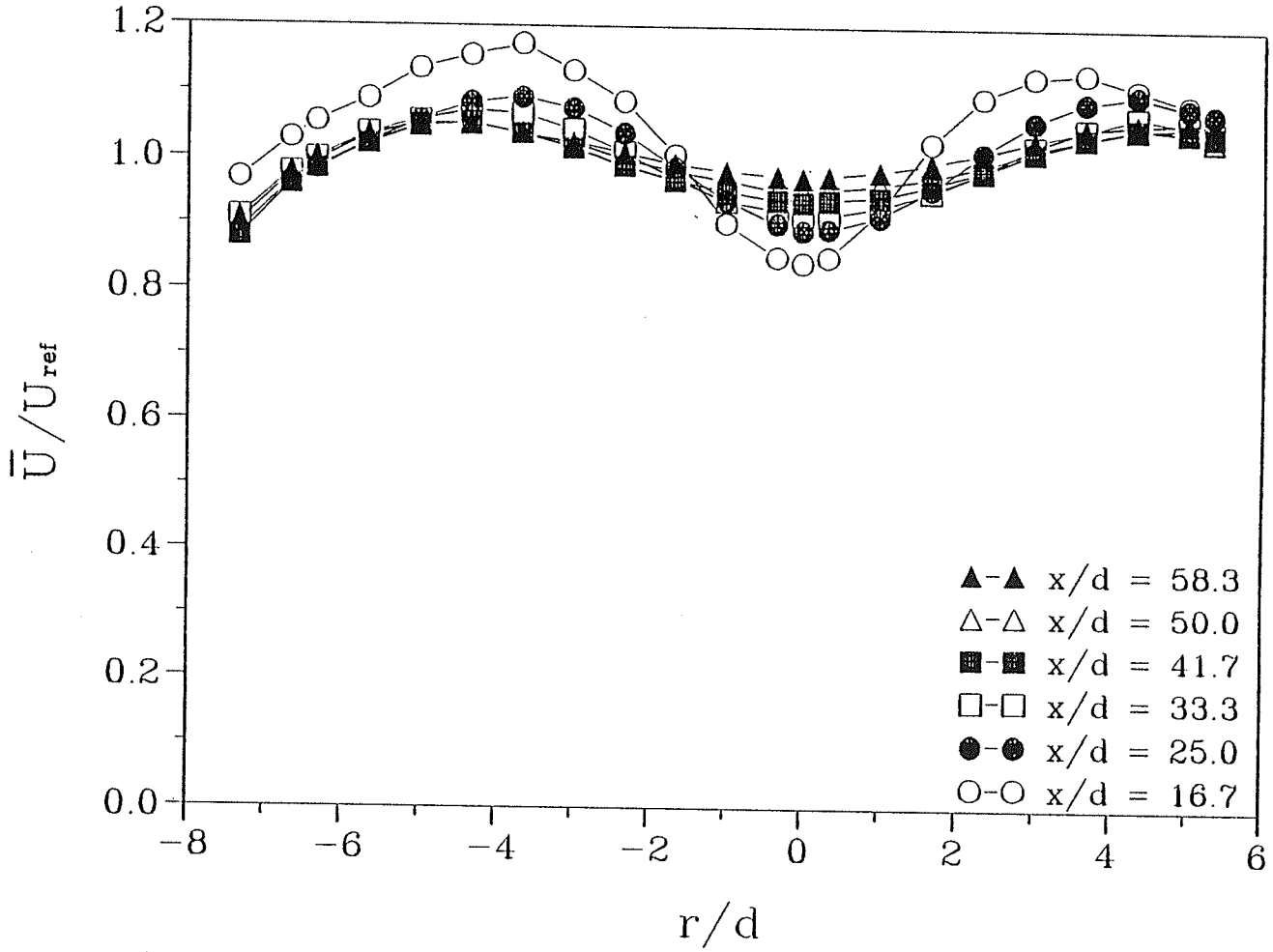

Figure 5. Transverse distributions of the mean velocity.

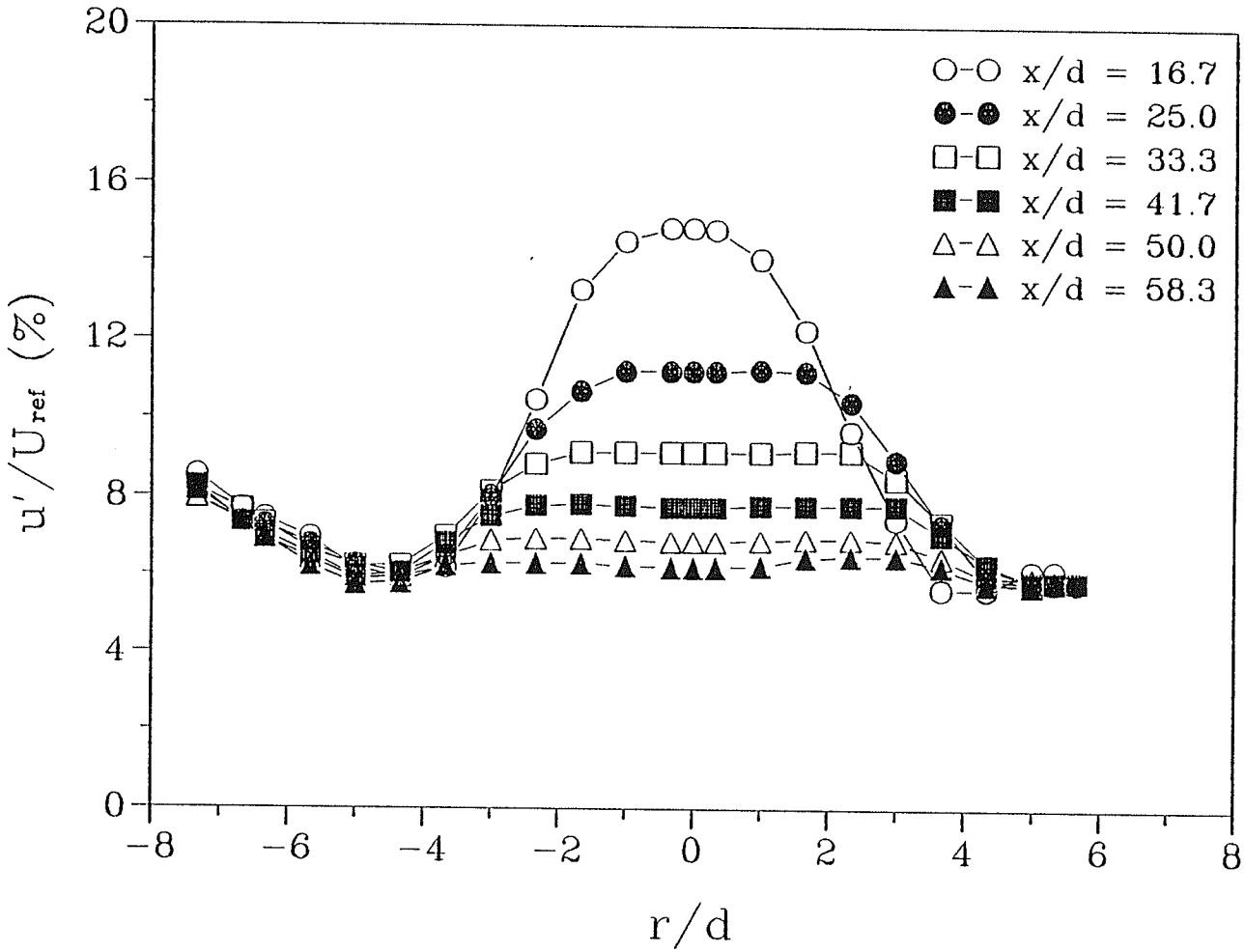

Figure 6. Transverse distributions of the r.m.s. velocity.

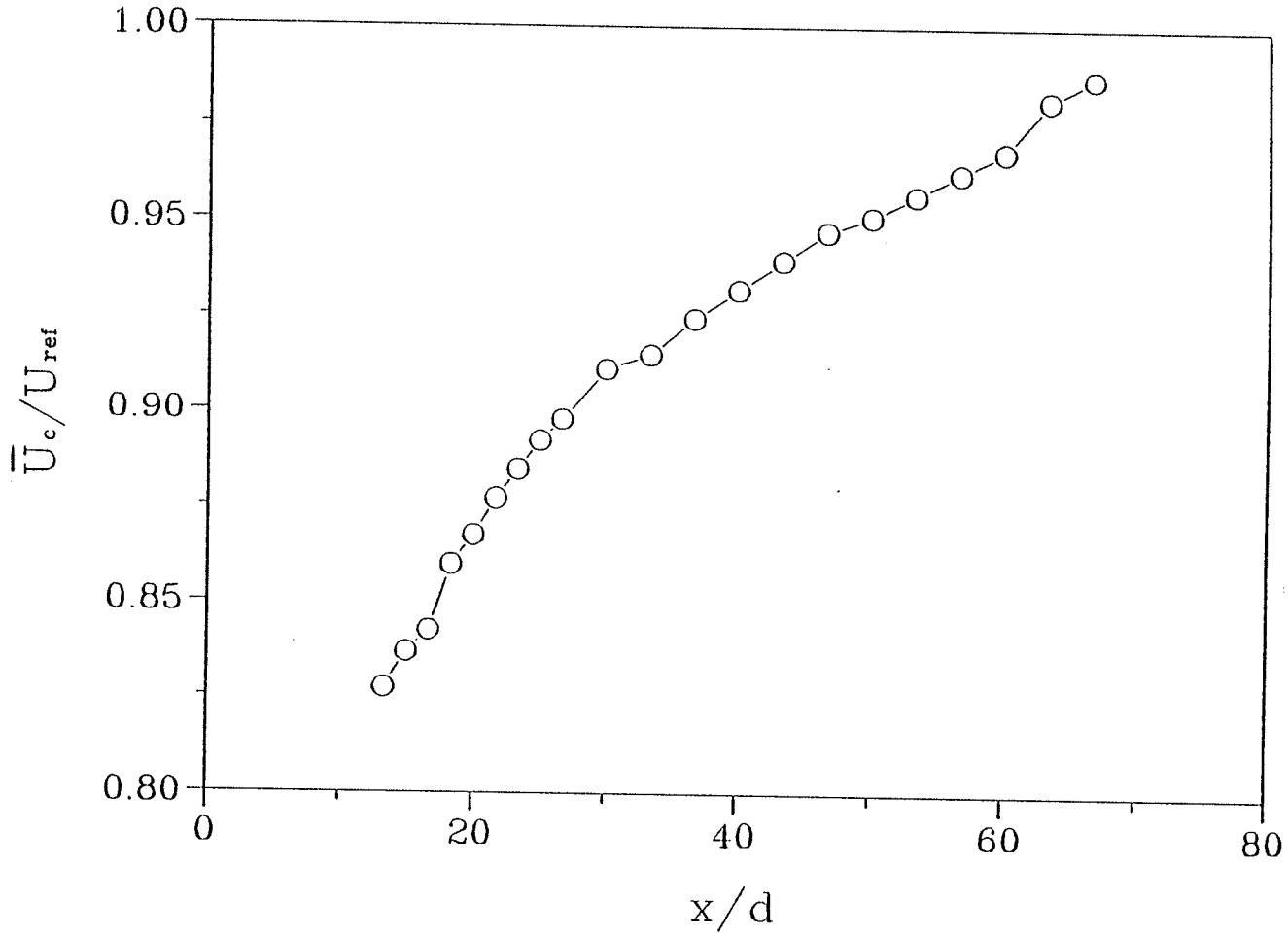

Figure 7. Downstream development of the centerline mean velocity.

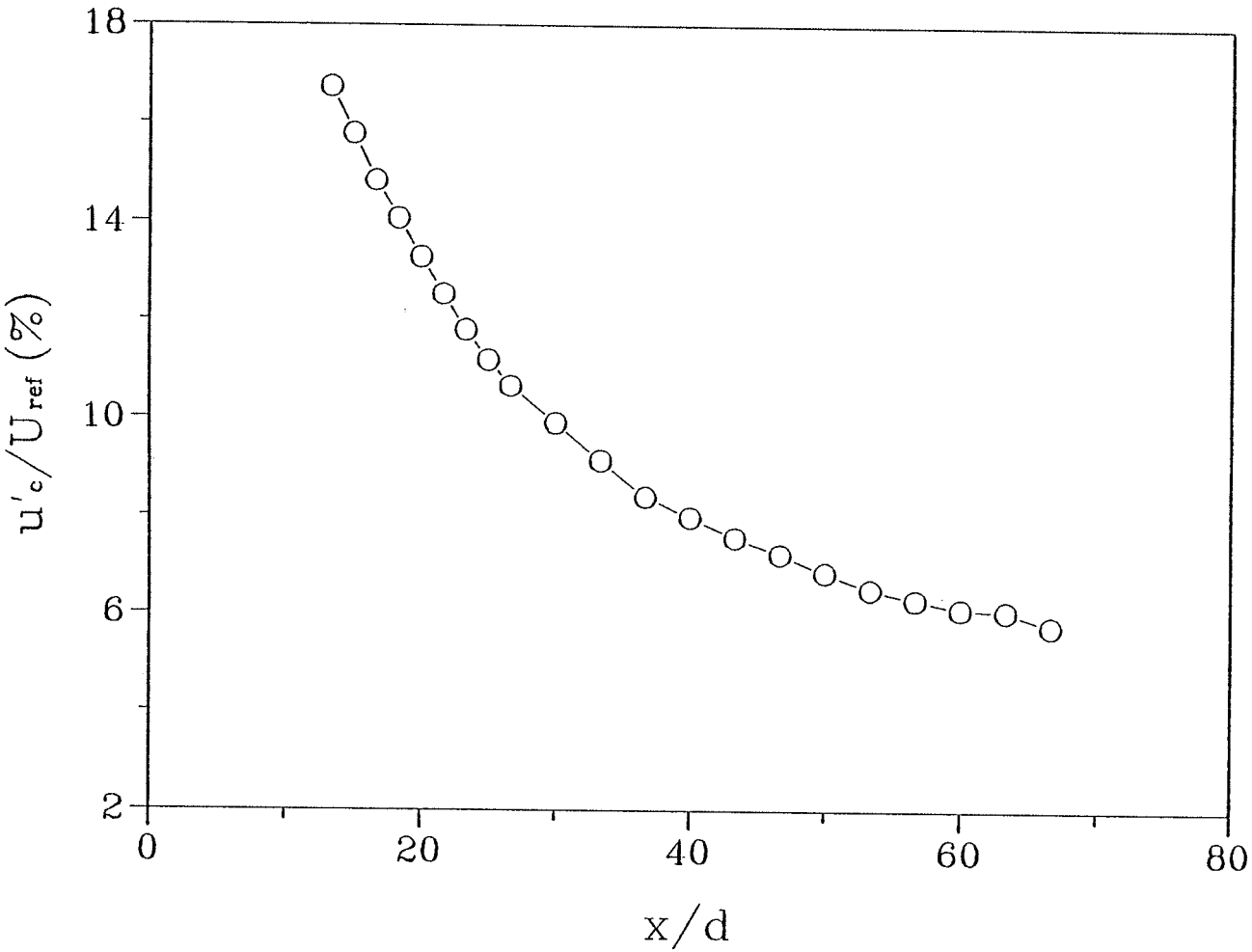

Figure 8. Downstream development of centerline r.m.s. velocity .

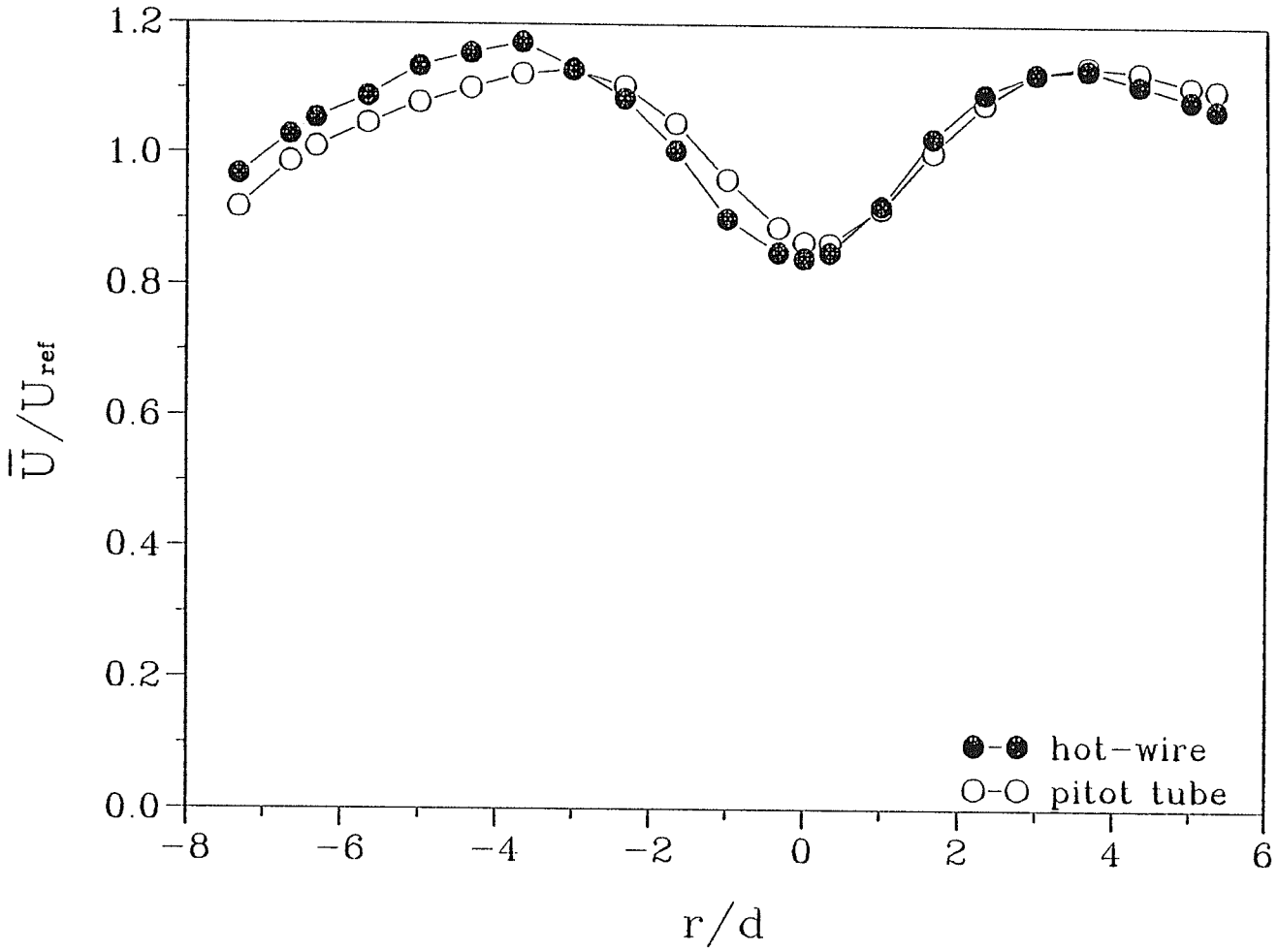

Figure 9. Transverse distributions of the mean velocity measured by both hot-wire and pitot tube at x/d = 16.7.

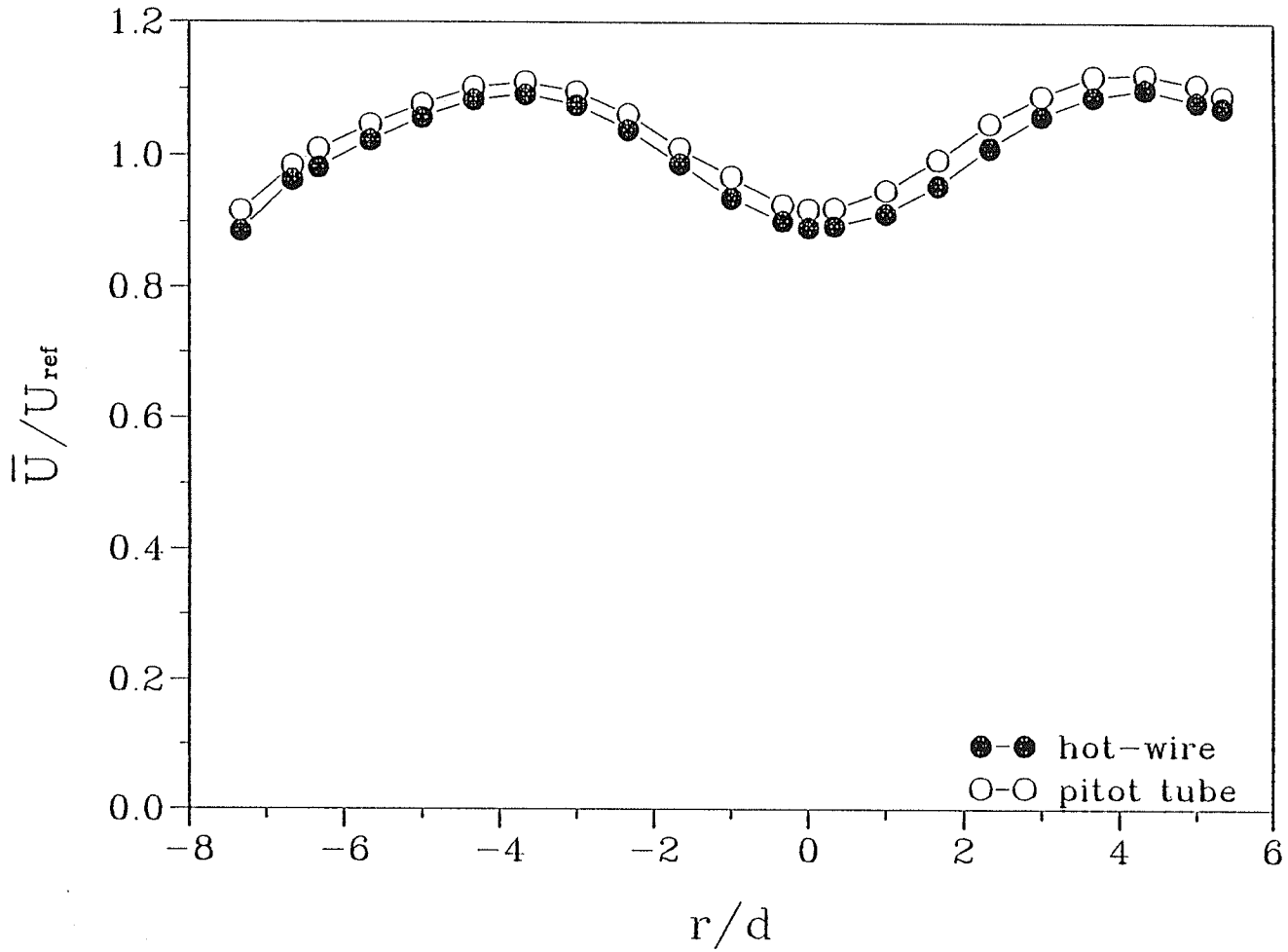

Figure 10. Transverse distributions of the mean velocity measured by both hot-wire and pitot tube at x/d = 25.0.

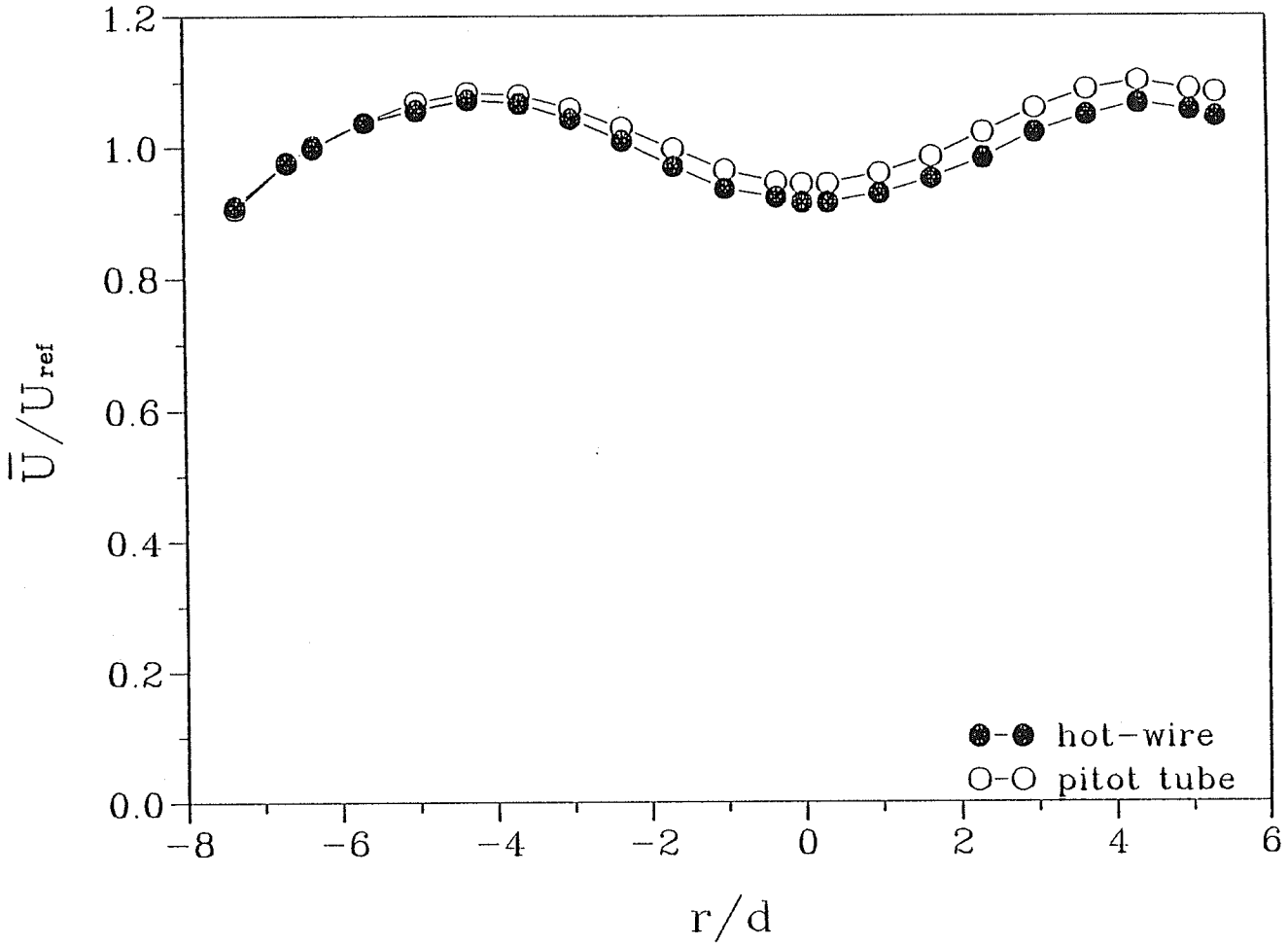

Figure 11. Transverse distributions of the mean velocity measured by both hot-wire and pitot tube at x/d = 33.3.

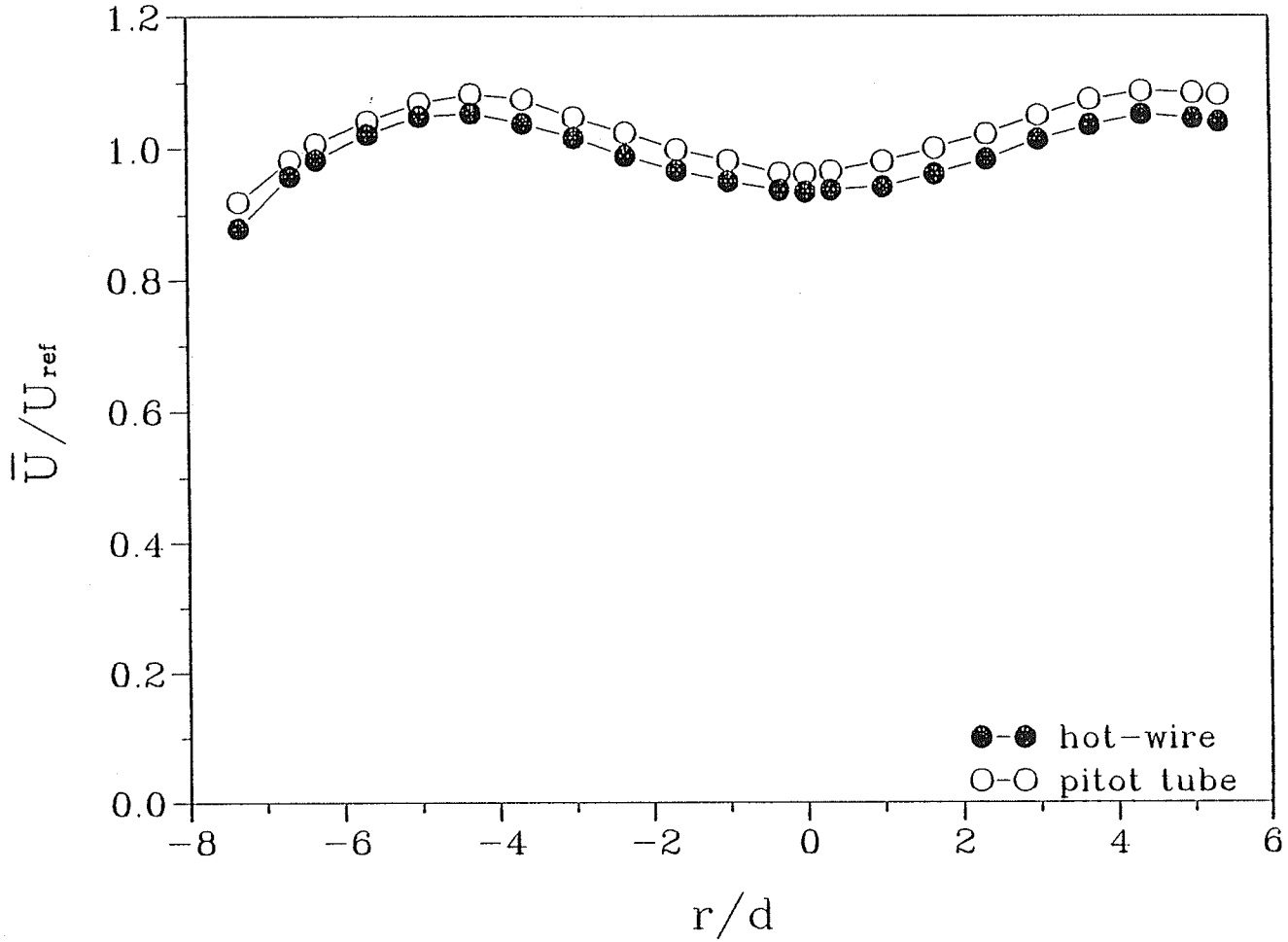

Figure 12. Transverse distributions of the mean velocity measured by both hot-wire and pitot tube at x/d = 41.7.

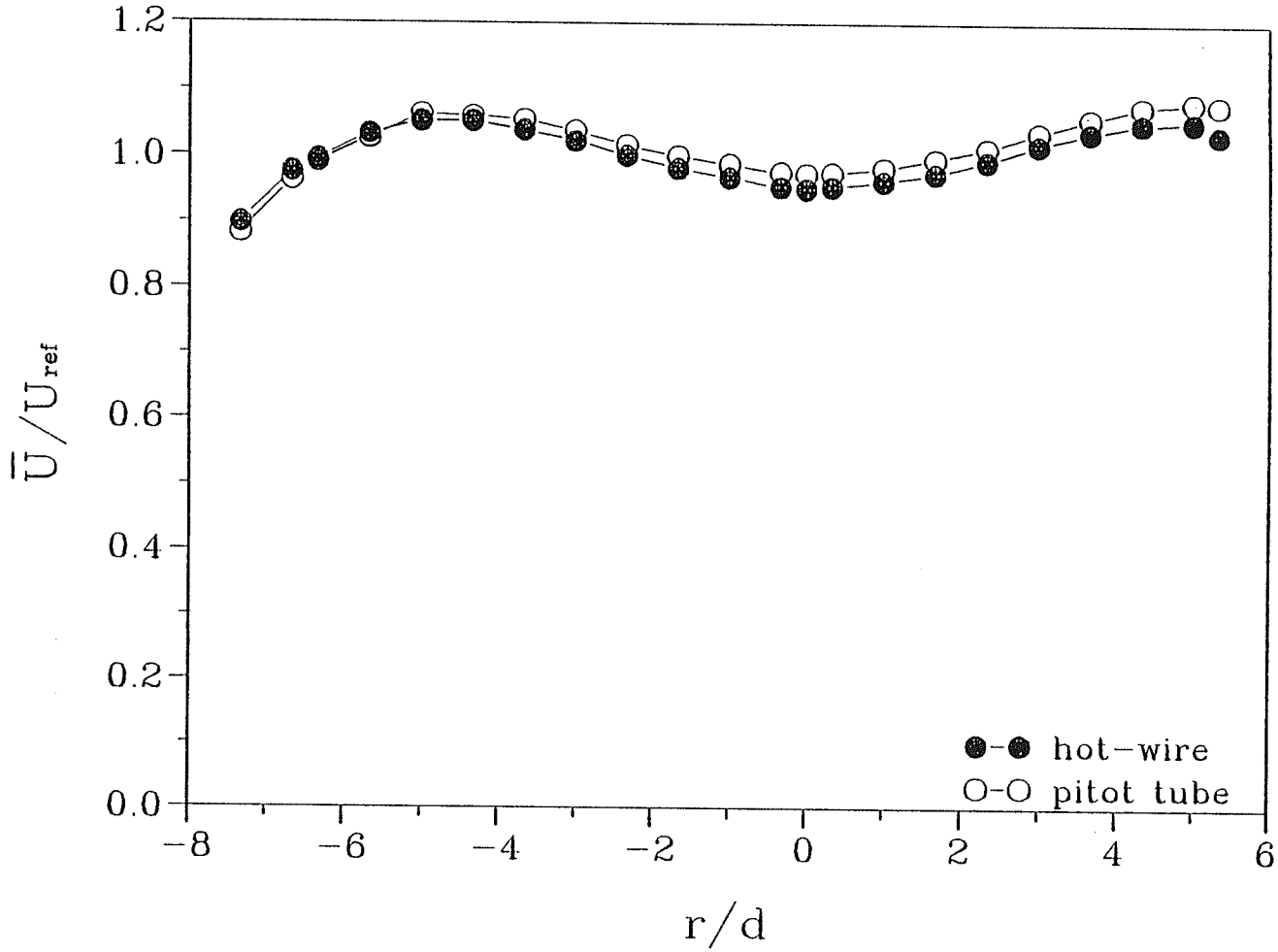

Figure 13. Transverse distributions of the mean velocity measured by both hot-wire and pitot tube at x/d = 50.0.

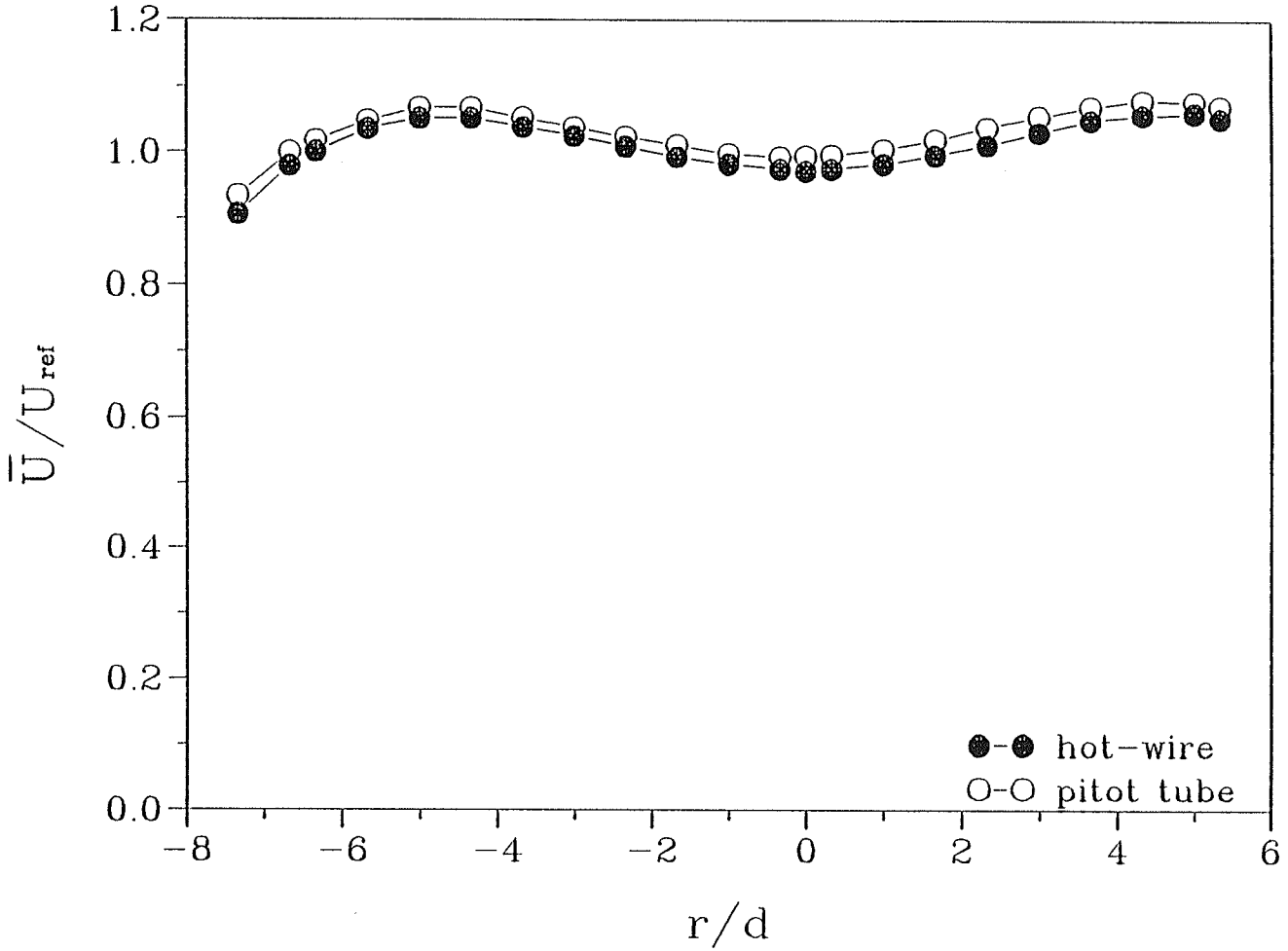

Figure 14. Transverse distributions of the mean velocity measured by both hot-wire and pitot tube at x/d = 58.3.

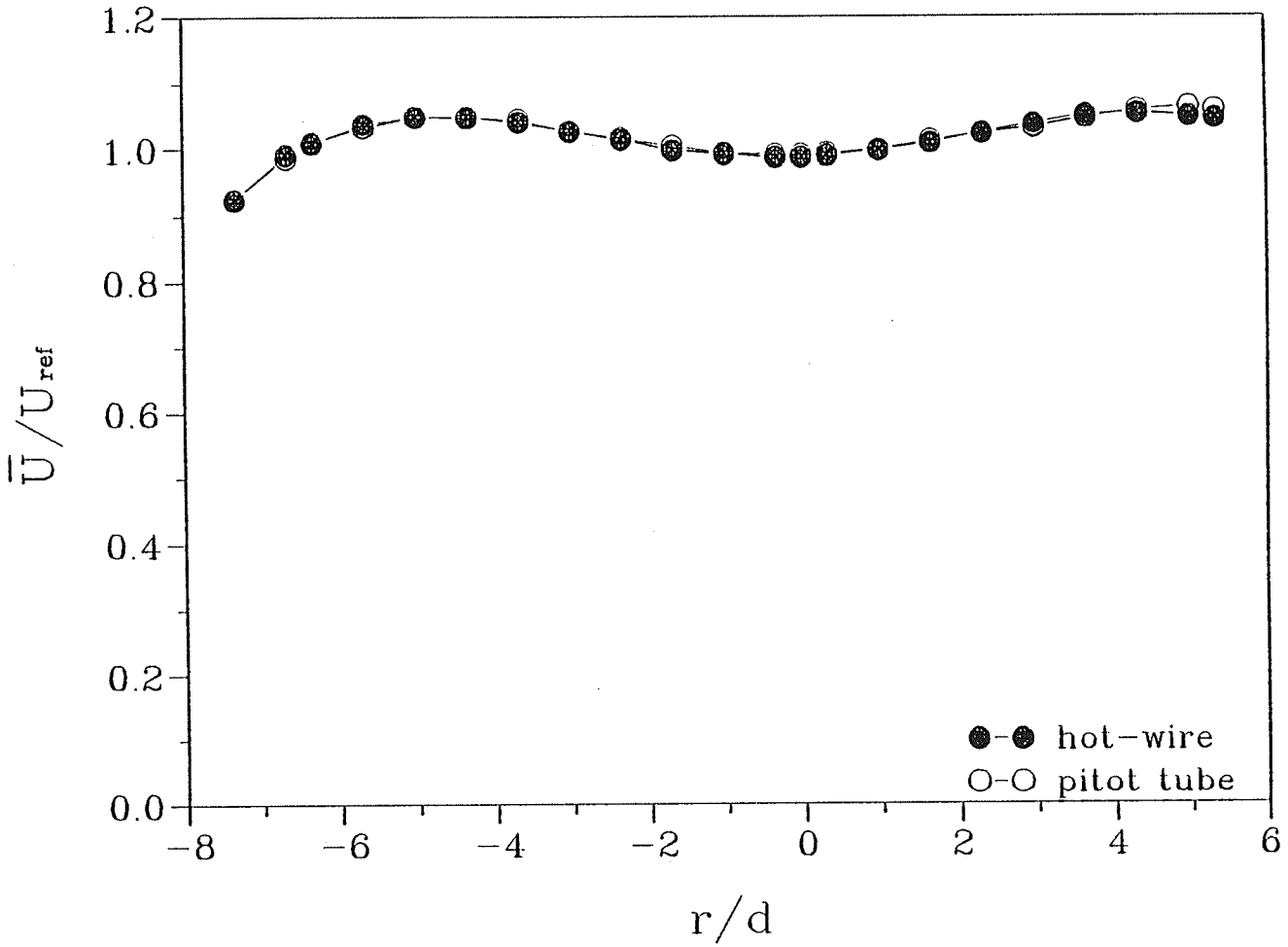

Figure 15. Transverse distributions of the mean velocity measured by both hot-wire and pitot tube at x/d = 66.7.

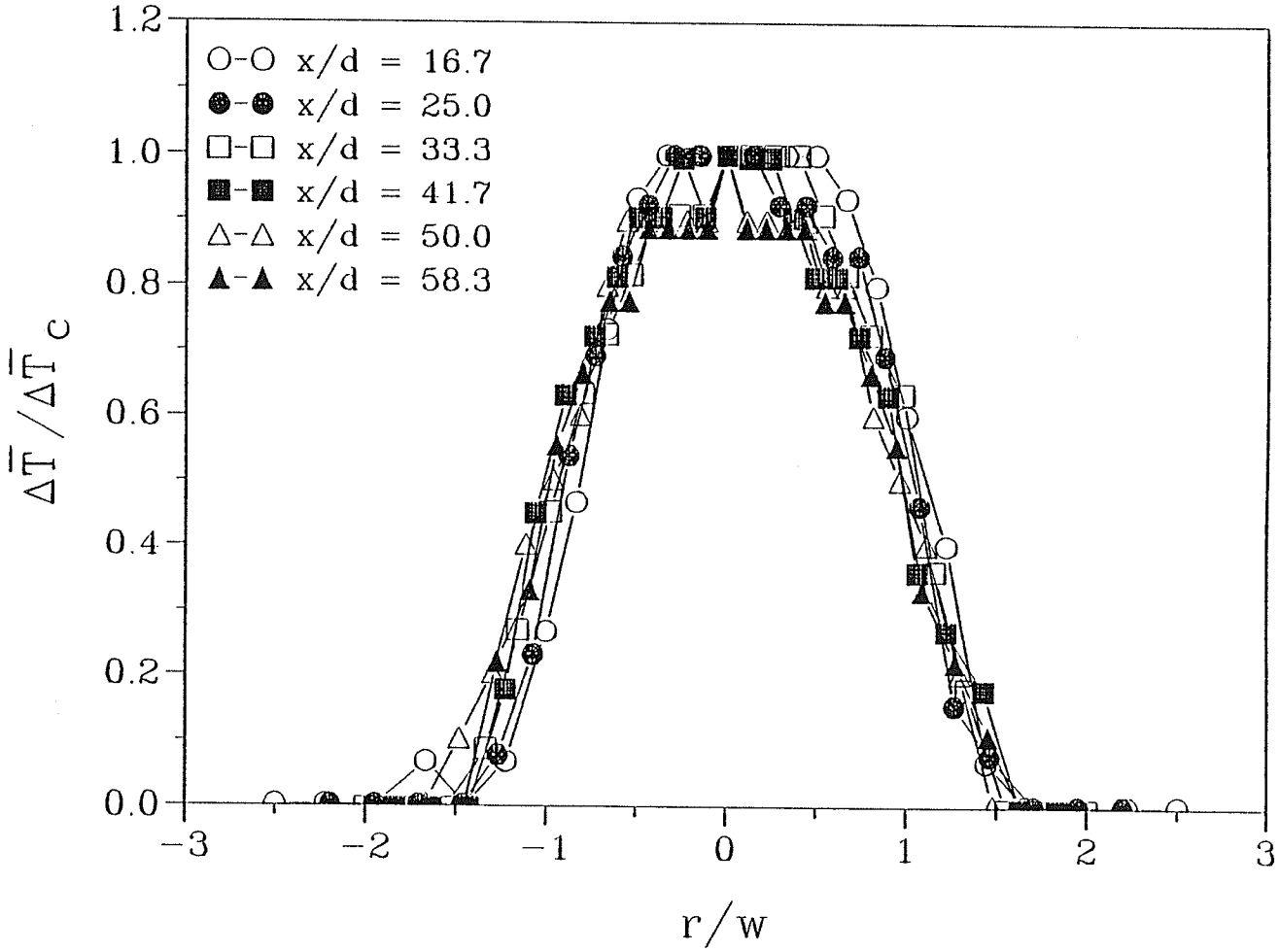

Figure 16. Transverse profiles of the mean temperature rise.

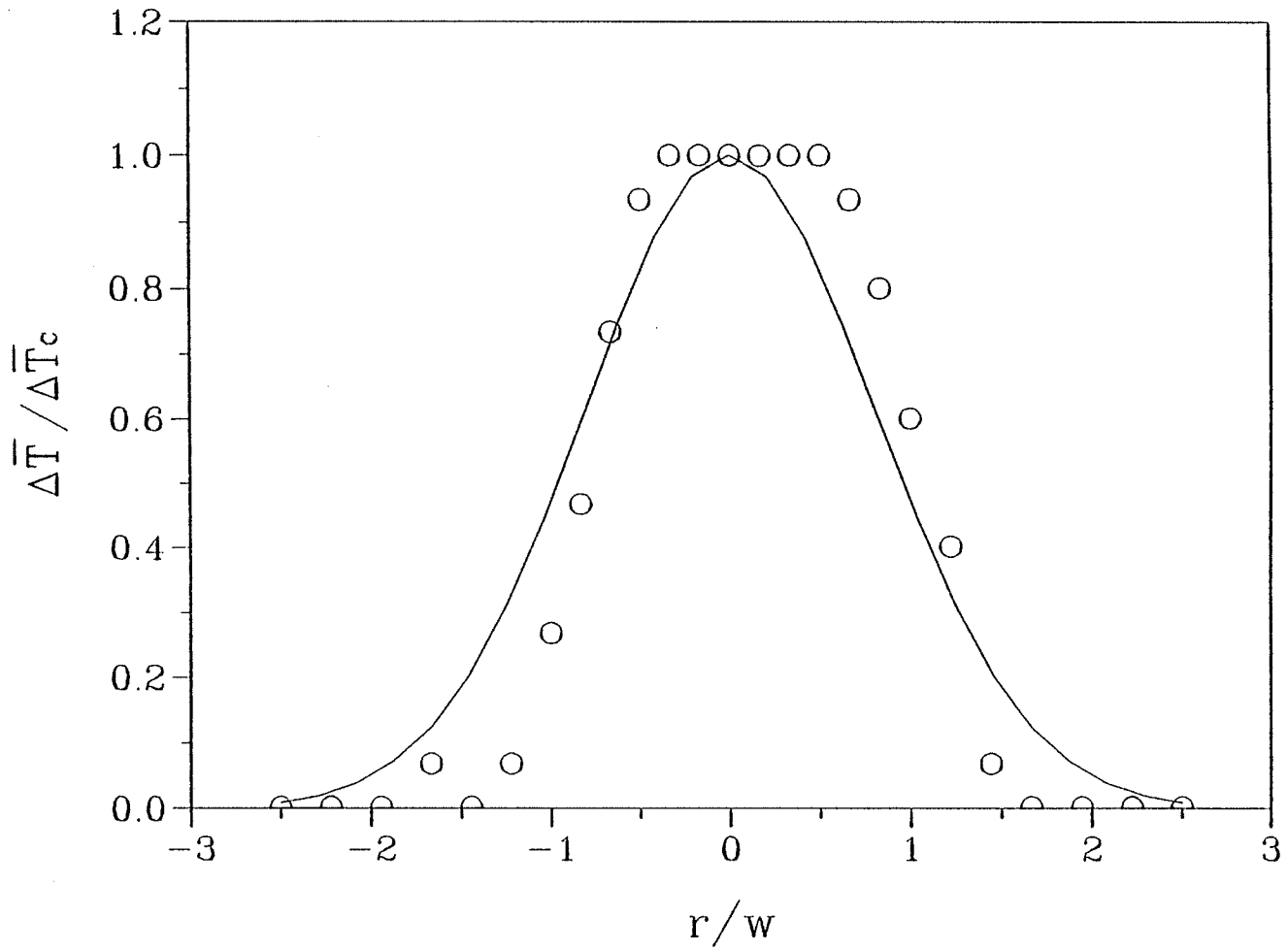

Figure 17. Transverse distribution of the mean temperature rise at x/d = 16.7 (solid smooth line represents the Gaussian distribution and the symbols of the open circle represent measured data).

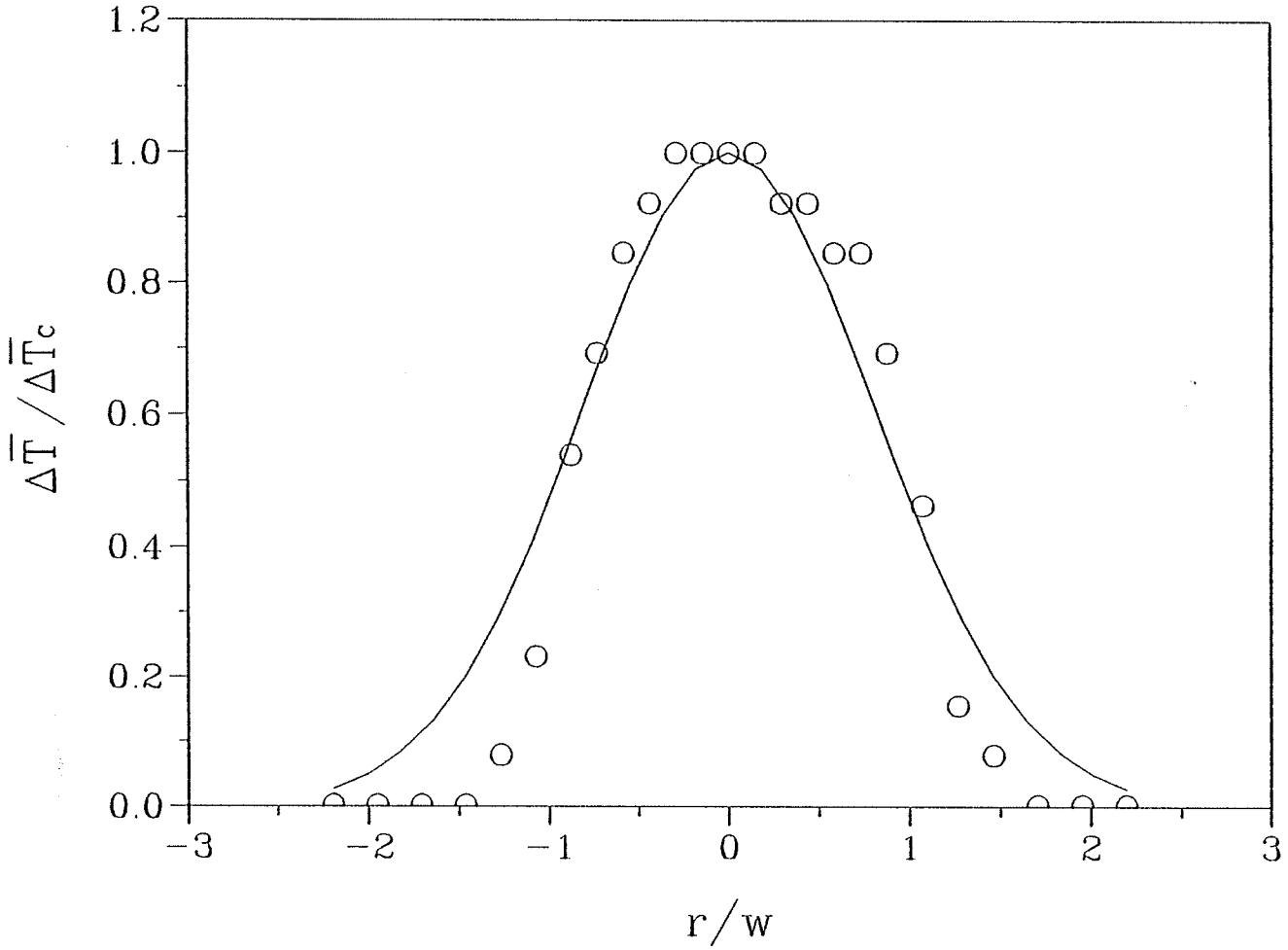

Figure 18. Transverse distribution of the mean temperature rise at x/d = 25.0 (symbols as in Figure 17.)

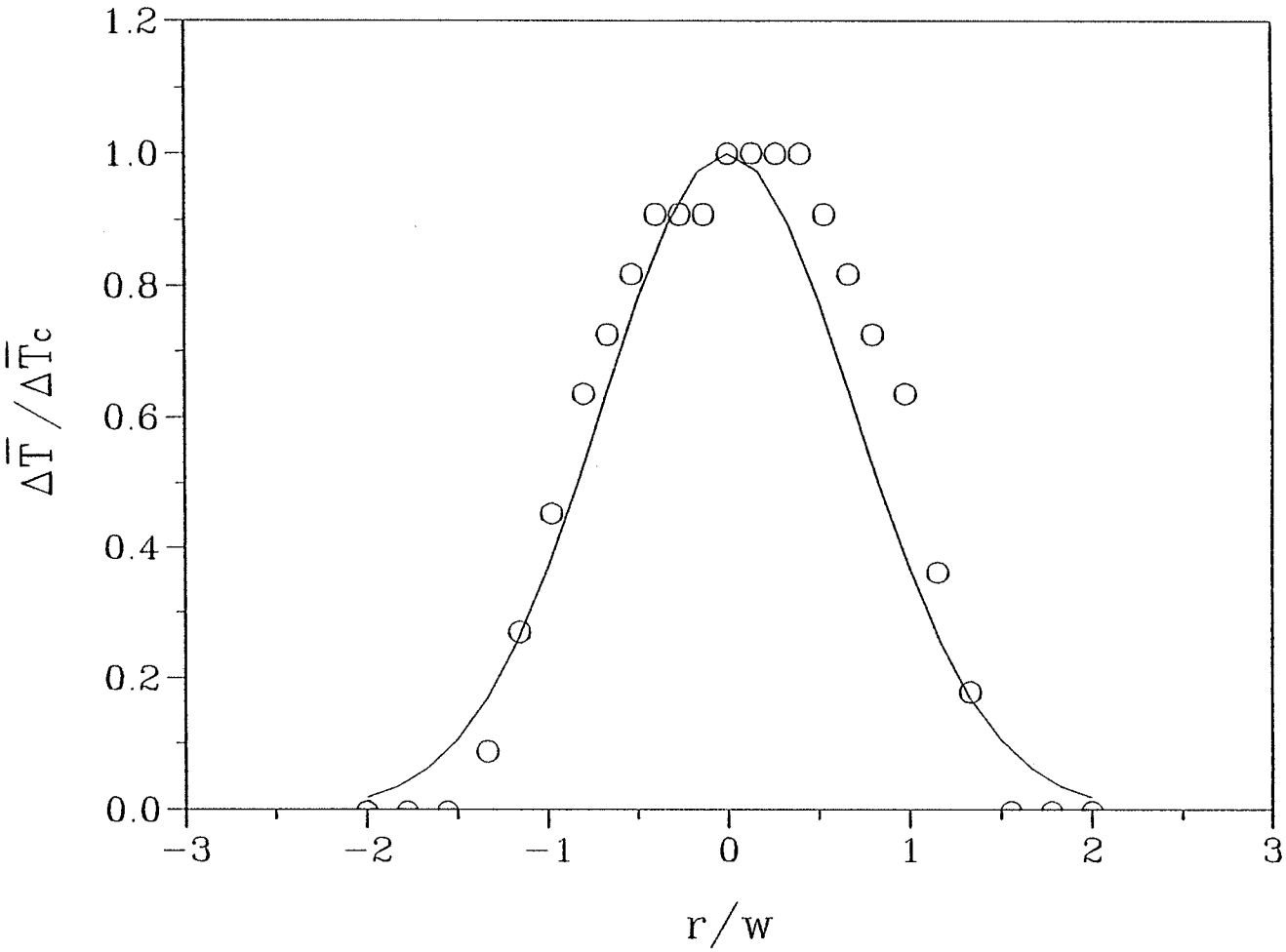

Figure 19. Transverse distribution of the mean temperature rise at x/d = 33.3 (symbols as in Figure 17.)

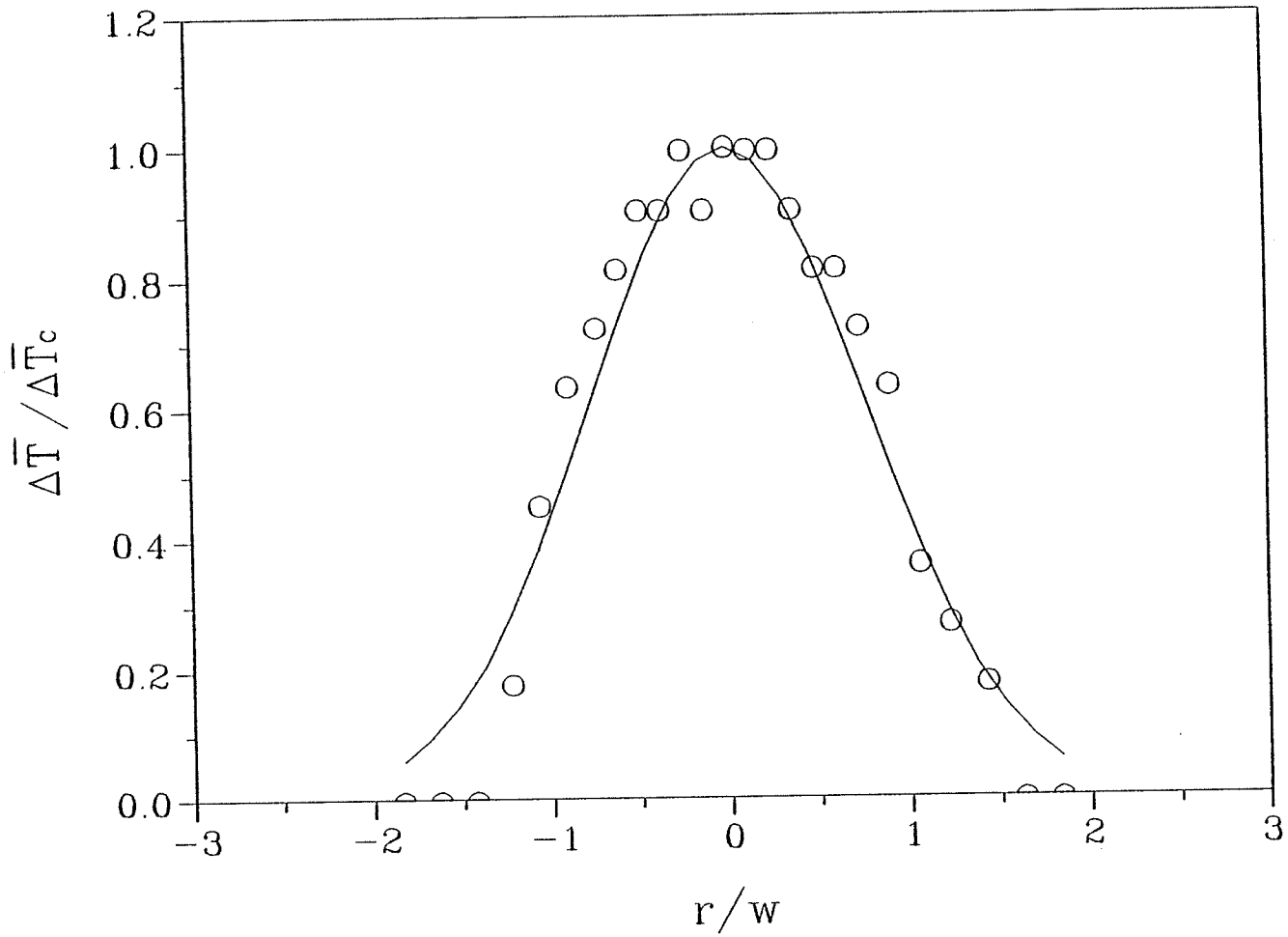

Figure 20. Transverse distribution of the mean temperature rise at x/d = 41.7 (symbols as in Figure 17.)

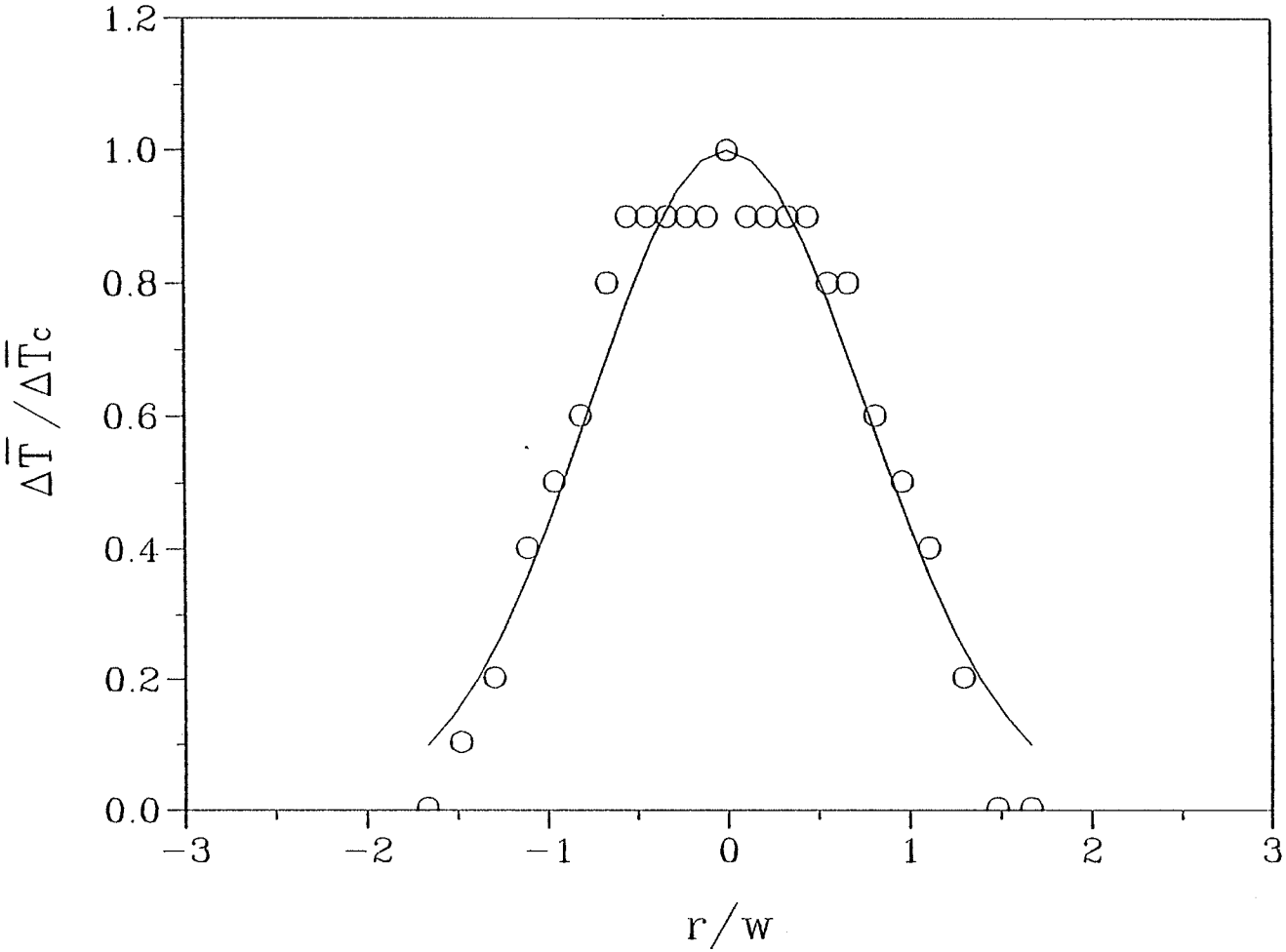

Figure 21. Transverse distribution of the mean temperature rise at x/d = 50.0 (symbols as in Figure 17.)

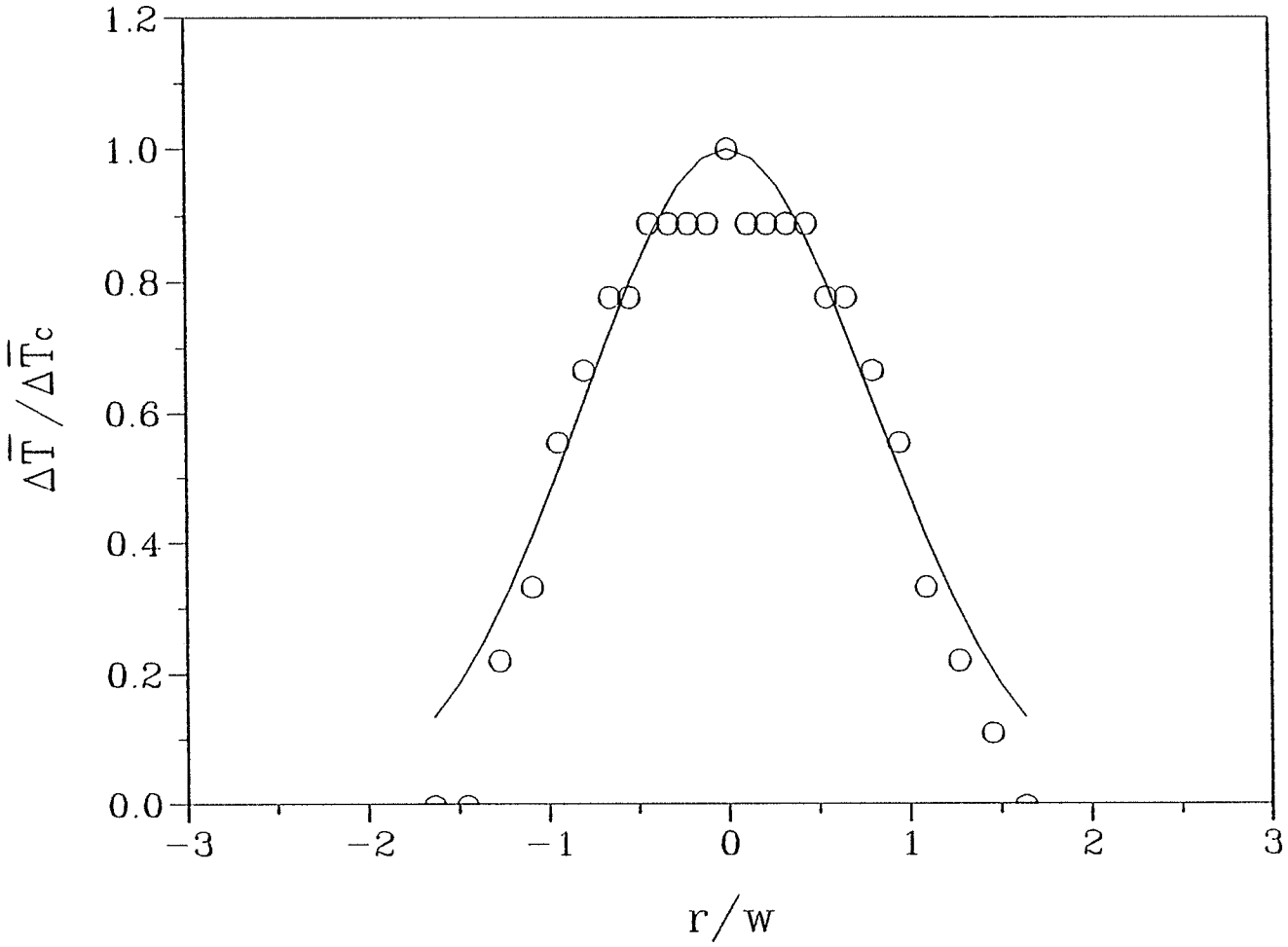

Figure 22. Transverse distribution of the mean temperature rise at x/d = 58.3 (symbols as in Figure 17.)

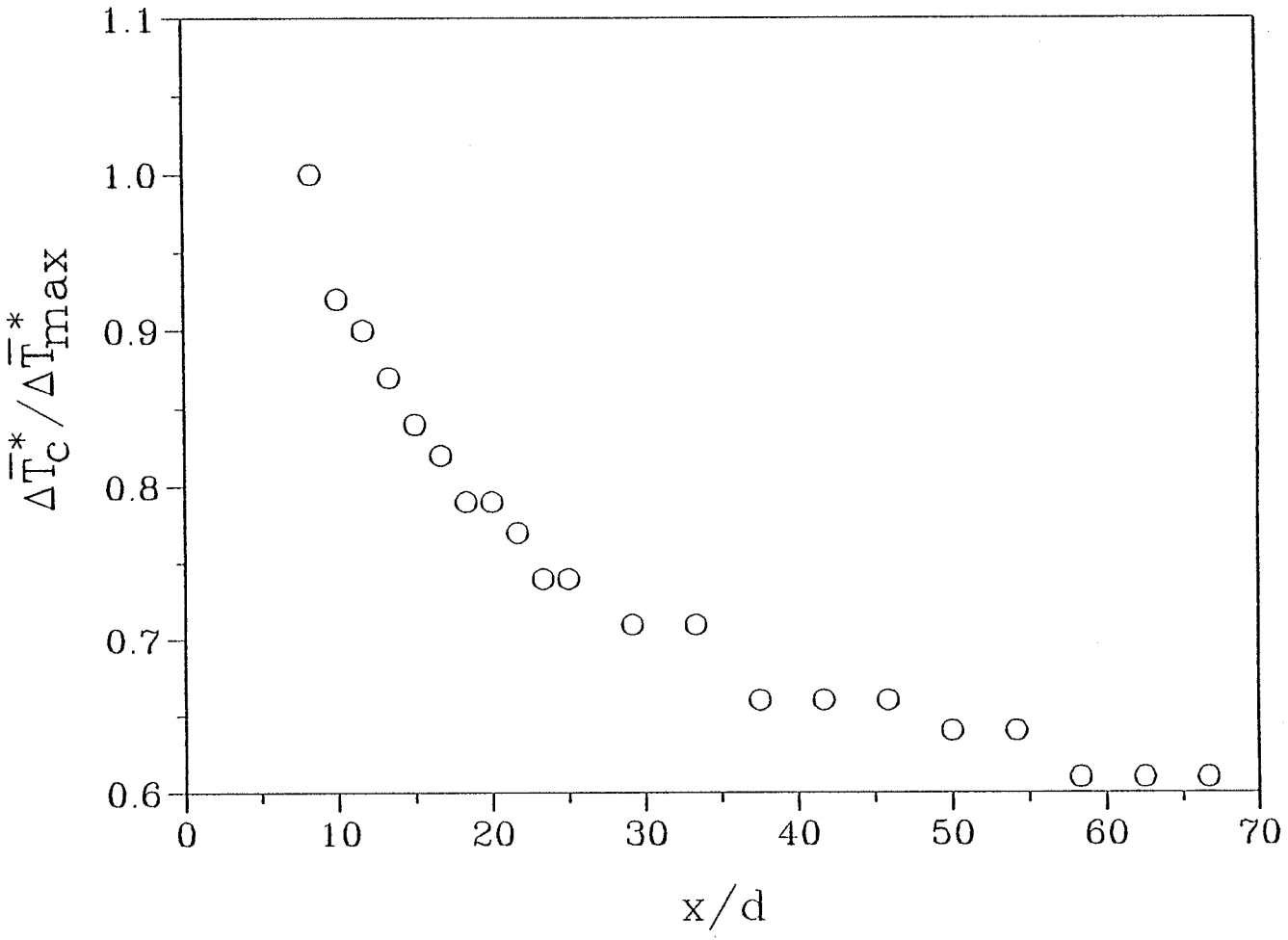

Figure 23. Downstream development of the centerline mean temperature.

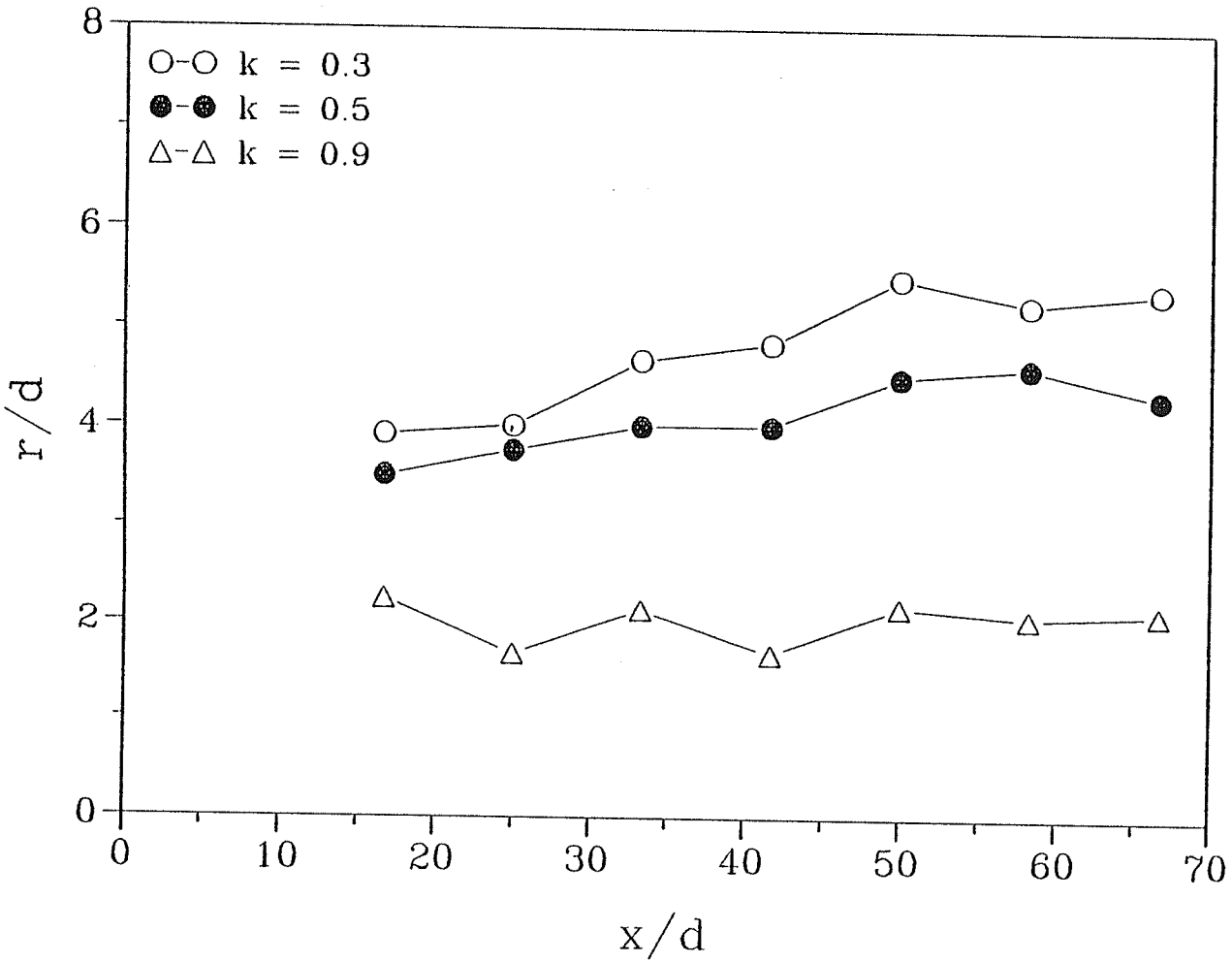

Figure 24. Locus of positions with $k = \Delta\overline{T} / \Delta\overline{T}_c = 0.9, 0.5, 0.3$ respectively.

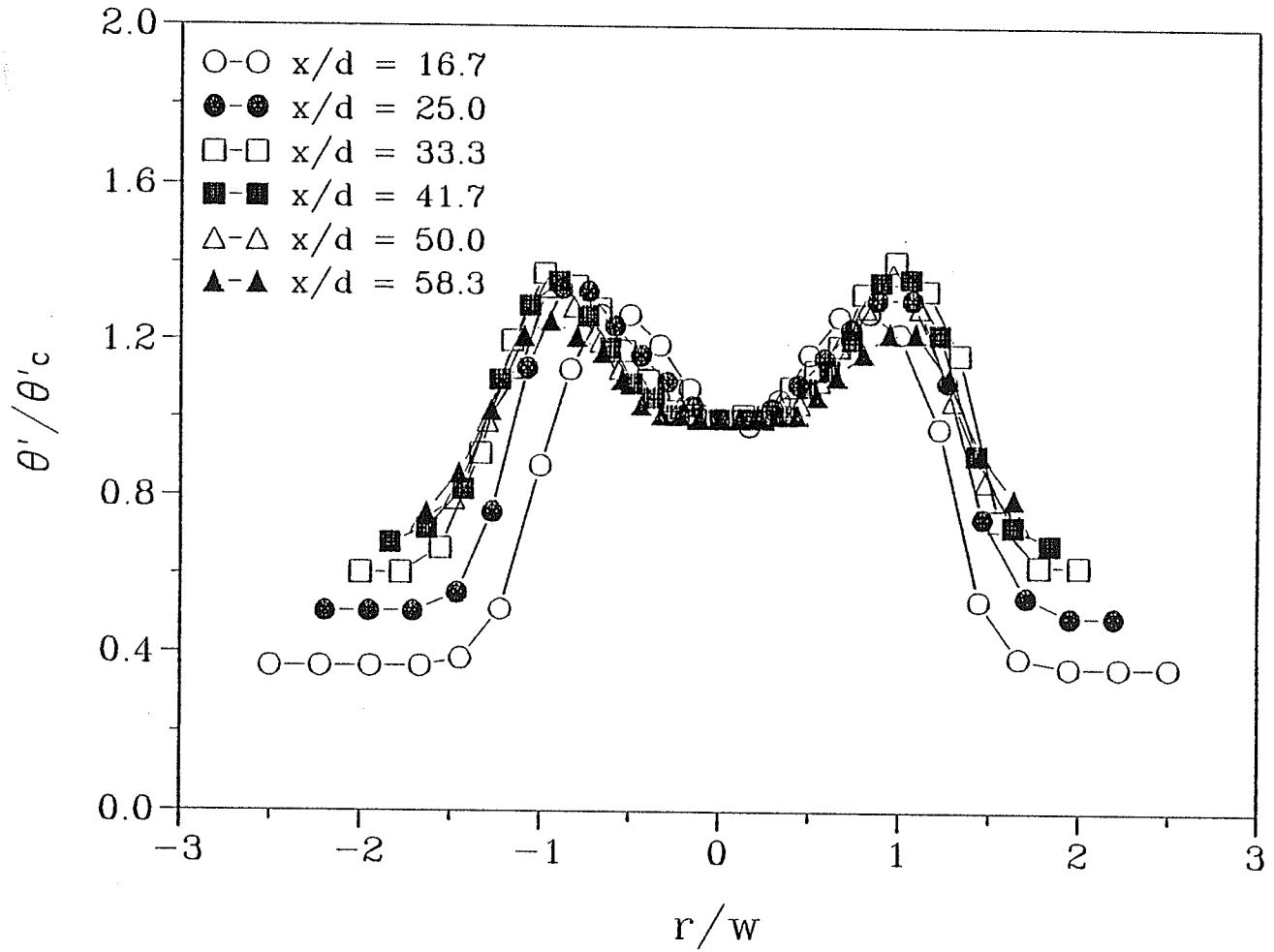

Figure 25. Transverse distributions of the r.m.s. temperature fluctuation.

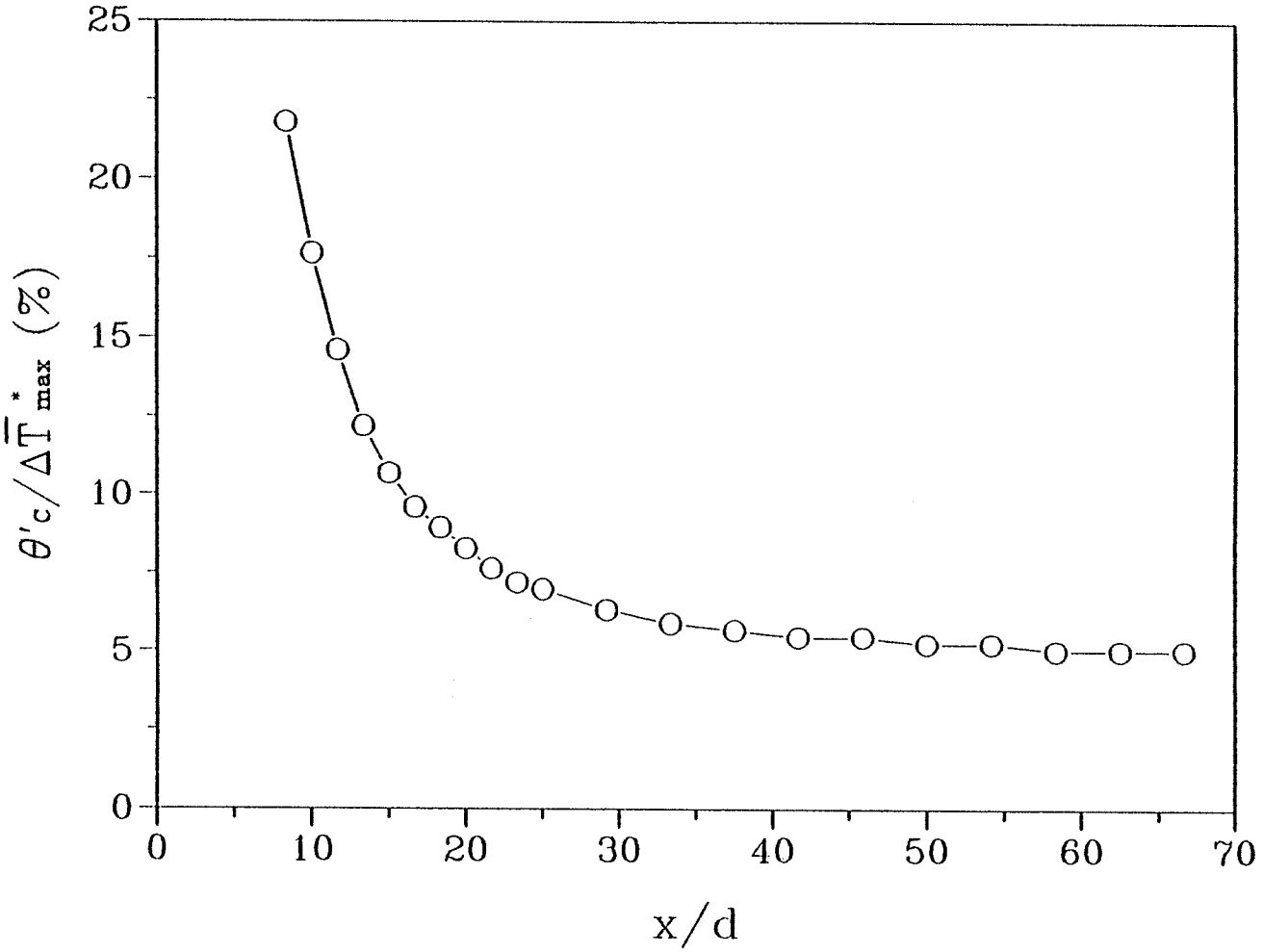

Figure 26. Downstream development of the centerline r.m.s. temperature fluctuation.

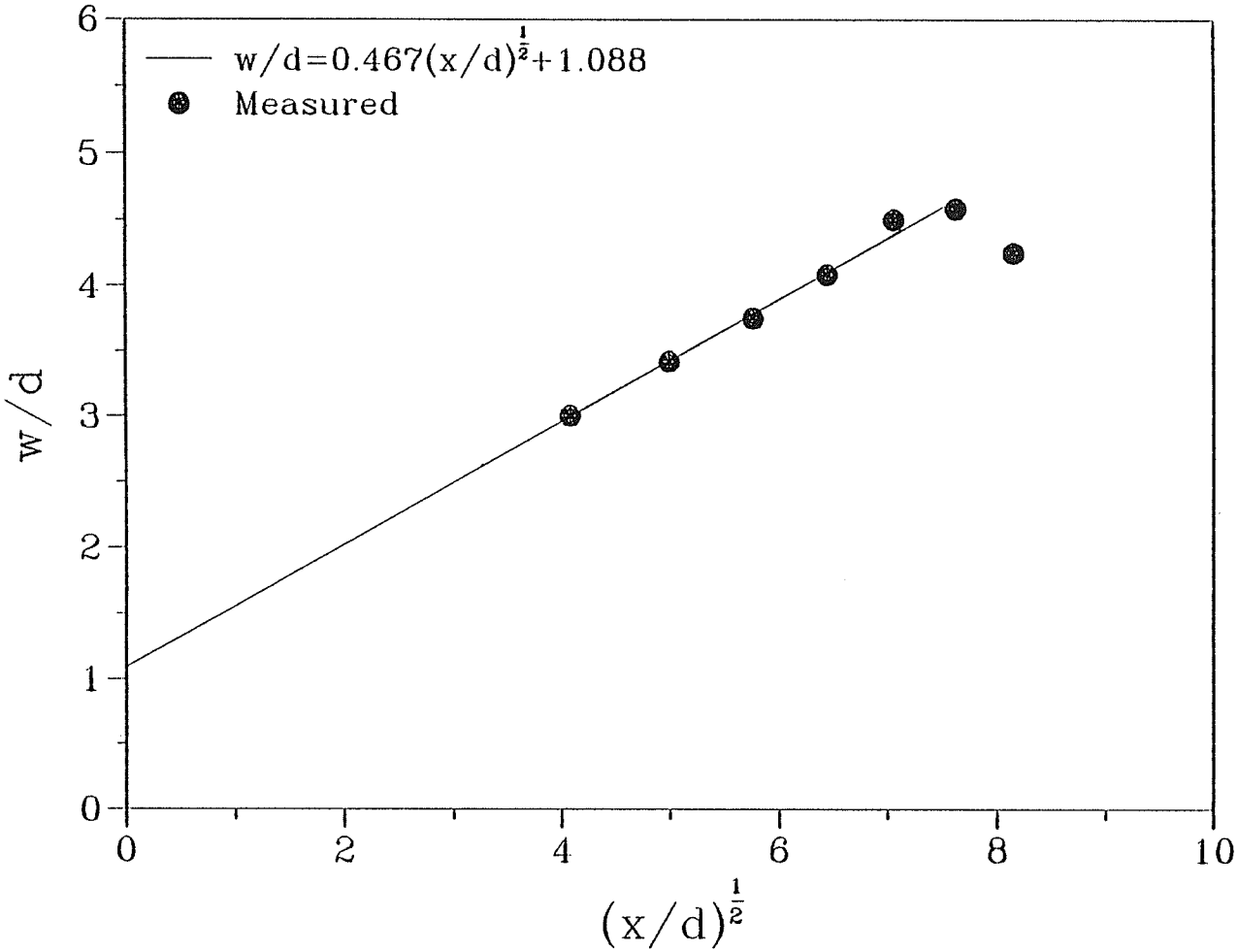

Figure 27. Downstream development of half-width of the wake.

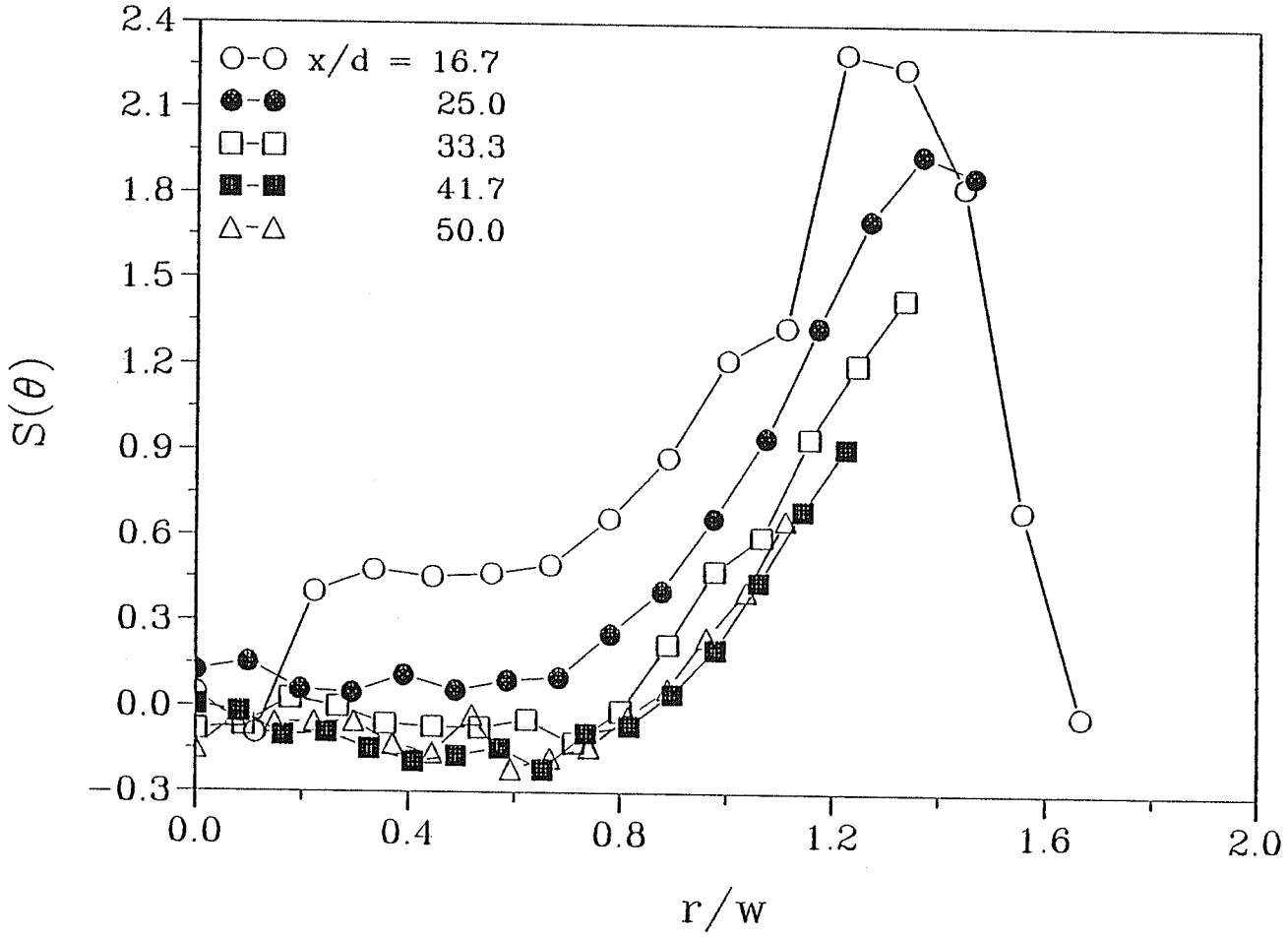

Figure 28. Transverse distributions of temperature skewness.

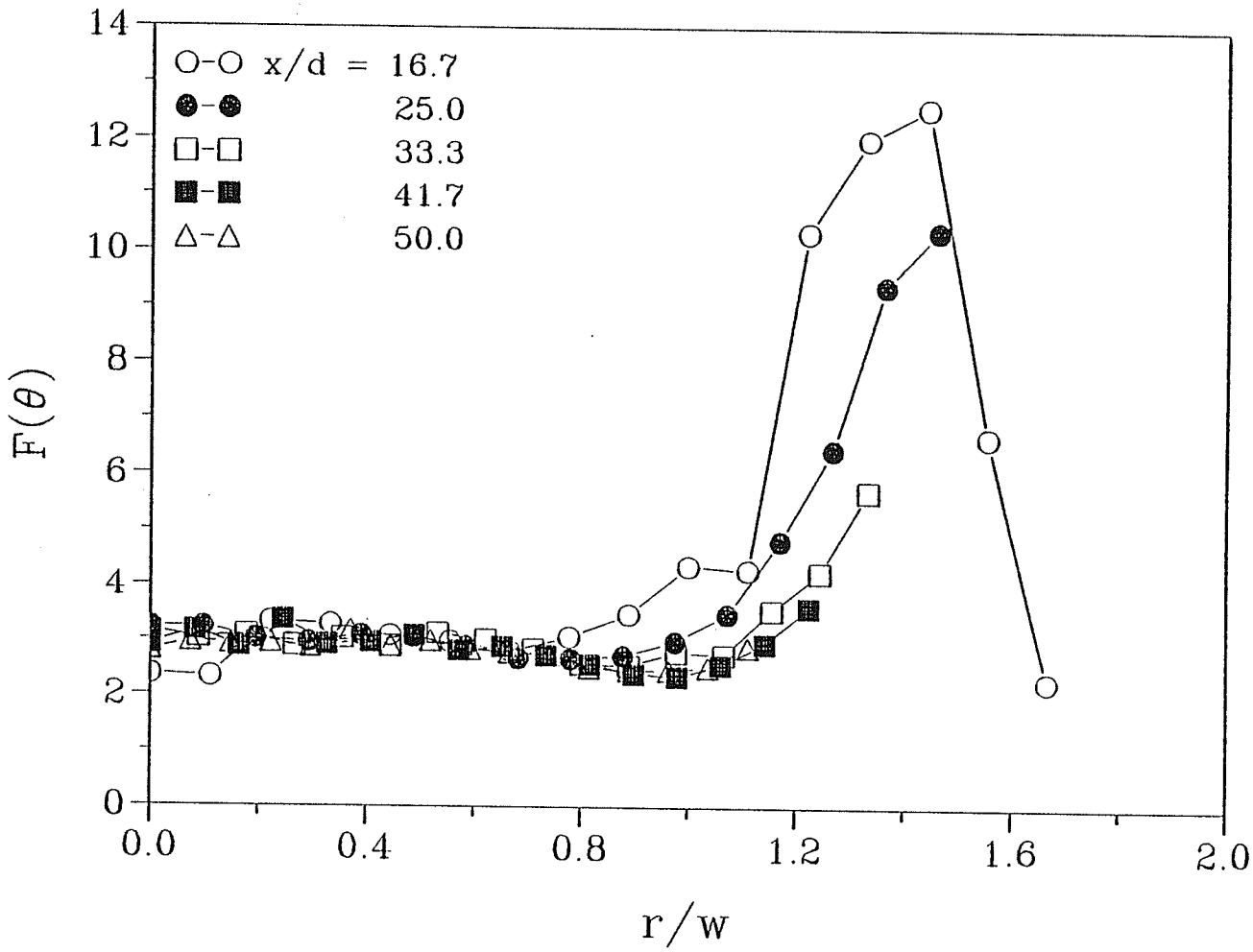

Figure 29. Transverse distributions of temperature flatness.

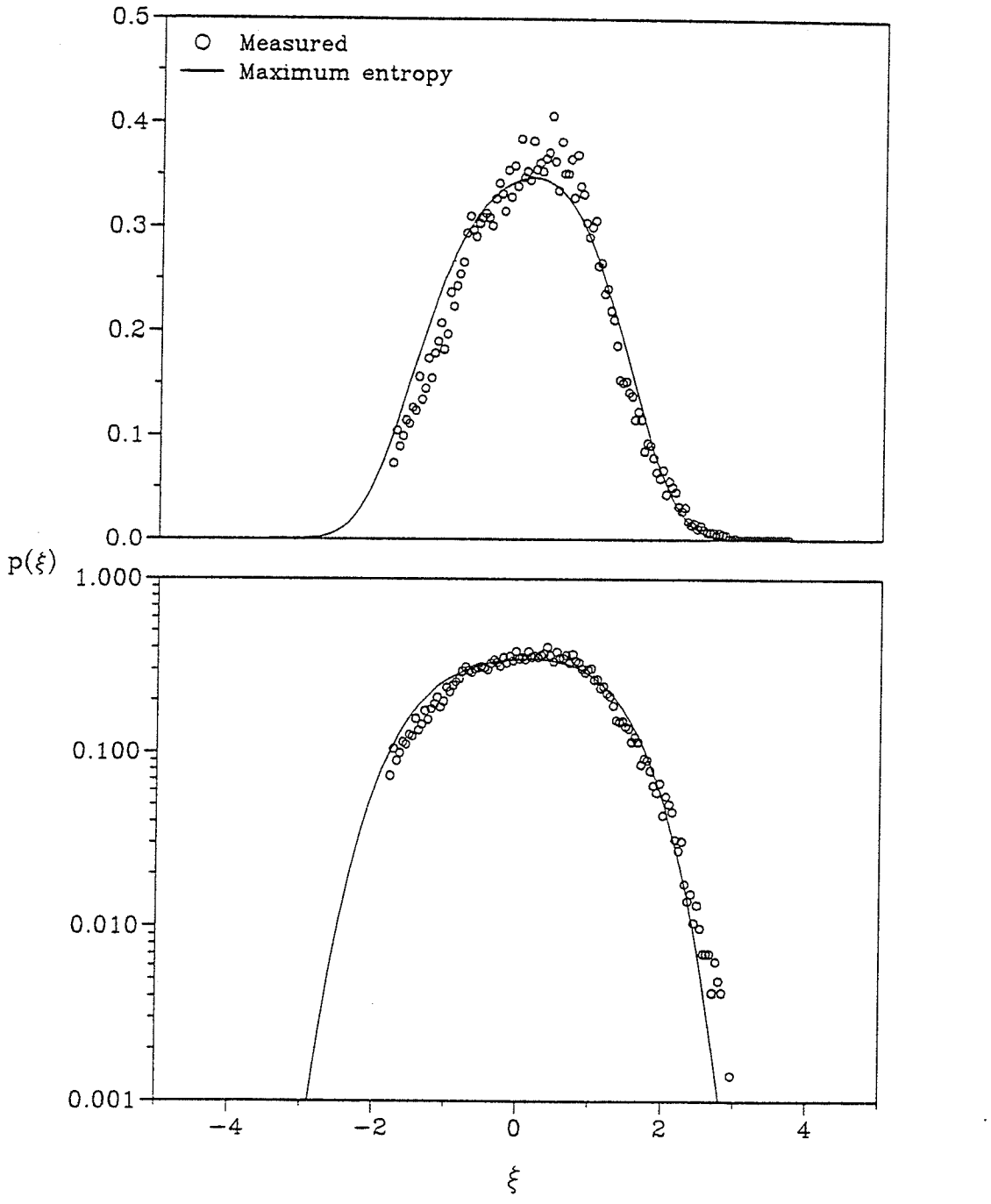

Figure 30. Distributions of probability density function of temperature fluctuation at r/d =0.0 and x/d = 16.7

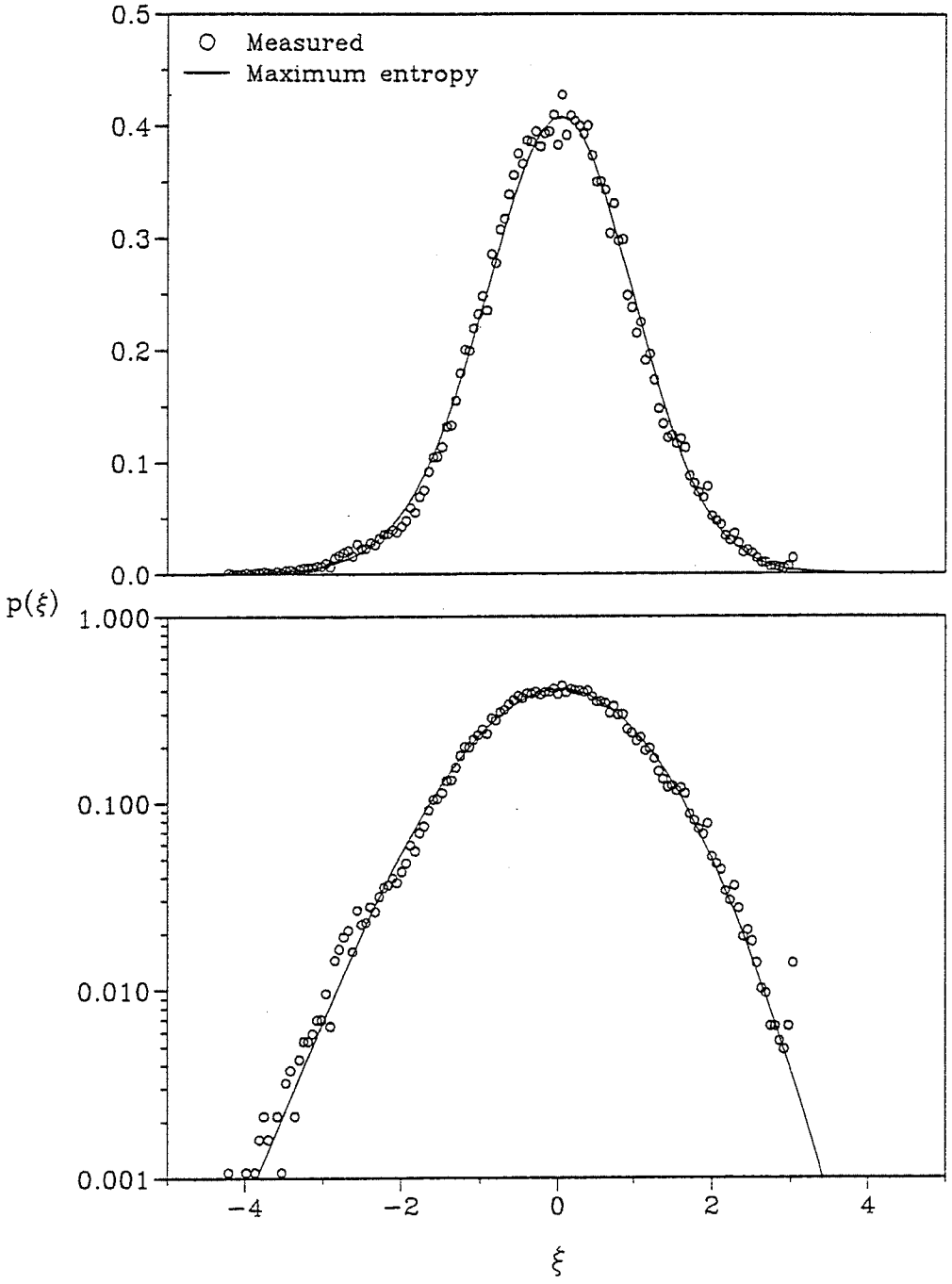

Figure 31. Distributions of probability density function of temperature fluctuation at r/d =0.0 and x/d = 25.0

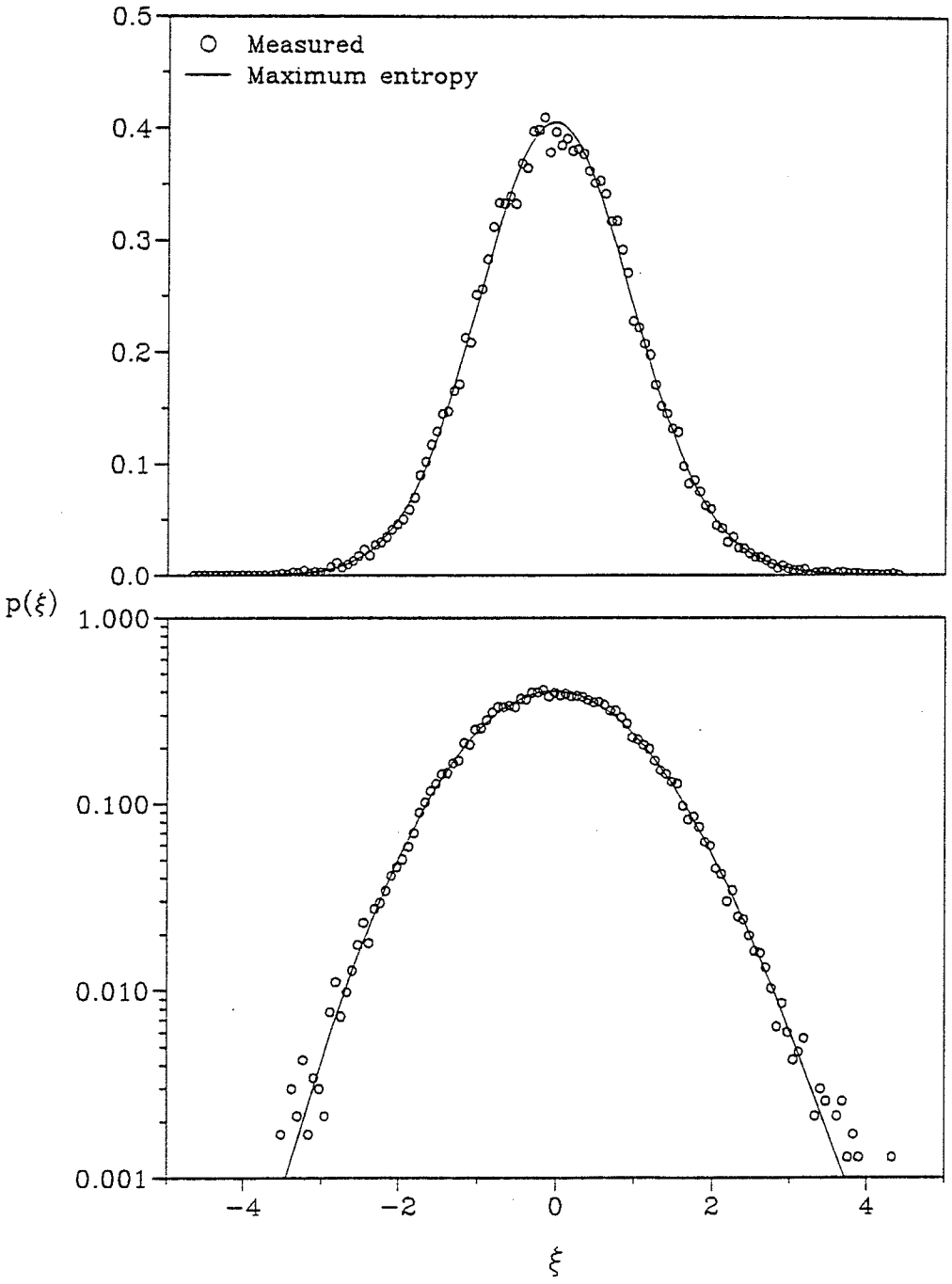

Figure 32. Distributions of probability density function of temperature fluctuation at r/d =0.0 and x/d = 33.3

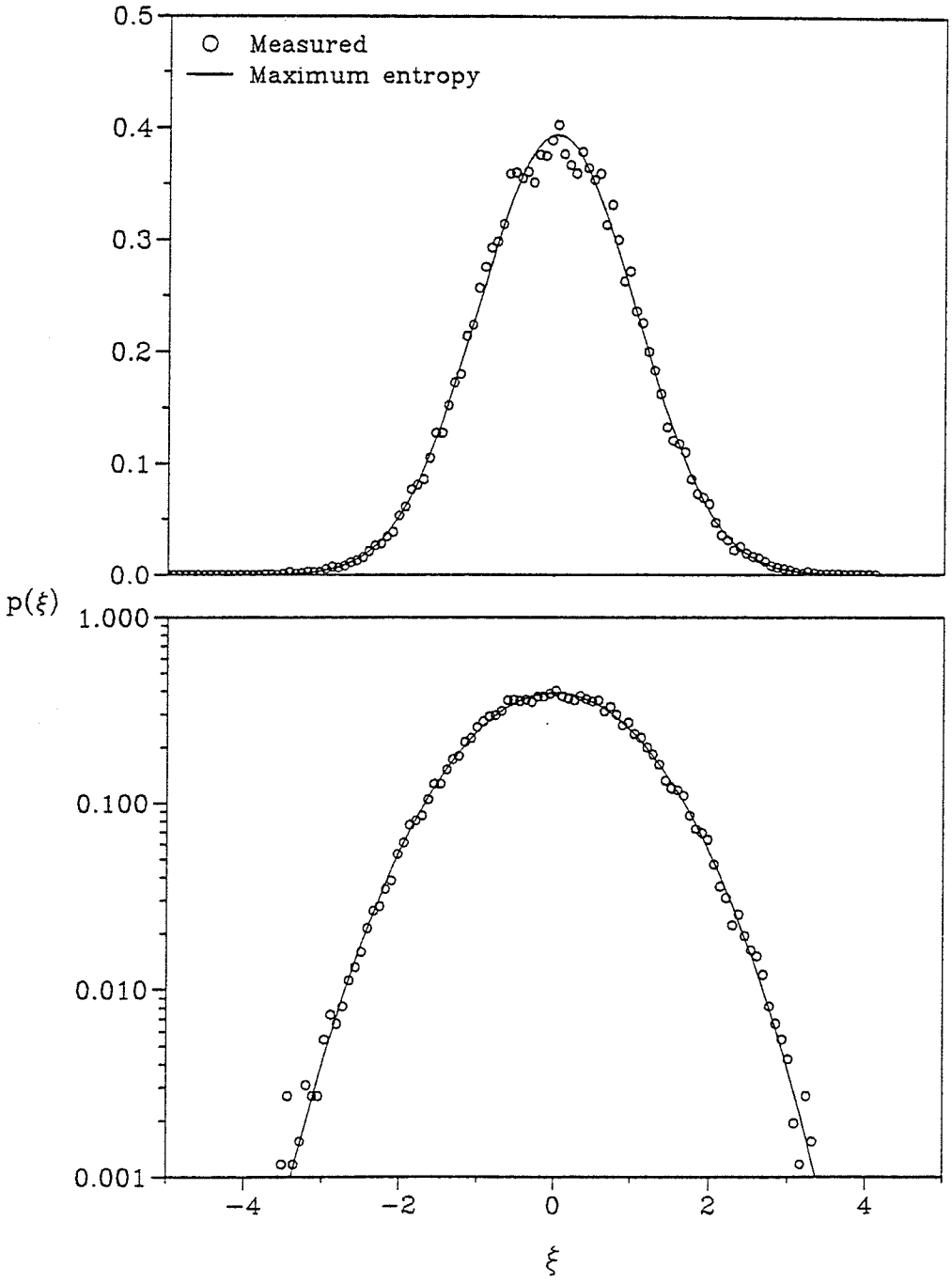

Figure 33. Distributions of probability density function of temperature fluctuation at r/d =0.0 and x/d = 41.7

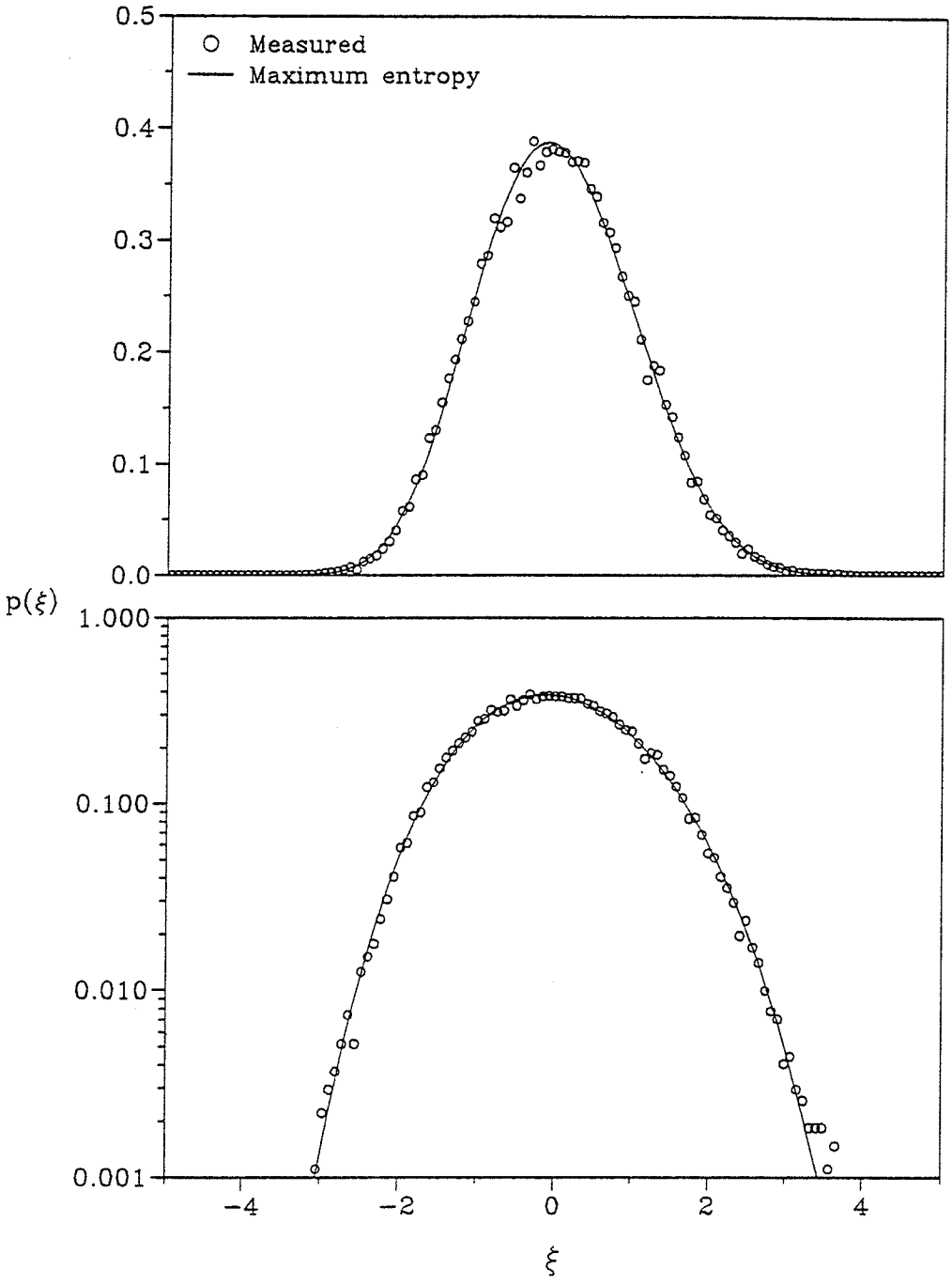

Figure 34. Distributions of probability density function of temperature fluctuation at r/d =0.0 and x/d = 50.0

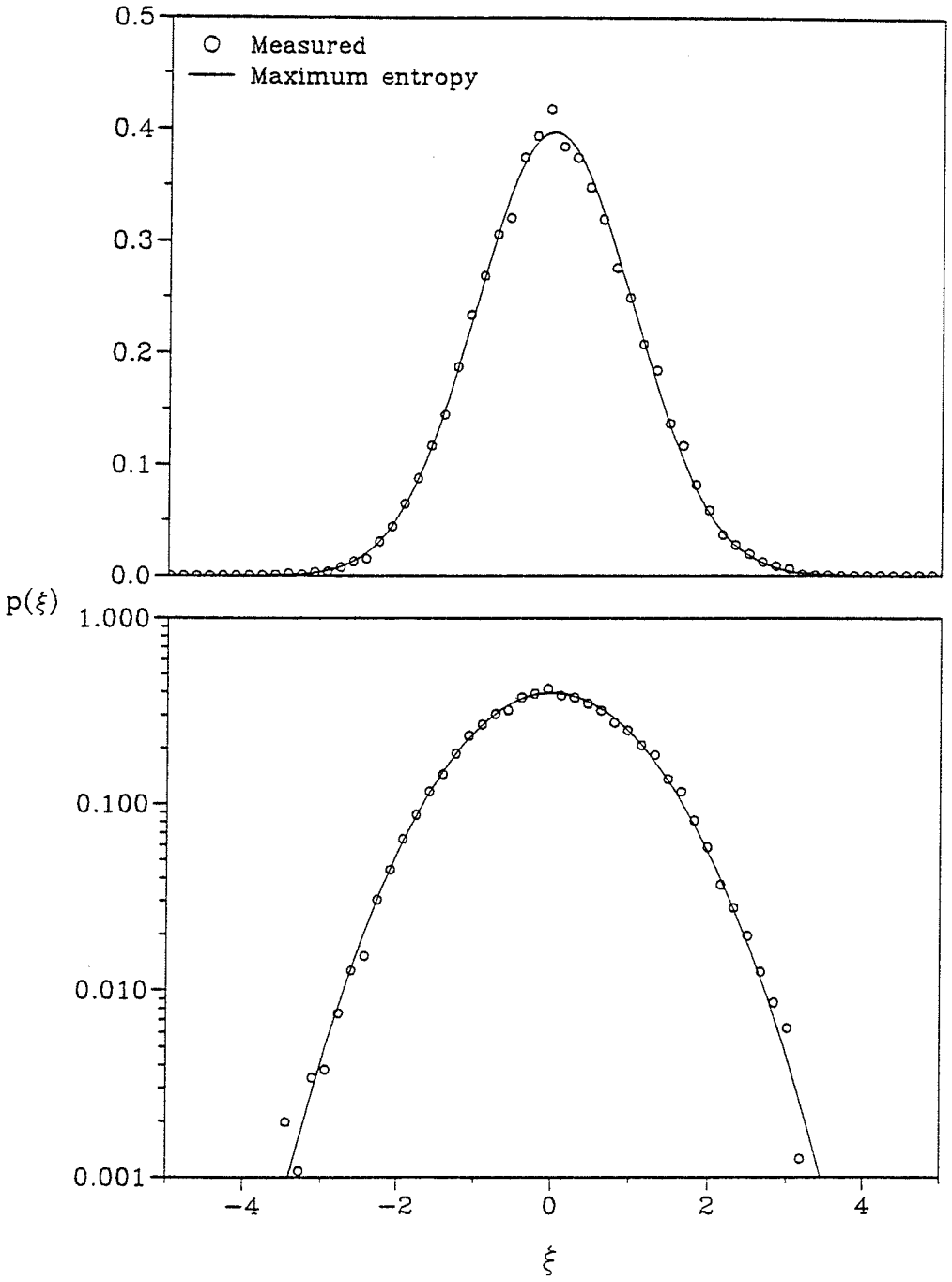

Figure 35. Distributions of probability density function of temperature fluctuation at r/d =0.0 and x/d = 58.3

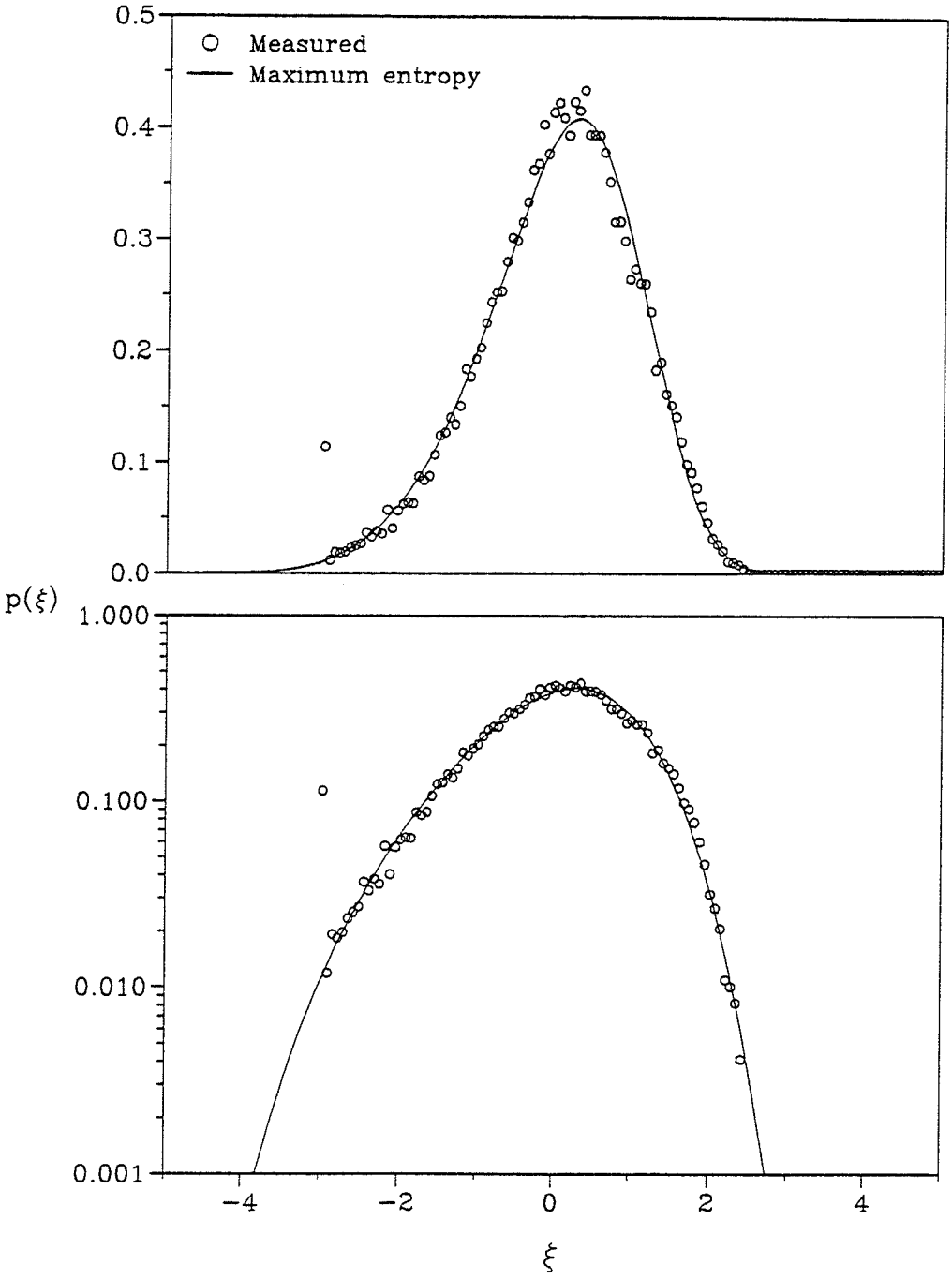

Figure 36. Distributions of probability density function of temperature fluctuation at r/d =1.3 and x/d = 16.7

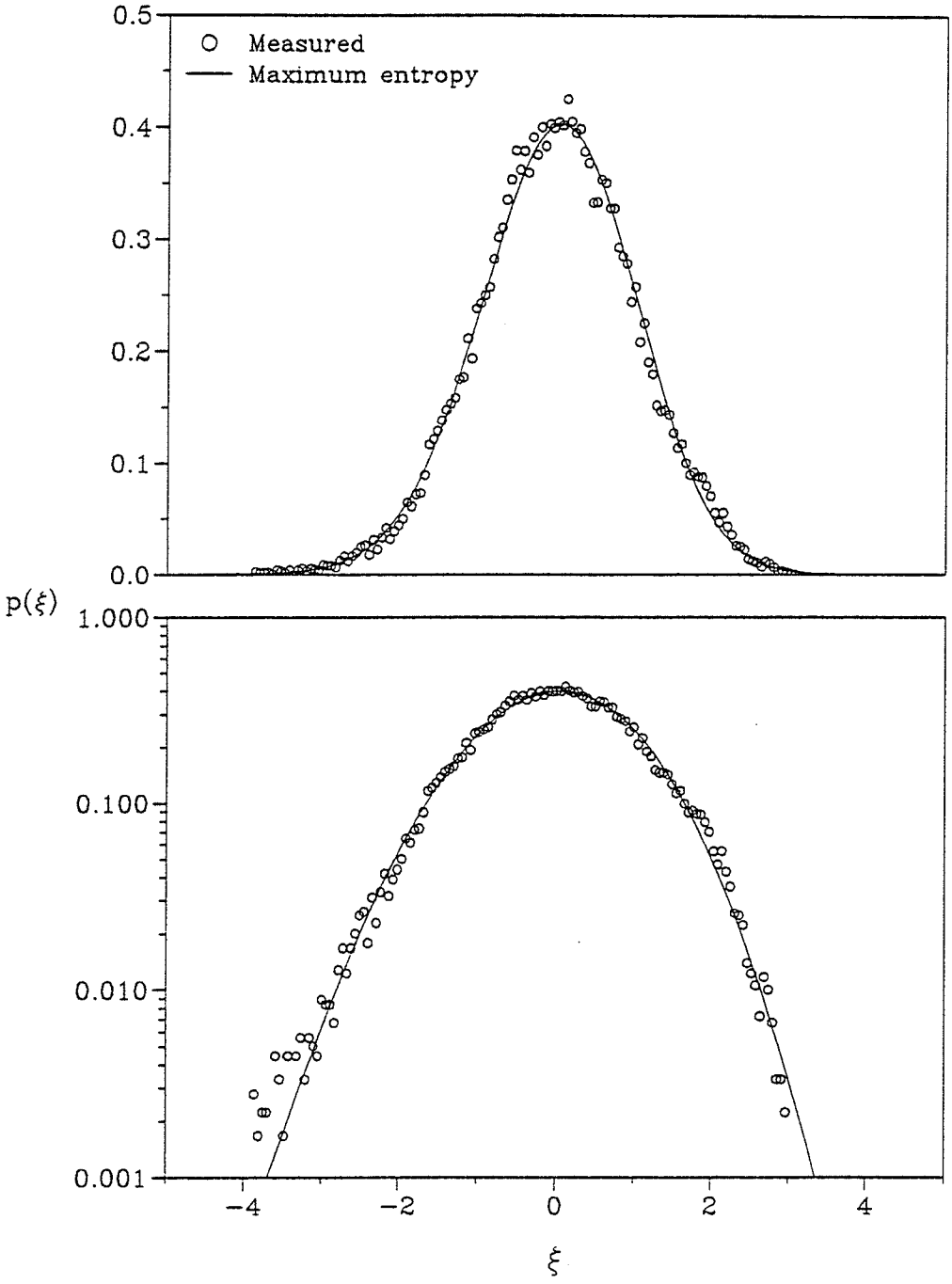

Figure 37. Distributions of probability density function of temperature fluctuation at r/d =1.3 and x/d = 25.0

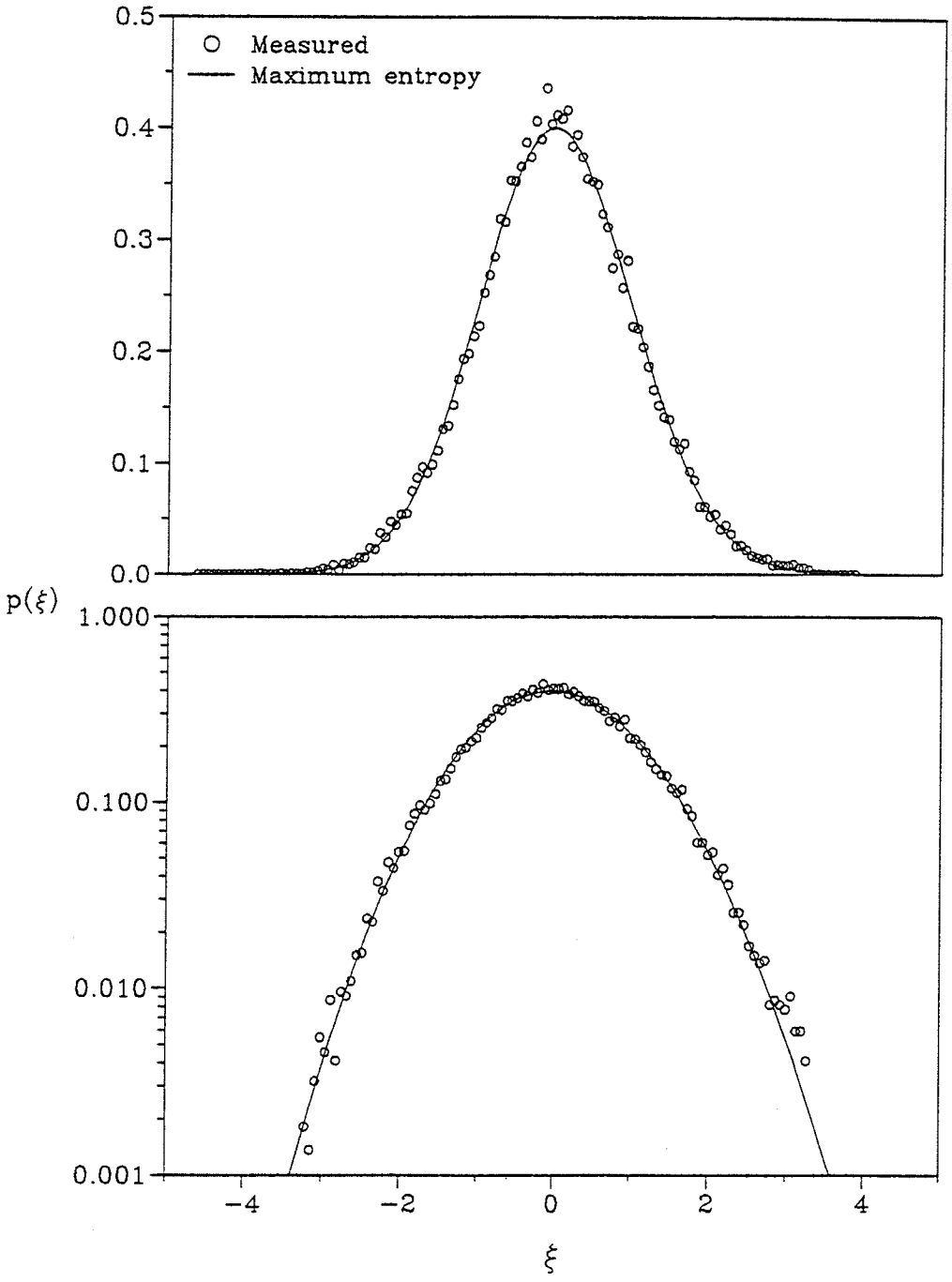

Figure 38. Distributions of probability density function of temperature fluctuation at r/d =1.3 and x/d = 33.3

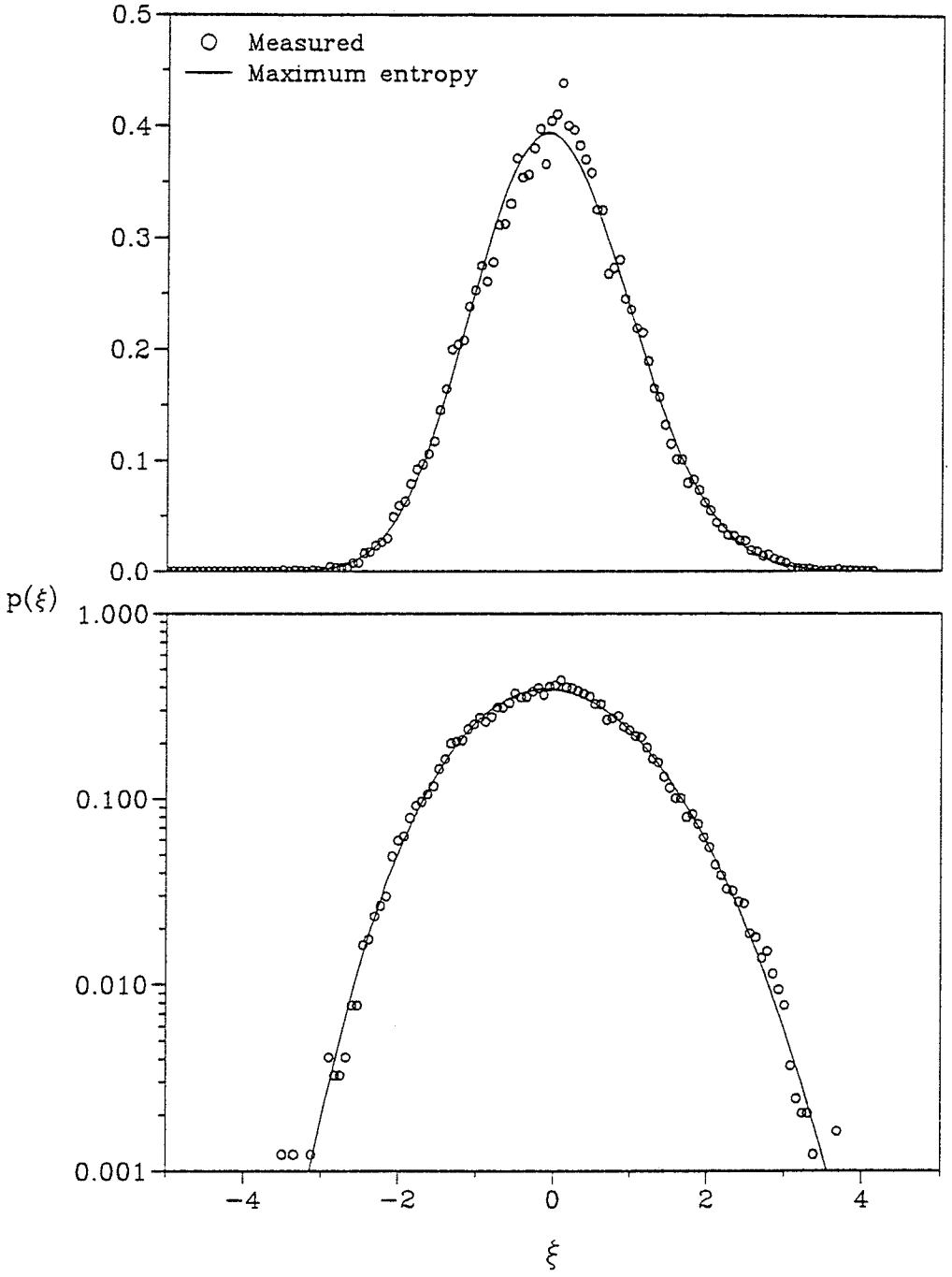

Figure 39. Distributions of probability density function of temperature fluctuation at r/d =1.3 and x/d = 41.7

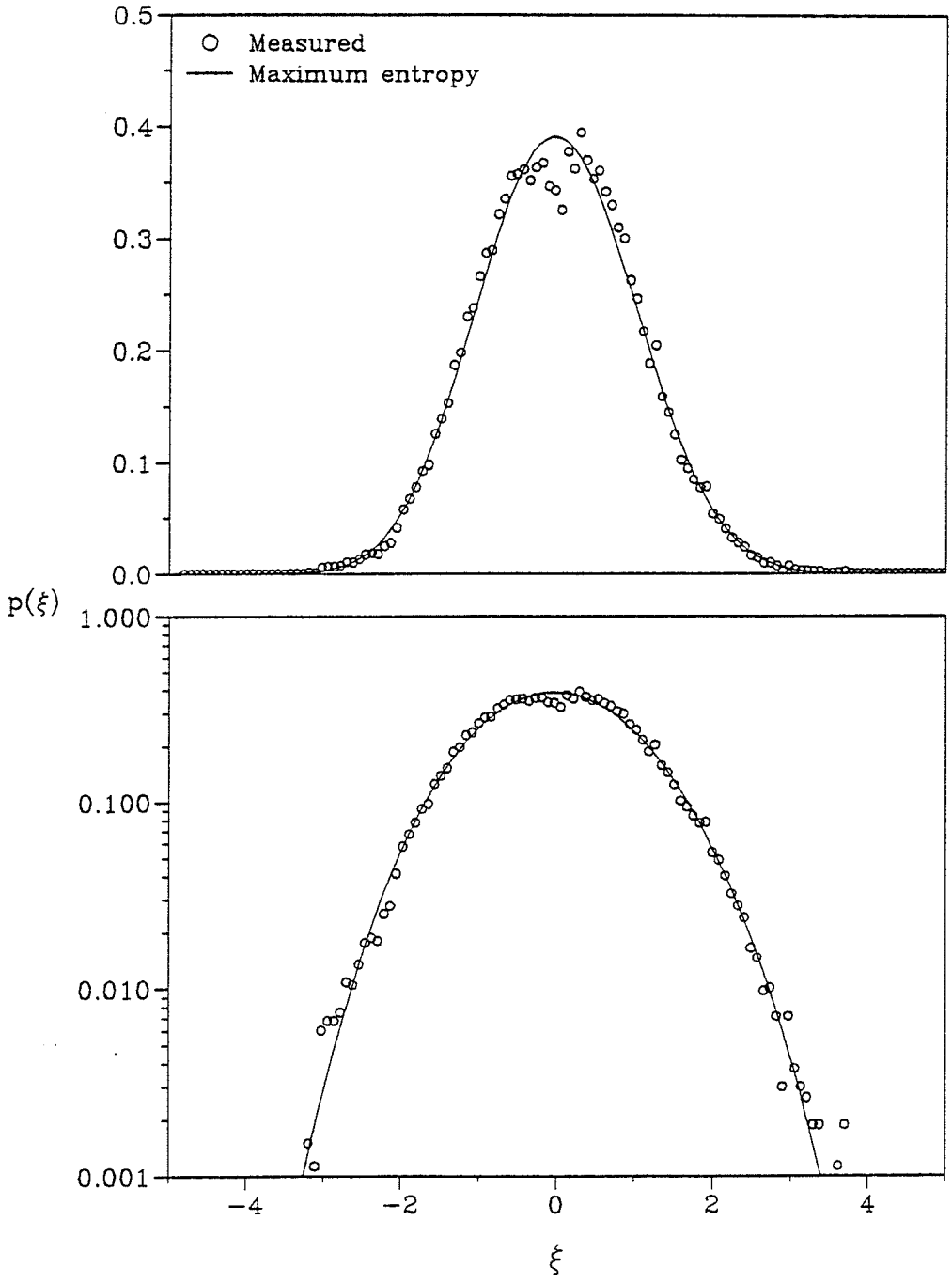

Figure 40. Distributions of probability density function of temperature fluctuation at r/d =1.3 and x/d = 50.0

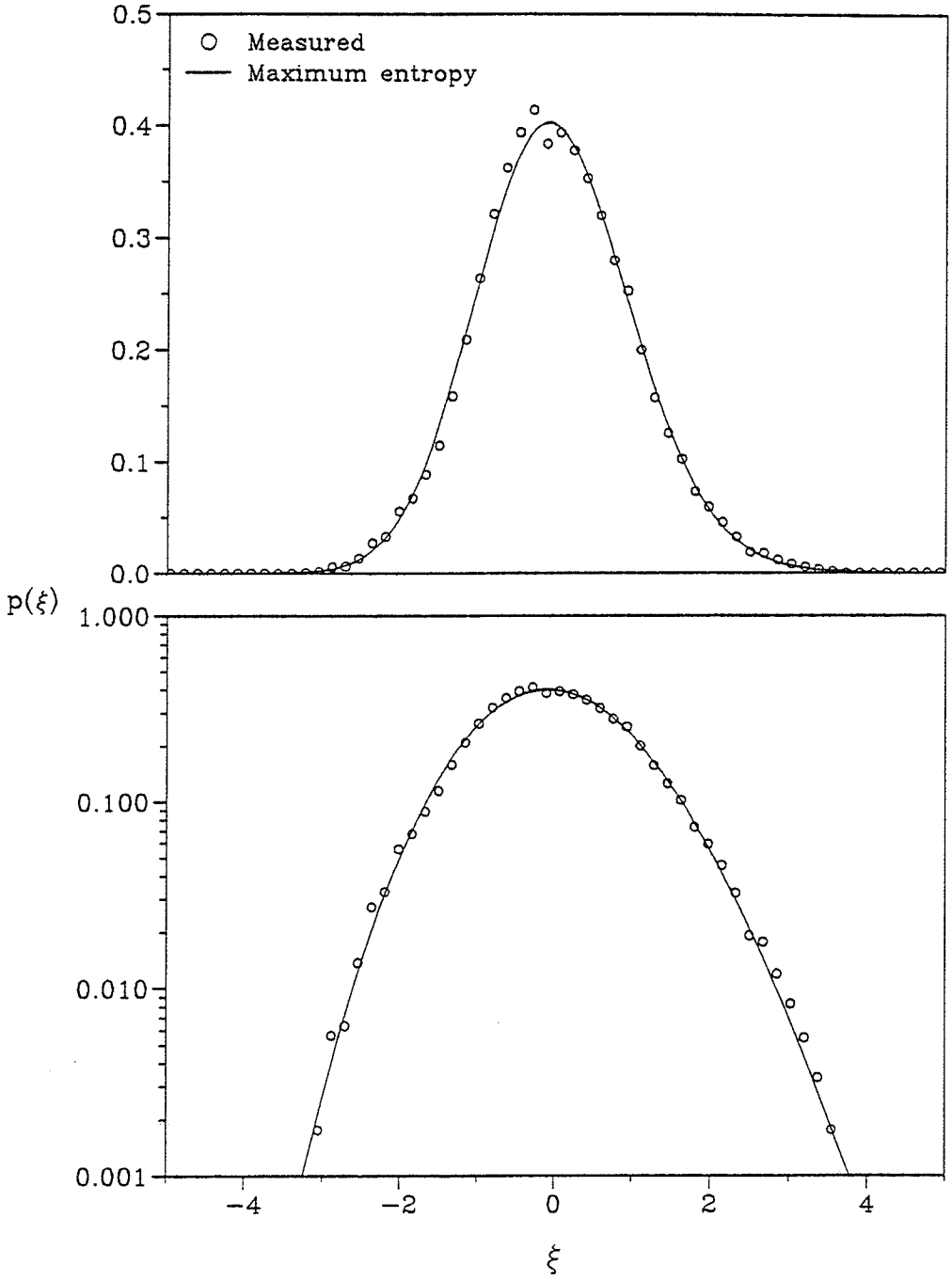

Figure 41. Distributions of probability density function of temperature fluctuation at r/d =1.3 and x/d = 58.3

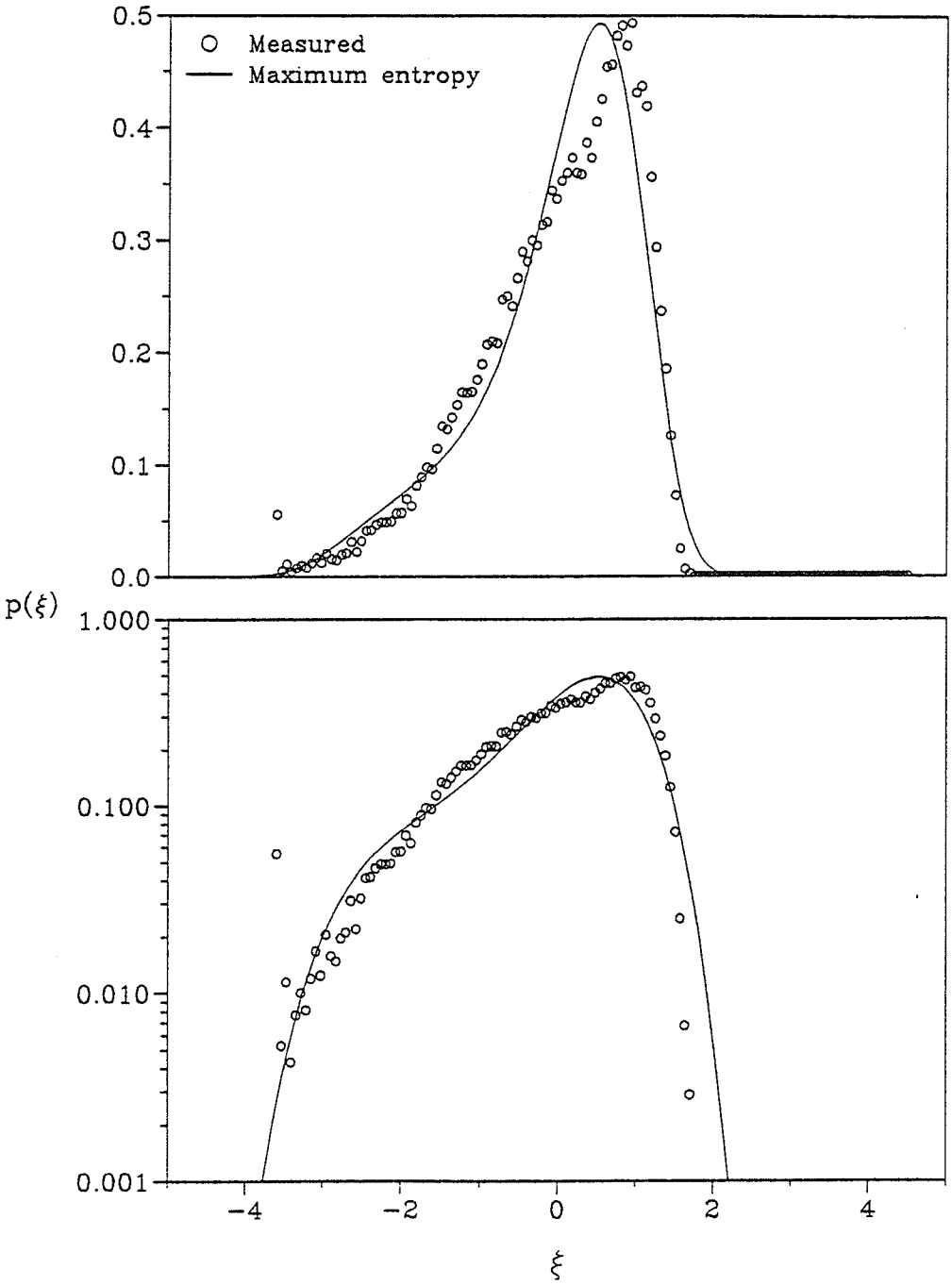

Figure 42. Distributions of probability density function of temperature fluctuation at r/d =2.7 and x/d = 16.7

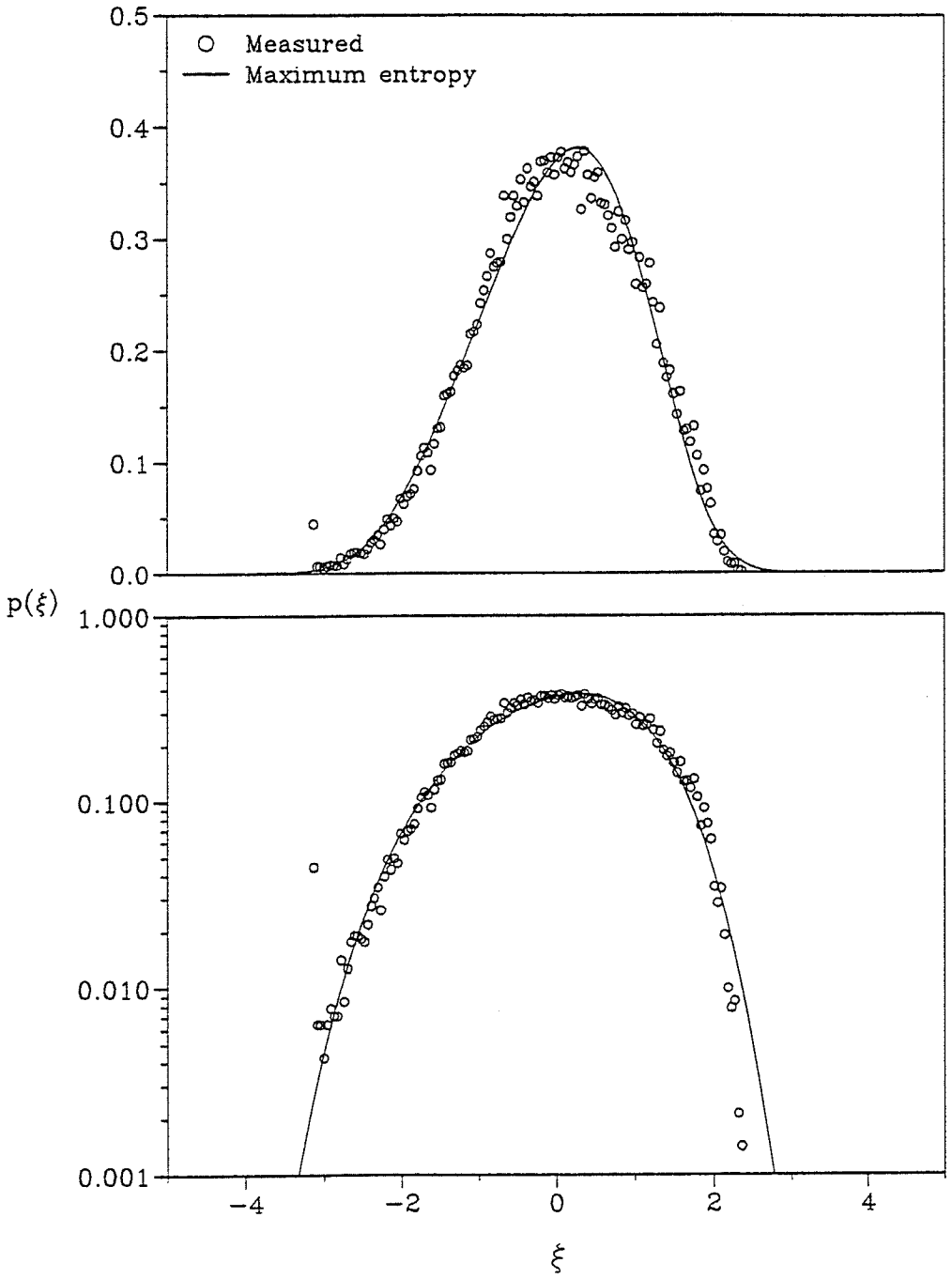

Figure 43. Distributions of probability density function of temperature fluctuation at r/d =2.7 and x/d = 25.0

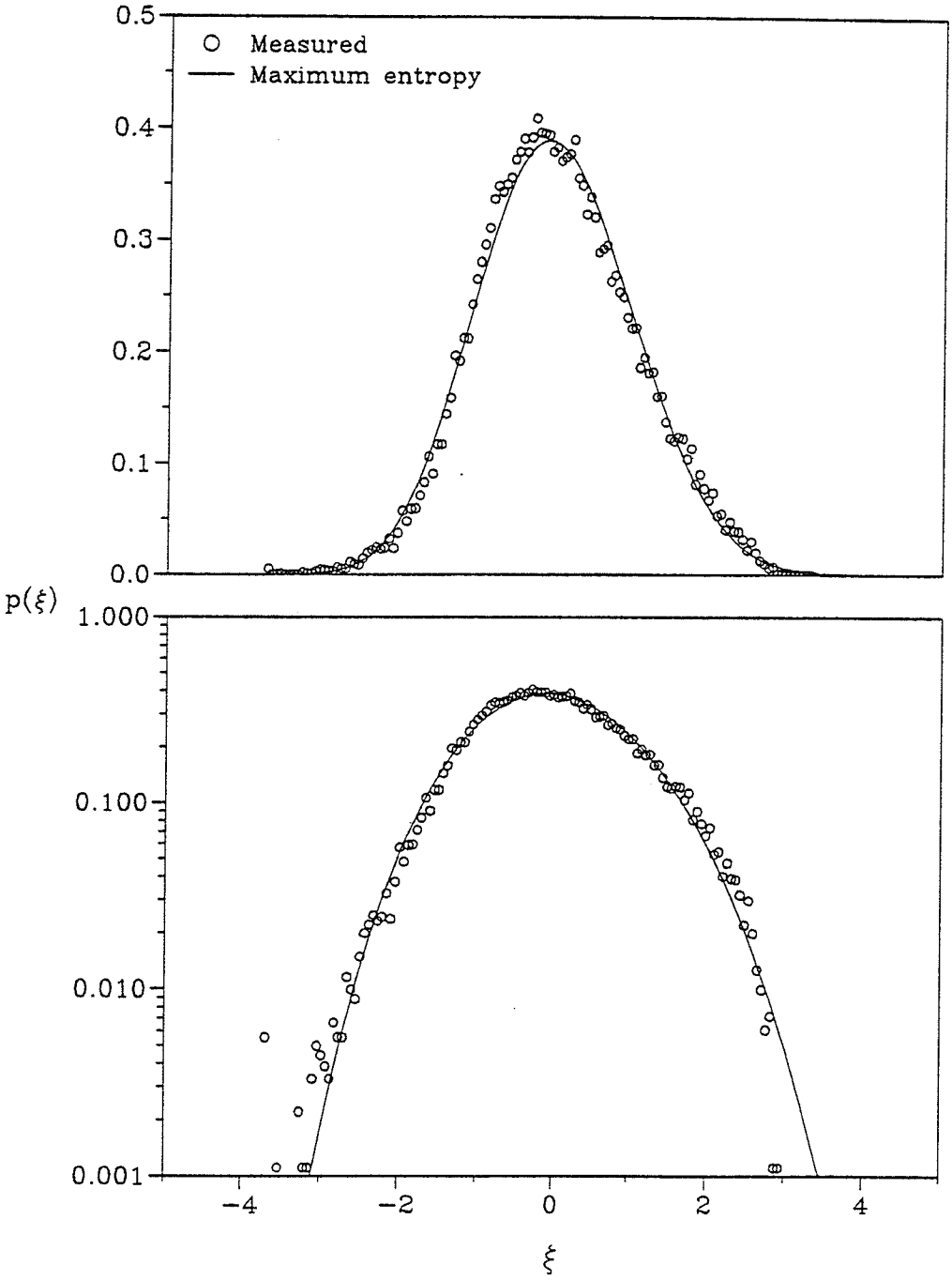

Figure 44. Distributions of probability density function of temperature fluctuation at r/d =2.7 and x/d = 33.3

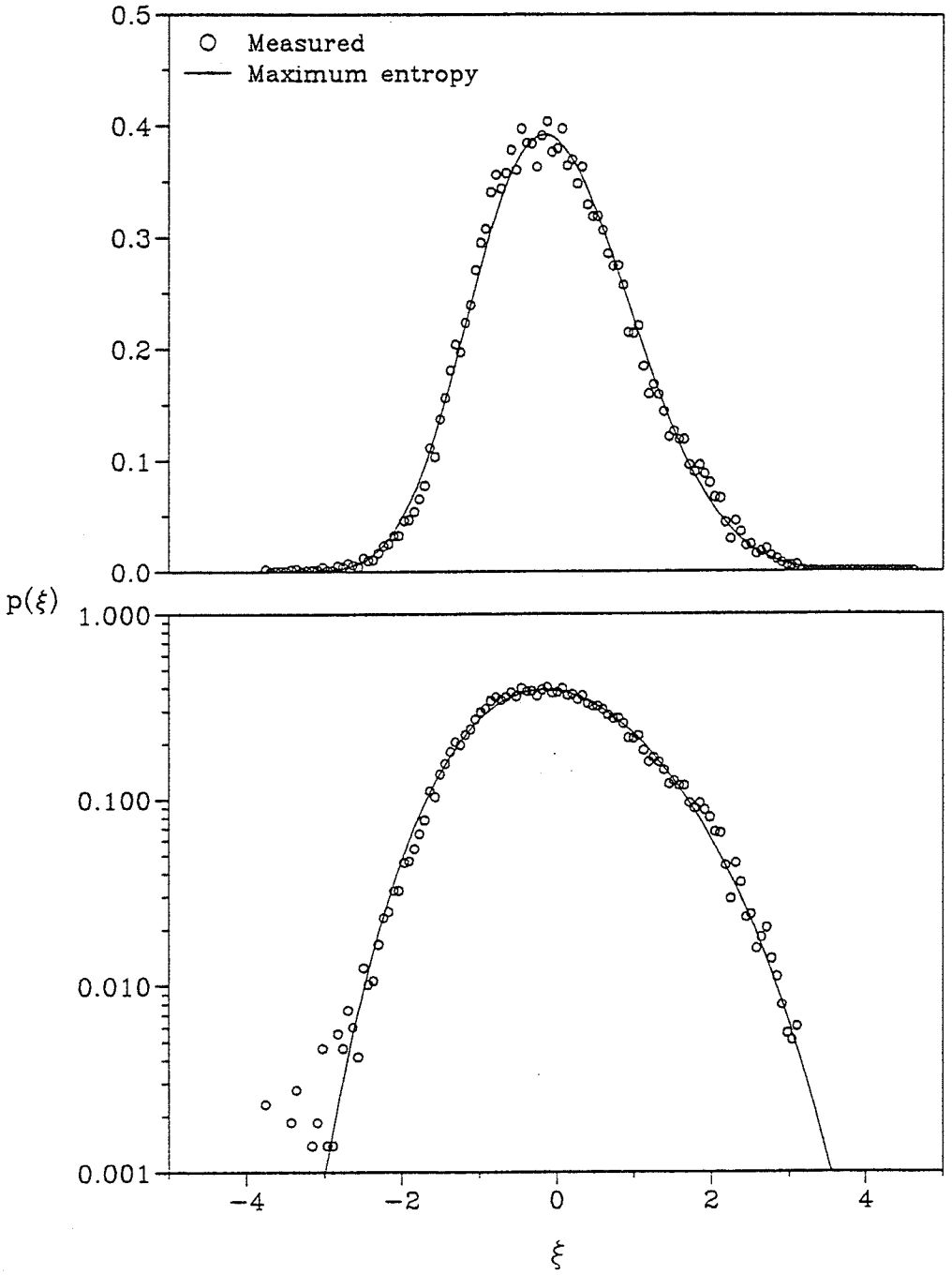

Figure 45. Distributions of probability density function of temperature fluctuation at r/d =2.7 and x/d = 41.7

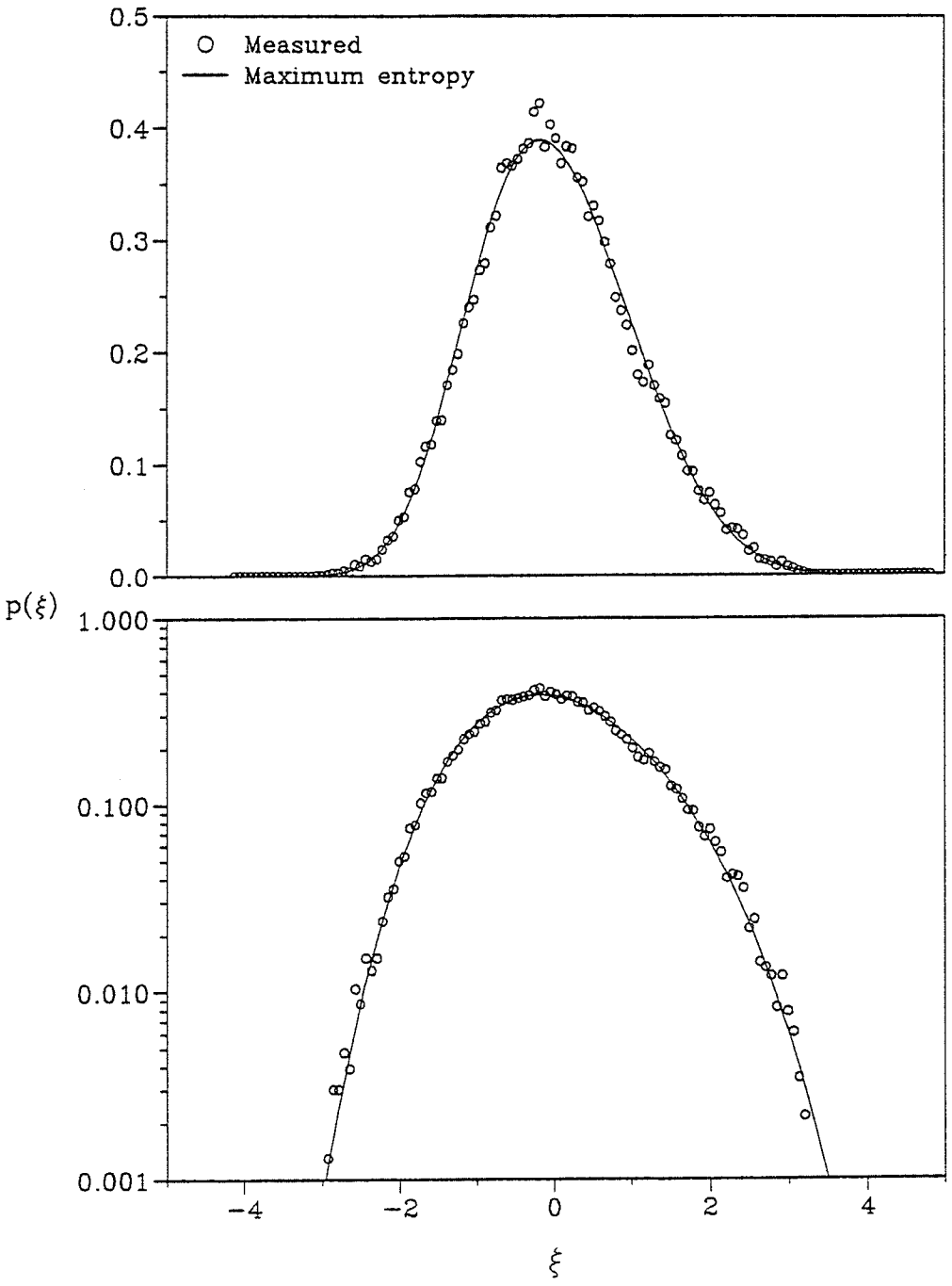

Figure 46. Distributions of probability density function of temperature fluctuation at r/d =2.7 and x/d = 50.0

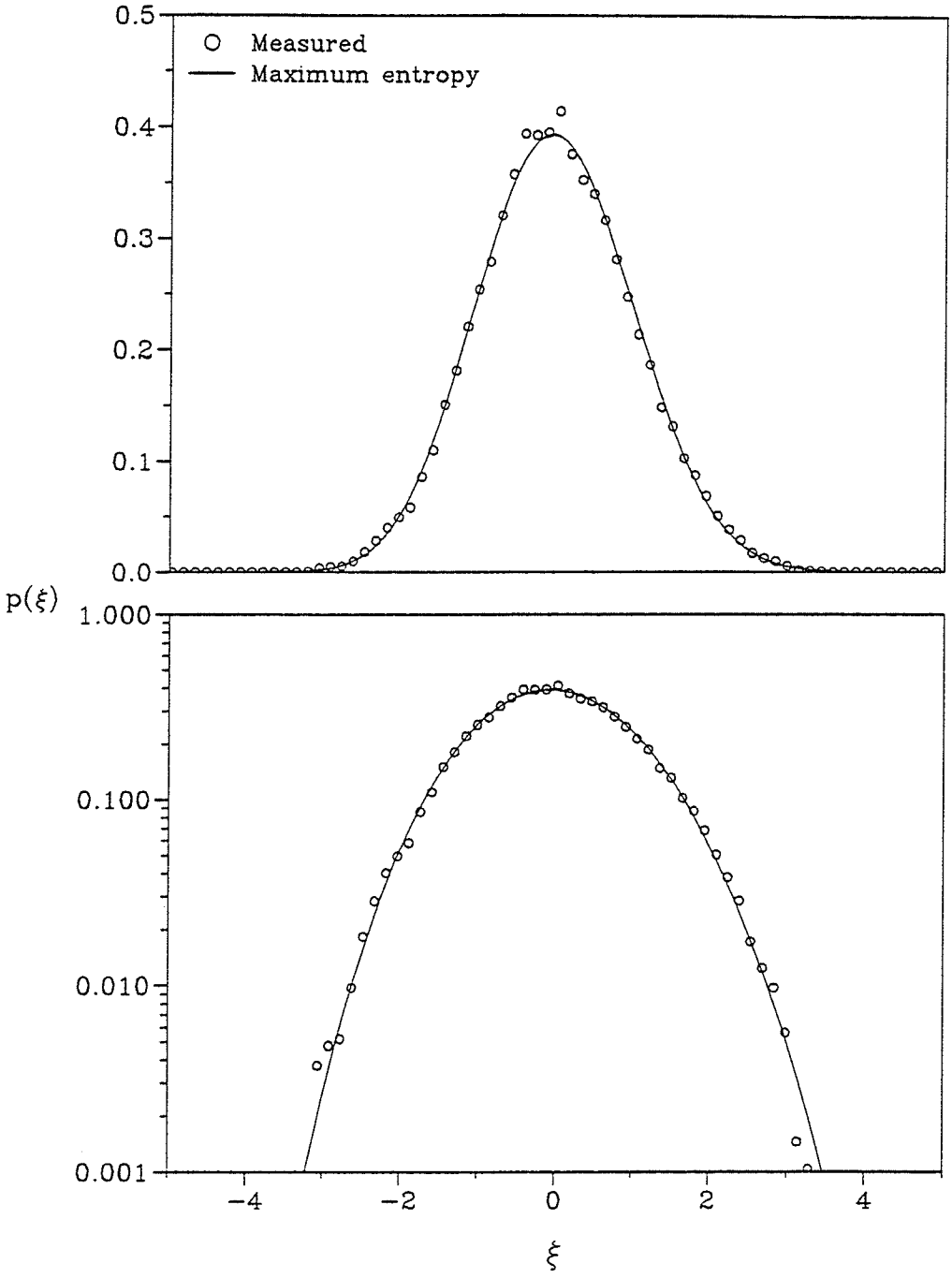

Figure 47. Distributions of probability density function of temperature fluctuation at r/d =2.7 and x/d = 58.3

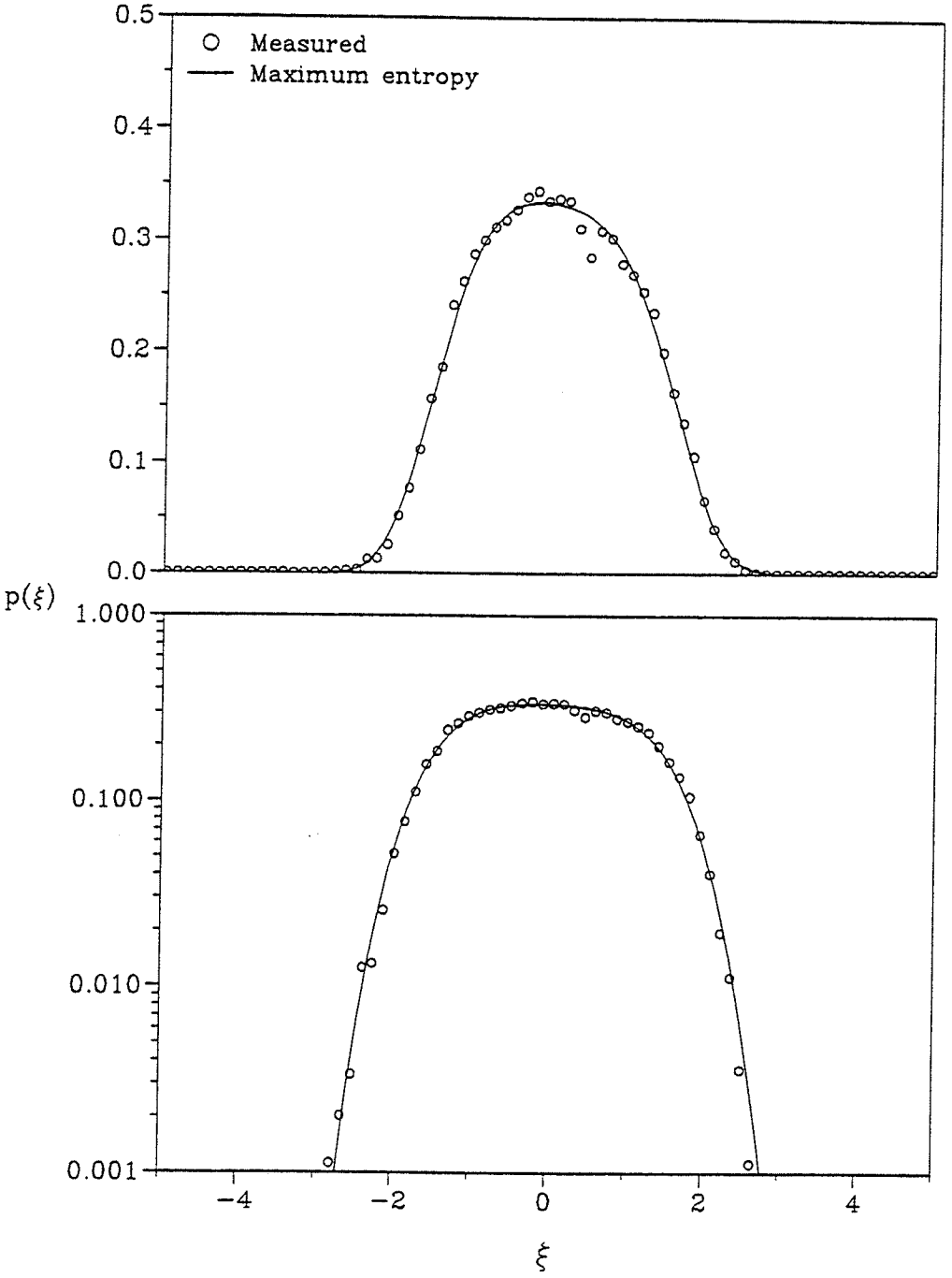

Figure 48. Distributions of probability density function of temperature fluctuation at r/d =5.0 and x/d = 16.7

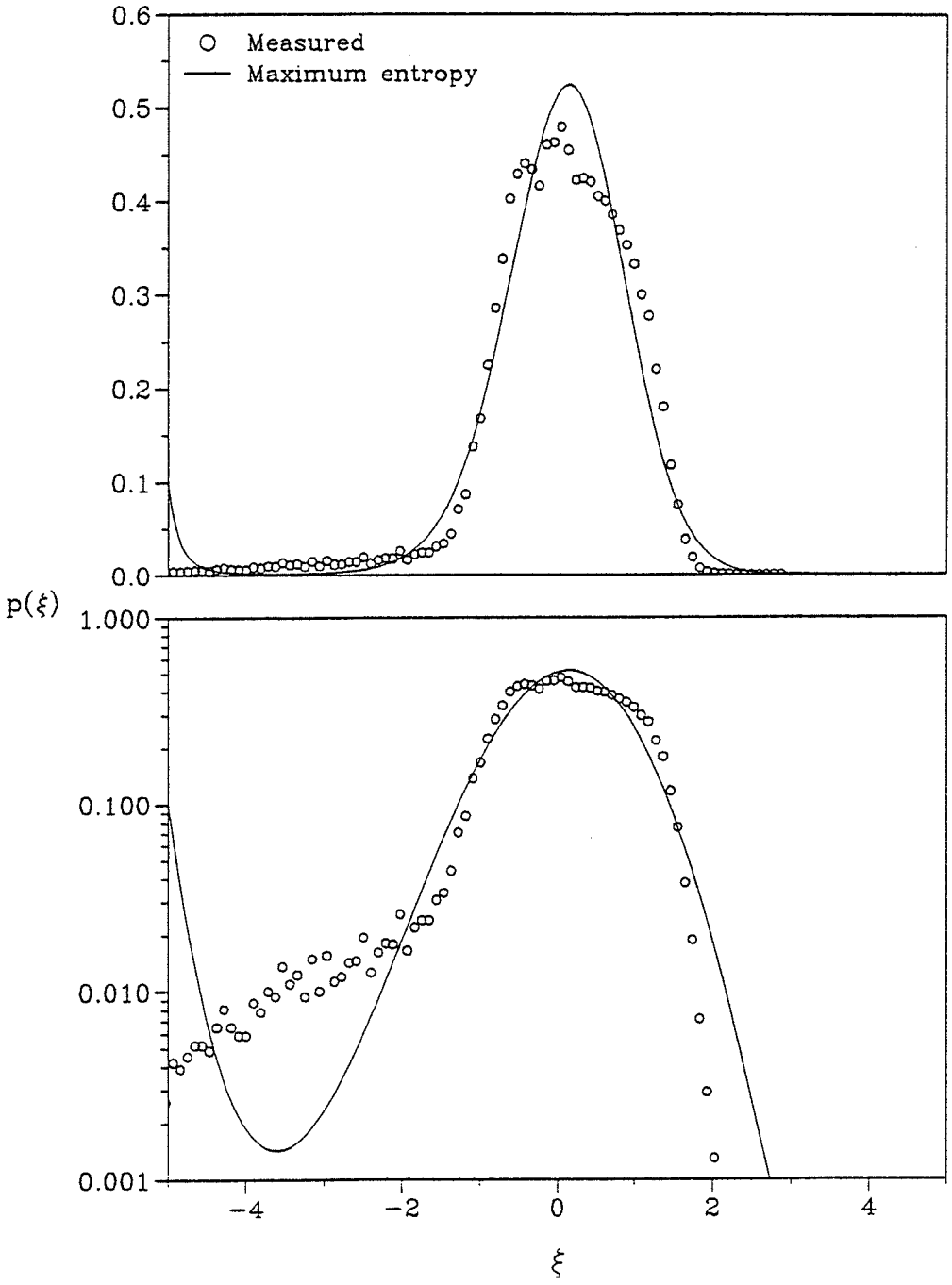

Figure 49. Distributions of probability density function of temperature fluctuation at r/d =5.0 and x/d = 25.0

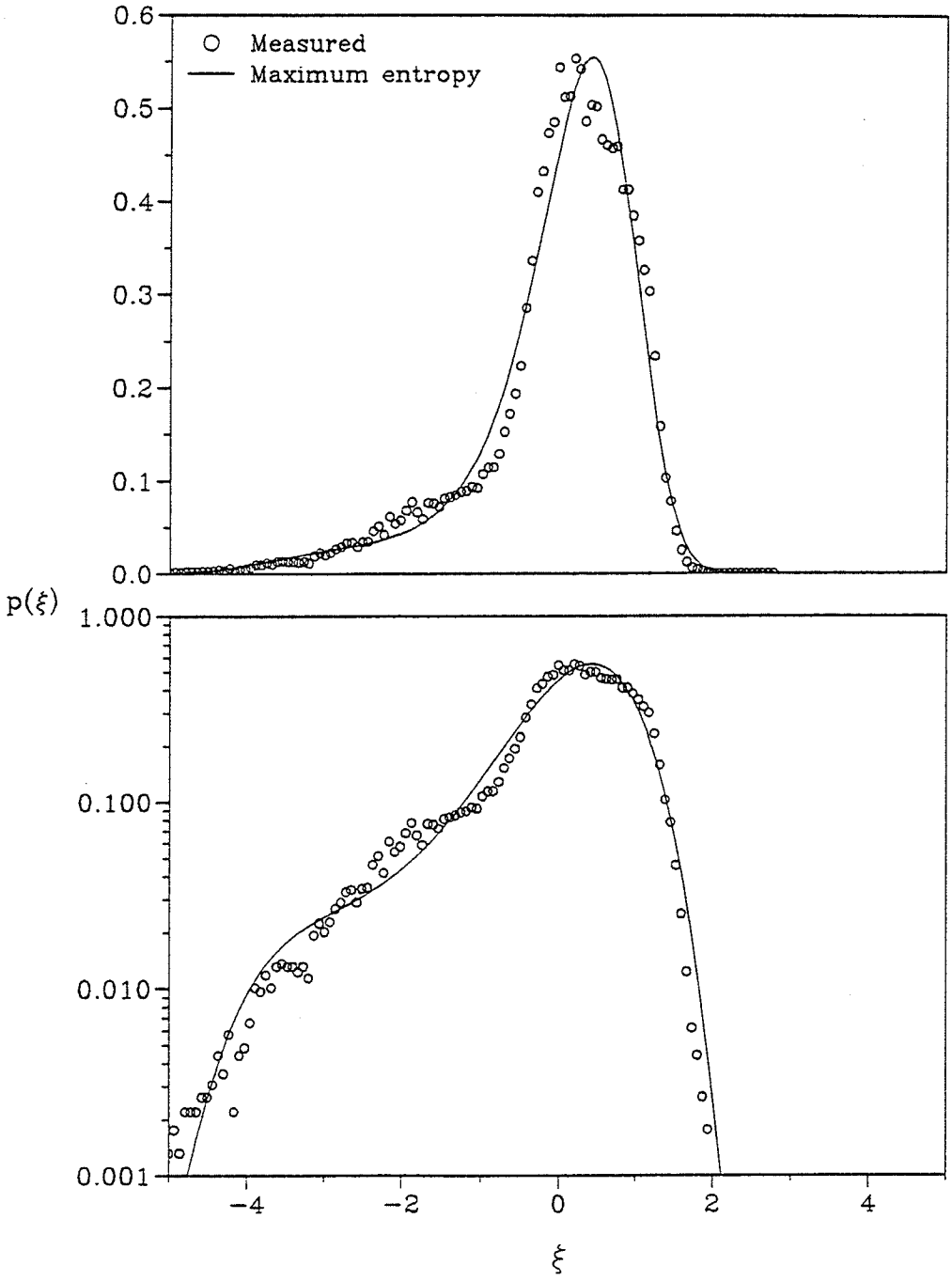

Figure 50. Distributions of probability density function of temperature fluctuation at r/d =5.0 and x/d = 33.3

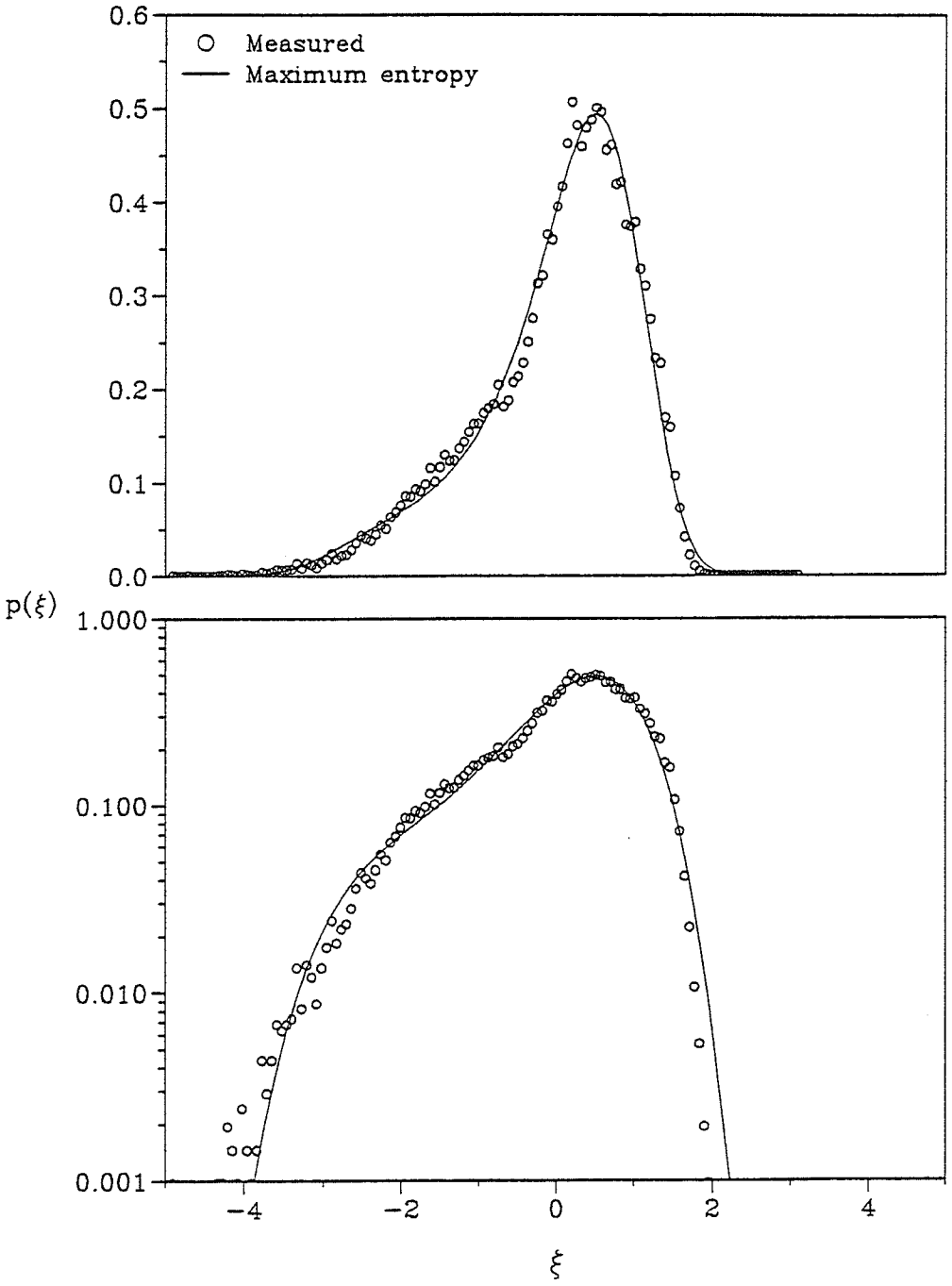

Figure 51. Distributions of probability density function of temperature fluctuation at r/d =5.0 and x/d = 41.7

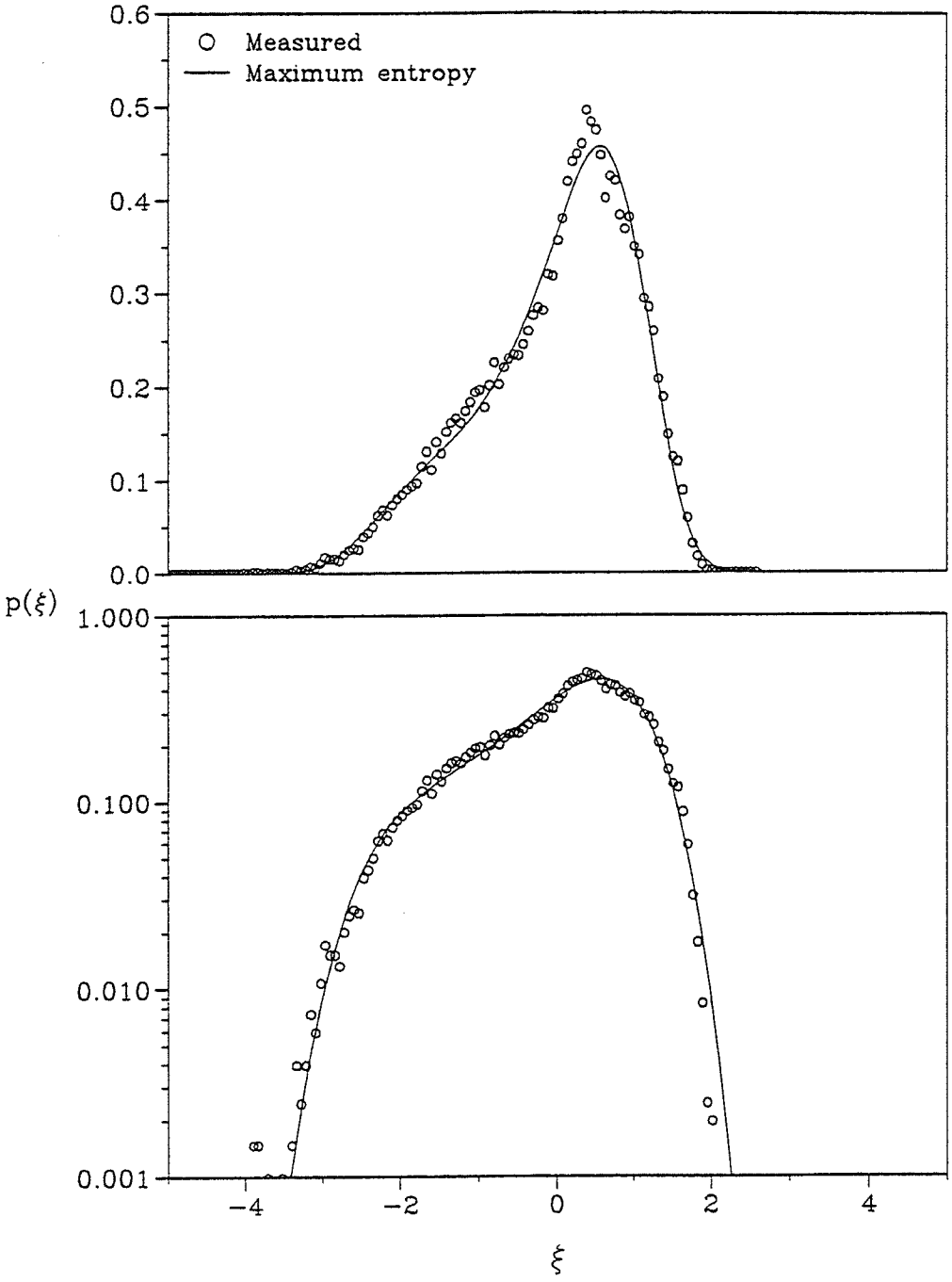

Figure 52. Distributions of probability density function of temperature fluctuation at r/d =5.0 and x/d = 50.0

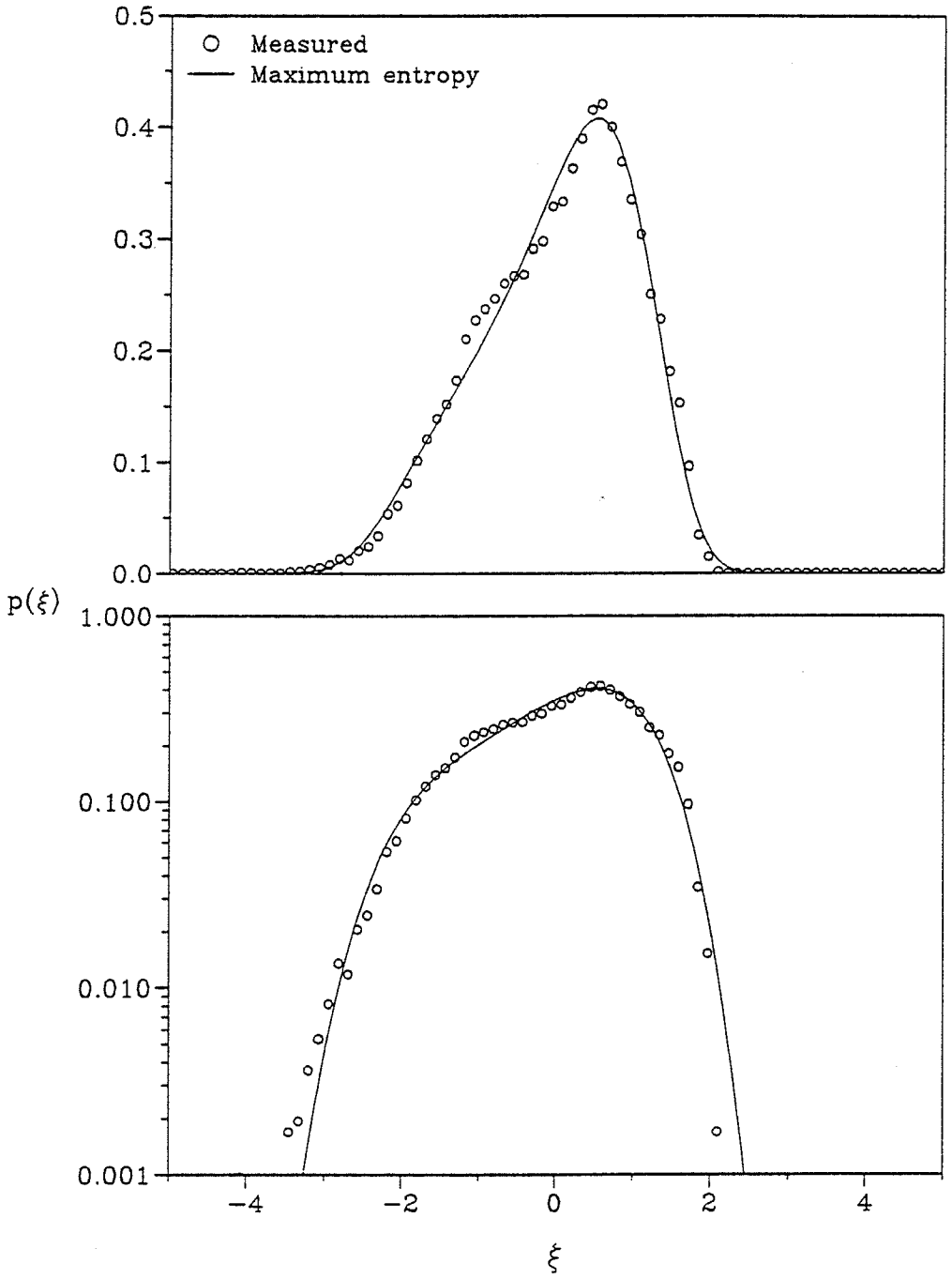

Figure 53. Distributions of probability density function of temperature fluctuation at r/d =5.0 and x/d = 58.3

APPENDIX

TABLE 1 (a)

Pitot tube measurements ($\overline{U} / U_{ref}$)

	x/d						
r/d	16.67	25.00	33.33	41.67	50.00	58.33	66.67
-7.33	0.92	0.92	0.91	0.92	0.88	0.93	0.93
-6.67	0.99	0.99	0.98	0.98	0.96	1.00	0.99
-6.33	1.01	1.01	1.00	1.01	0.99	1.02	1.01
-5.67	1.05	1.05	1.04	1.04	1.03	1.05	1.03
-5.00	1.08	1.08	1.07	1.07	1.06	1.07	1.05
-4.33	1.10	1.10	1.08	1.08	1.06	1.07	1.05
-3.67	1.12	1.11	1.08	1.07	1.05	1.05	1.04
-3.00	1.13	1.10	1.06	1.05	1.04	1.04	1.03
-2.33	1.11	1.06	1.03	1.02	1.02	1.02	1.02
-1.67	1.05	1.01	1.00	1.00	1.00	1.01	1.00
-1.00	0.96	1.01	0.96	0.98	0.99	1.00	0.99
-0.33	0.89	0.93	0.95	0.96	0.98	0.99	0.99
0.00	0.87	0.92	0.94	0.96	0.97	0.99	0.99
0.33	0.87	0.92	0.94	0.97	0.97	1.00	0.99
1.00	0.92	0.95	0.96	0.98	0.98	1.00	1.00
1.67	1.00	0.99	0.99	1.00	1.00	1.02	1.01
2.33	1.08	1.05	1.02	1.02	1.01	1.04	1.02
3.00	1.13	1.09	1.06	1.05	1.04	1.06	1.03
3.67	1.14	1.12	1.09	1.07	1.06	1.07	1.05
4.33	1.13	1.12	1.10	1.09	1.08	1.08	1.06
5.00	1.11	1.11	1.09	1.08	1.08	1.08	1.06
5.33	1.10	1.09	1.08	1.08	1.08	1.07	1.06

TABLE 1 (b)

Pitot tube measurements ($\overline{U} / U_{ref}$)

	x/d					
r/d	83.33	100.00	116.67	133.33	150.00	166.67
-7.33	0.95	0.95	0.97	0.87	0.89	0.90
-6.67	1.00	1.01	1.02	0.96	0.96	0.98
-6.33	1.02	1.03	1.03	0.99	0.99	1.00
-5.67	1.04	1.04	1.05	1.02	1.03	1.04
-5.00	1.05	1.05	1.06	1.05	1.05	1.06
-4.33	1.05	1.04	1.05	1.06	1.06	1.07
-3.67	1.04	1.04	1.05	1.06	1.07	1.07
-3.00	1.03	1.03	1.04	1.05	1.06	1.07
-2.33	1.02	1.02	1.03	1.05	1.06	1.07
-1.67	1.01	1.01	1.03	1.05	1.05	1.06
-1.00	1.00	1.01	1.02	1.04	1.05	1.06
-0.33	1.00	1.01	1.02	1.04	1.05	1.06
0.00	1.00	1.01	1.02	1.04	1.05	1.05

TABLE 2 (a)

Hot-wire measurements (radial distributions)

r/d	x/d = 16.67		x/d = 25.00		x/d = 33.33		x/d = 41.67	
	$\overline{U} / U_{ref}$	u' / U_{ref} (%)	$\overline{U} / U_{ref}$	u' / U_{ref} (%)	$\overline{U} / U_{ref}$	u' / U_{ref} (%)	$\overline{U} / U_{ref}$	u' / U_{ref} (%)
-7.33	0.93	9.17	0.86	8.74	0.89	8.82	0.89	9.30
-6.67	0.98	8.29	0.93	7.79	0.96	8.22	0.98	8.26
-6.33	1.01	8.02	0.95	7.71	0.98	7.84	1.00	7.88
-5.67	1.04	7.44	0.99	7.17	1.02	7.09	1.04	7.33
-5.00	1.08	6.59	1.02	6.65	1.04	6.68	1.07	6.67
-4.33	1.10	6.37	1.05	6.39	1.05	6.68	1.07	6.78
-3.67	1.12	6.64	1.05	6.86	1.05	7.48	1.06	7.66
-3.00	1.08	8.51	1.04	8.51	1.02	8.74	1.03	8.42
-2.33	1.04	11.26	1.00	10.31	0.99	9.49	1.01	8.75
-1.67	0.96	14.25	0.95	11.34	0.95	9.80	0.98	8.81
-1.00	0.86	15.59	0.90	11.86	0.92	9.80	0.97	8.75
-0.33	0.81	15.92	0.87	11.86	0.90	9.80	0.95	8.72
0.00	0.80	15.92	0.86	11.86	0.90	9.80	0.95	8.72
0.33	0.81	15.90	0.86	11.86	0.90	9.80	0.95	8.72
1.00	0.88	15.10	0.88	11.91	0.91	9.80	0.96	8.75
1.67	0.98	13.15	0.92	11.86	0.93	9.85	0.98	8.75
2.33	1.05	10.38	0.98	11.09	0.96	9.85	1.00	8.75
3.00	1.08	7.96	1.02	9.49	1.00	9.08	1.03	8.75
3.67	1.08	6.04	1.05	7.73	1.03	7.94	1.05	7.88
4.33	1.06	6.04	1.06	6.24	1.05	6.70	1.07	7.06
5.00	1.04	6.56	1.04	6.19	1.04	6.19	1.06	6.56
5.33	1.02	6.59	1.04	6.19	1.03	6.24	1.06	6.56

TABLE 2 (b)

Hot-wire measurements (radial distributions)

r/d	x/d = 50.00		x/d = 58.33		x/d = 66.67	
	$\overline{U} / U_{ref}$	u' / U_{ref} (%)	$\overline{U} / U_{ref}$	u' / U_{ref} (%)	$\overline{U} / U_{ref}$	u' / U_{ref} (%)
-7.33	0.90	8.86	0.91	9.07	0.91	8.59
-6.67	0.97	8.20	0.98	8.22	0.98	8.01
-6.33	0.99	7.71	1.00	7.74	1.00	7.47
-5.67	1.03	7.11	1.04	6.94	1.02	6.78
-5.00	1.05	6.56	1.05	6.41	1.04	6.14
-4.33	1.05	6.62	1.05	6.46	1.04	5.93
-3.67	1.04	7.16	1.04	6.91	1.03	6.22
-3.00	1.02	7.66	1.02	6.99	1.01	6.41
-2.33	1.00	7.71	1.01	6.99	1.00	6.41
-1.67	0.98	7.71	0.99	6.99	0.98	6.35
-1.00	0.97	7.66	0.98	6.94	0.98	6.22
-0.33	0.95	7.60	0.97	6.89	0.97	6.30
0.00	0.95	7.60	0.97	6.89	0.97	6.35
0.33	0.95	7.60	0.97	6.89	0.98	6.35
1.00	0.96	7.66	0.98	6.94	0.98	6.38
1.67	0.97	7.71	1.00	7.15	1.00	6.46
2.33	0.99	7.71	1.01	7.21	1.01	6.46
3.00	1.01	7.66	1.03	7.21	1.02	6.43
3.67	1.03	7.16	1.05	6.94	1.04	6.41
4.33	1.05	6.62	1.06	6.46	1.04	6.03
5.00	1.05	6.62	1.06	6.41	1.04	5.93
5.33	1.03	6.56	1.05	6.51	1.03	6.25

TABLE 2 (c)

Hot-wire measurements (radial distributions)

r/d	x/d = 53.33		x/d = 100.00		x/d = 116.67	
	$\overline{U} / U_{ref}$	u' / U_{ref} (%)	$\overline{U} / U_{ref}$	u' / U_{ref} (%)	$\overline{U} / U_{ref}$	u' / U_{ref} (%)
-7.33	0.84	8.30	0.87	8.12	0.90	7.78
-6.67	0.92	7.59	0.94	7.27	0.97	6.95
-6.33	0.95	7.21	0.97	6.82	0.99	6.38
-5.67	0.99	6.25	1.00	5.81	1.01	5.44
-5.00	1.00	5.58	1.01	5.24	1.02	4.87
-4.33	1.01	5.47	1.02	5.06	1.02	4.69
-3.67	1.00	5.54	1.01	5.06	1.02	4.67
-3.00	0.99	5.60	1.00	5.03	1.02	4.64
-2.33	0.98	5.58	1.00	5.01	1.01	4.62
-1.67	0.97	5.49	0.99	4.92	1.01	4.60
-1.00	0.97	5.35	0.98	4.85	1.01	4.53
-0.33	0.96	5.22	0.98	4.76	1.01	4.48
0.00	0.96	5.17	0.98	4.76	1.01	4.46

TABLE 2 **(d)**

Hot-wire measurements (radial distributions)

r/d	x/d = 133.33		x/d = 150.00		x/d = 166.67	
	$\overline{U} / U_{ref}$	u' / U_{ref} (%)	$\overline{U} / U_{ref}$	u' / U_{ref} (%)	$\overline{U} / U_{ref}$	u' / U_{ref} (%)
-7.33	0.87	8.38	0.86	8.26	0.90	8.14
-6.67	0.96	7.61	0.96	7.58	0.98	7.35
-6.33	0.99	7.19	0.99	7.09	1.01	6.91
-5.67	1.03	6.11	1.03	6.04	1.05	5.88
-5.00	1.05	5.25	1.05	5.20	1.07	4.97
-4.33	1.06	4.74	1.06	4.55	1.08	4.43
-3.67	1.07	4.53	1.07	4.27	1.09	4.11
-3.00	1.06	4.50	1.07	4.22	1.09	4.01
-2.33	1.06	4.48	1.06	4.20	1.09	3.99
-1.67	1.05	4.46	1.06	4.20	1.08	3.99
-1.00	1.05	4.46	1.05	4.20	1.08	3.99
-0.33	1.05	4.41	1.05	4.18	1.08	3.97
0.00	1.05	4.39	1.05	4.15	1.07	3.97

TABLE 3

Hot-wire measurements (axial distributions)

r/d =0.0										
x/d	13.33	15.00	16.67	18.33	20.00	21.67	23.33	25.00	26.67	30.00
$\overline{U} / U_{ref}$	0.83	0.84	0.84	0.86	0.87	0.88	0.88	0.89	0.90	0.91
$u' / U_{ref}(\%)$	16.74	15.79	14.83	14.07	13.29	12.53	11.79	11.18	10.65	9.89
x/d	33.33	36.67	40.00	43.33	46.67	50.00	53.33	56.67	60.00	63.33
$\overline{U} / U_{ref}$	0.91	0.92	0.93	0.94	0.95	0.95	0.96	0.96	0.97	0.98
$u' / U_{ref}(\%)$	9.13	8.39	7.97	7.55	7.21	6.83	6.49	6.28	6.09	6.05

TABLE 4

Cold wire measurements (radial distributions)

r/d	x/d=16.67		x/d=25.00		x/d=33.33		x/d=41.67		x/d=50.00		x/d=58.33		x/d=66.67	
	$\Delta\overline{T}/\Delta\overline{T}_c$	$\theta'/\Delta\overline{T}_c$	$\Delta\overline{T}/\Delta\overline{T}_c$	$\theta'/\Delta\overline{T}_c$	$\Delta\overline{T}/\Delta\overline{T}_c$	$\theta'/\Delta\overline{T}_c$	$\Delta\overline{T}/\Delta\overline{T}_c$	$\theta'/\Delta\overline{T}_c$	$\Delta\overline{T}/\Delta\overline{T}_c$	$\theta'/\Delta\overline{T}_c$	$\Delta\overline{T}/\Delta\overline{T}_c$	$\theta'/\Delta\overline{T}_c$	$\Delta\overline{T}/\Delta\overline{T}_c$	$\theta'/\Delta\overline{T}_c$
-7.50	0.00	0.10	0.00	0.11	0.00	0.13	0.00	0.14	0.00	0.13	0.00	0.15	0.00	0.17
-6.67	0.00	0.10	0.00	0.11	0.00	0.13	0.00	0.14	0.10	0.15	0.00	0.17	0.11	0.20
-5.83	0.00	0.10	0.00	0.11	0.00	0.15	0.00	0.16	0.20	0.18	0.22	0.20	0.22	0.23
-5.00	0.07	0.10	0.00	0.12	0.09	0.20	0.18	0.22	0.40	0.21	0.33	0.24	0.33	0.25
-4.33	0.00	0.11	0.08	0.17	0.27	0.26	0.45	0.26	0.50	0.25	0.56	0.25	0.44	0.25
-3.67	0.07	0.14	0.23	0.25	0.45	0.30	0.64	0.27	0.60	0.24	0.67	0.24	0.67	0.24
-3.00	0.27	0.24	0.54	0.30	0.64	0.29	0.73	0.25	0.80	0.22	0.78	0.23	0.78	0.23
-2.50	0.47	0.31	0.69	0.30	0.73	0.28	0.82	0.24	0.90	0.21	0.78	0.22	0.78	0.22
-2.00	0.73	0.35	0.85	0.28	0.82	0.26	0.91	0.22	0.90	0.20	0.89	0.20	0.78	0.22
-1.50	0.93	0.35	0.92	0.26	0.91	0.24	0.91	0.21	0.90	0.20	0.89	0.20	0.89	0.22
-1.00	1.00	0.32	1.00	0.25	0.91	0.24	1.00	0.20	0.90	0.19	0.89	0.20	0.89	0.22
-0.50	1.00	0.29	1.00	0.23	0.91	0.22	0.91	0.20	0.90	0.18	0.89	0.20	0.89	0.21
0.00	1.00	0.27	1.00	0.22	1.00	0.22	0.91	0.20	1.00	0.18	1.00	0.20	1.00	0.21
0.50	0.93	0.27	1.00	0.22	0.91	0.22	1.00	0.20	0.90	0.18	0.89	0.20	0.89	0.21
1.00	1.00	0.29	0.92	0.23	1.00	0.22	1.00	0.20	0.90	0.18	0.89	0.20	0.89	0.21
1.50	1.00	0.32	0.92	0.24	1.00	0.24	0.91	0.20	0.90	0.19	0.89	0.20	0.89	0.22
2.00	0.93	0.34	0.85	0.26	0.91	0.25	0.82	0.22	0.90	0.19	0.89	0.20	0.89	0.22
2.50	0.80	0.35	0.85	0.28	0.82	0.26	0.82	0.23	0.80	0.20	0.78	0.21	0.78	0.22
3.00	0.60	0.33	0.69	0.29	0.73	0.29	0.73	0.24	0.80	0.22	0.78	0.22	0.78	0.23
3.67	0.40	0.27	0.46	0.29	0.64	0.31	0.64	0.27	0.60	0.24	0.67	0.23	0.67	0.24
4.33	0.07	0.15	0.15	0.25	0.36	0.29	0.36	0.27	0.50	0.25	0.56	0.24	0.44	0.26
5.00	0.00	0.11	0.08	0.17	0.18	0.26	0.27	0.24	0.40	0.24	0.33	0.24	0.33	0.26
5.83	0.00	0.10	0.00	0.12	0.00	0.16	0.18	0.18	0.20	0.19	0.22	0.22	0.11	0.24
6.67	0.00	0.10	0.00	0.11	0.00	0.14	0.00	0.15	0.00	0.15	0.11	0.18	0.00	0.20
7.50	0.00	0.10	0.00	0.11	0.00	0.14	0.00	0.14	0.00	0.13	0.00	0.16	0.00	0.18

TABLE 5

Cold wire measurements (axial distributions)

x/d	$\Delta\overline{T}_c^* / \Delta\overline{T}_{max}^*$	$\theta_c' / \Delta\overline{T}_{max}^*$ (%)	x/d	$\Delta\overline{T}_c^* / \Delta\overline{T}_{max}^*$	$\theta_c' / \Delta\overline{T}_{max}^*$ (%)
8.33	1.00	21.79	29.17	0.71	6.31
10.00	0.92	17.65	33.33	0.71	5.88
11.67	0.90	14.60	37.50	0.66	5.66
13.33	0.87	12.20	41.67	0.66	5.44
15.00	0.84	10.67	45.83	0.66	5.44
16.67	0.82	9.58	50.00	0.64	5.23
18.33	0.79	8.93	54.17	0.64	5.23
20.00	0.79	8.28	58.33	0.61	5.01
21.67	0.77	7.62	62.50	0.61	5.01
23.33	0.74	7.19	66.67	0.61	5.01
25.00	0.74	6.97	-	-	-

TABLE 6 (a)

The skewness and flatness distributions

r/d	x/d = 16.67		x/d = 25.00		x/d = 33.33		x/d = 41.67		x/d = 50.00		x/d = 58.33		x/d = 66.67	
	$F(\theta)$	$S(\theta)$	$F(\theta)$	$S(\theta)$	$F(\theta)$	$S(\theta)$	$F(\theta)$	$S(\theta)$	$F(\theta)$	$S(\theta)$	$F(\theta)$	$S(\theta)$	$F(\theta)$	$S(\theta)$
0.00	2.37	-0.05	3.23	-0.13	3.16	0.08	2.91	-0.01	2.80	0.15	2.97	0.01	2.85	-0.01
0.33	2.33	0.09	3.23	-0.15	3.03	0.06	3.17	0.02	2.96	0.04	2.98	0.14	2.93	-0.04
0.67	3.34	-0.40	3.02	-0.06	3.09	-0.03	2.88	0.10	2.93	0.06	3.15	-0.05	3.04	-0.01
1.00	3.28	-0.48	2.95	-0.05	2.89	0.00	3.36	0.09	2.94	0.05	2.91	0.09	2.84	0.09
1.33	3.08	-0.45	3.09	-0.11	3.03	0.06	2.91	0.15	2.86	0.05	3.10	0.17	2.80	0.05
1.67	2.97	-0.47	3.06	-0.06	2.89	0.07	2.95	0.19	3.18	0.13	2.87	0.04	2.87	0.04
2.00	2.80	-0.50	2.89	-0.09	3.12	0.07	3.09	0.17	2.89	0.16	3.03	0.11	2.95	0.13
2.33	3.06	-0.66	2.67	-0.10	3.00	0.04	2.81	0.14	2.98	0.03	3.02	0.25	3.02	0.21
2.67	3.47	-0.88	2.66	-0.26	2.83	0.13	2.87	0.22	2.82	0.22	2.89	0.09	2.89	0.20
3.00	4.35	-1.22	2.72	-0.41	2.57	0.01	2.72	0.09	2.77	0.18	2.98	0.15	2.88	0.27
3.33	4.28	-1.33	2.98	-0.67	2.53	-0.22	2.57	0.06	2.72	0.14	2.78	0.24	2.86	0.14
3.67	10.32	-2.30	3.49	-0.95	2.79	-0.48	2.39	-0.05	2.51	0.03	2.63	0.09	2.68	0.10
4.00	12.00	-2.25	4.82	-1.33	2.73	-0.60	2.34	-0.20	2.46	-0.07	2.44	0.10	2.67	0.09
4.33	12.57	-1.83	6.45	-1.71	3.55	-0.95	2.56	-0.44	2.46	-0.25	2.33	-0.09	2.44	-0.05
4.67	6.68	-0.70	9.37	-1.94	4.25	-1.21	2.95	-0.69	2.51	-0.41	2.49	-0.29	2.45	-0.13
5.00	2.27	0.03	10.36	-1.87	5.70	-1.43	3.61	-0.91	2.88	-0.66	2.62	-0.45	28.53	-4.70

TABLE 6 (b)

The skewness and flatness distributions

r/d	x/d = 83.33		x/d = 100.00		x/d = 116.67		x/d = 133.33		x/d = 150.00		x/d = 166.67	
	$F(\theta)$	$S(\theta)$	$F(\theta)$	$S(\theta)$	$F(\theta)$	$S(\theta)$	$F(\theta)$	$S(\theta)$	$F(\theta)$	$S(\theta)$	$F(\theta)$	$S(\theta)$
0.00	2.81	0.05	2.84	0.07	2.92	-0.06	2.69	0.04	2.72	0.09	2.70	-0.04
0.33	2.68	0.05	2.73	0.02	2.81	0.02	2.80	-0.01	2.53	0.03	2.66	-0.01
0.67	2.74	0.08	2.86	0.04	2.76	0.03	2.66	0.01	2.64	0.06	2.59	-0.03
1.00	2.66	0.00	2.85	0.06	2.58	0.03	2.60	0.03	2.66	0.03	2.54	-0.04
1.33	2.71	0.08	2.71	0.09	2.72	0.06	2.59	0.06	2.56	-0.01	2.62	0.06
1.67	2.85	-0.02	2.77	0.06	2.69	0.09	2.68	-0.01	2.63	-0.01	2.60	-0.05
2.00	2.81	0.03	2.75	0.03	2.59	-0.01	2.65	0.02	2.68	0.02	2.58	-0.01
2.33	2.87	0.17	2.86	0.06	2.71	0.02	2.64	0.08	2.68	0.13	2.70	0.03
2.67	2.84	0.08	2.76	-0.01	2.75	0.02	2.69	0.01	2.66	-0.04	2.64	0.03
3.00	2.74	0.12	2.78	0.09	2.78	0.05	2.64	0.11	2.71	0.03	2.53	0.00
3.33	2.74	0.14	2.60	0.09	2.65	0.11	2.69	0.05	2.57	0.06	2.67	0.06
3.67	2.75	0.08	2.78	0.06	2.85	0.07	2.65	-0.01	2.77	0.09	2.62	0.04
4.00	2.65	0.03	2.68	-0.01	2.81	0.07	2.70	0.03	2.61	0.02	2.67	0.01
4.33	2.60	0.00	2.61	-0.01	2.76	0.10	2.65	-0.08	2.78	0.06	2.54	0.03
4.67	2.66	-0.09	2.53	-0.05	2.74	-0.06	2.71	-0.04	2.58	-0.03	2.78	-0.12
5.00	2.54	-0.14	2.53	-0.10	2.60	-0.08	2.63	-0.01	2.59	-0.03	2.62	0.05

TABLE 7

The parameters of the curve fitting and

the development of the wake width

Function: $\Delta\overline{T} / \Delta\overline{T}_c = e^{A(r/w)^2}$							
x/d	16.67	25.00	33.33	41.67	50.00	58.33	66.67
A	-0.750	-0.750	-1.000	-0.833	-0.833	-0.750	-0.833
R^2 *	0.936	0.961	0.950	0.966	0.958	0.963	0.951
w (mm)	18.0	20.5	22.5	24.5	27.0	27.5	25.5

* R is regression coefficient.